Final Report

UTILITY OF HIGH ALKALINITY CEMENTS FOR CONTROL OF REINFORCING STEEL CORROSION IN CONCRETE (BD 546-1)

submitted to

Florida Department of Transportation Research Center
605 Suwannee Street
Tallahassee, Florida 32399

submitted by

William H. Hartt and Jorge A. Suarez
Center for Marine Materials
Florida Atlantic University – Sea tech Campus
101 North Beach Road
Dania Beach, Florida 33004
(954) 924-7243 (voice) (954) 924-7270 (fax)
hartt@oe.fau.edu

David R. Lankard
Lankard Materials Laboratory
400 Frank Road
Columbus, Ohio 43207

March 26, 2007

Disclaimer

The opinions, findings, and conclusions expressed in this publication are those of the author and not necessarily those of the State of Florida Department of Transportation.

SI* (MODERN METRIC) CONVERSION FACTORS

APPROXIMATE CONVERSIONS TO SI UNITS

SYMBOL	WHEN YOU KNOW	MULTIPLY BY	TO FIND	SYMBOL
		LENGTH		
in	inches	25.4	millimeters	mm
ft	feet	0.305	meters	m
yd	yards	0.914	meters	m
mi	miles	1.61	kilometers	km
		AREA		
in^2	square inches	645.2	square millimeters	mm^2
ft^2	square feet	0.093	square meters	m^2
yd^2	square yard	0.836	square meters	m^2
ac	acres	0.405	hectares	ha
mi^2	square miles	2.59	square kilometers	km^2
		VOLUME		
fl oz	fluid ounces	29.57	milliliters	mL
gal	gallons	3.785	liters	L
ft^3	cubic feet	0.028	cubic meters	m^3
yd^3	cubic yards	0.765	cubic meters	m^3
		MASS		
oz	ounces	28.35	grams	g
lb	pounds	0.454	kilograms	kg
T	short tons (2000 lb)	0.907	megagrams (or "metricton")	Mg (or "t")
		TEMPERATURE (exact degrees)		
°F	Fahrenheit	5 (F-32)/9 or (f-32)/1.8	Celsius	°C
		ILLUMINATION		
fc	foot-candles	10.76	lux	lx
fl	foot-Lamberts	3.426	$candela/m^2$	cd/m^2
		FORCE and PRESSURE or STRESS		
lbf	poundforce	4.45	newtons	N
lbf/in^2	poundforce per square inch	6.89	kilopascals	kPa

APPROXIMATE CONVERSIONS FROM SI UNITS

SYMBOL	WHEN YOU KNOW	MULTIPLY BY	TO FIND	SYMBOL
		LENGTH		
mm	millimeters	0.039	inches	in
m	meters	3.28	feet	ft
m	meters	1.09	yards	yd
km	kilometers	0.621	miles	mi
		AREA		
mm^2	square millimeters	0.0016	square inches	in^2
m^2	square meters	10.764	square feet	ft^2
m^2	square meters	1.195	square yards	yd^2
ha	hectares	2.47	acres	ac
km^2	square kilometers	0.386	square miles	mi^2
		VOLUME		
mL	milliliters	0.034	fluid ounces	fl oz
L	liters	0.264	gallons	gal
m^3	cubic meters	35.314	cubic feet	ft^3
m^3	cubic meters	1.307	cubic yards	yd^3
		MASS		
g	grams	0.035	ounces	oz
kg	kilograms	2.202	pounds	lb
Mg (or "t")	megagrams (or "metric ton")	1.103	short tons (2000 lb)	T
		TEMPERATURE (exact degrees)		
°C	Celsius	1.8C+32	Fahrenheit	°F
		ILLUMINATION		
lx	lux	0.0929	foot-candles	fc
cd/m^2	$candela/m^2$	0.2919	foot-Lamberts	fl
		FORCE and PRESSURE or STRESS		
N	newtons	0.225	poundforce	lbf
kPa	kilopascals	0.145	poundforce per square inch	lbf/in^2

*SI is the symbol for the International System of Units. Approxiamte rounding should be made to comply with Section 4 of ASTM E380. (Revised March 2003.)

Technical Report Documentation Page

1. Report No.	2. Government Accession No.	3. Recipient's Catalog No.

4. Title and Subtitle	5. Report Date
Utility of High Alkalinity Cement for Control of Reinforcing Steel Corrosion in Concrete	March, 2007
	6. Performing Organization Code FAU-OE-CMM-06-3
7. Author(s) William H. Hartt, Jorge A. Suarez, and David R. Lankard	8. Performing Organization Report No.
9. Performing Organization Name and Address Center for Marine Materials Florida Atlantic University – Sea Tech Campus 101 North Beach Road Dania Beach, Florida 33004	10. Work Unit No. (TRAIS)
	11. Contract or Grant No. BD 564-1
12. Sponsoring Agency Name and Address Florida Department of Transportation 605 Suwannee Street, MS 30 Tallahassee, FL 32399	13. Type of Report and Period Covered Final Report
	14. Sponsoring Agency Code

15. Supplementary Notes

16. Abstract

Corrosion of reinforcing steel in concrete exposed to sea water has been documented as a major cause of bridge deterioration, both nationwide and in Florida. Previous research has indicated, however, that as much as a 10-fold increase in time-to-corrosion can be realized by using high alkalinity ($Na_2O_e \approx 1.00$) compared to normal alkalinity ($Na_2O_e \leq 0.60$) cement. Consequently, if high alkalinity cements (HACs) can be specified for bridge construction, significantly enhanced corrosion resistance can be realized at no additional cost. However, a concern regarding HACs is the possibility of alkali-silica reaction (ASR) which can compromise concrete integrity. The objective of the present project was to determine the likelihood of ASR when HACs are used with aggregates common to Florida bridge construction. Experiments involved cements of three Na_2O_e (0.5, 1.0, and 1.2), a local silica sand, and seven coarse aggregates, three of which were limestone from different Florida quarries and two were Georgia and Nova Scotia granites. The concretes also included Spratt limestone and Sudbury gravel, which have been documented previously as being severely and moderately ASR susceptible, respectively. Most mix designs were based on FDOT Class V concrete. In addition, some concretes were admixed with an ASR inhibitor ($LiNO_3$); and most contained fly ash. Measurements of concrete 1) pore water pH, 2) length change, 3) compressive and flexural strengths, and 4) electrical resistivity were made periodically for times up to two years. Petrographic analysis was performed on samples of the aggregates and on all concretes at the end of one year with additional macroscopic examinations after two years. Only mixes with Sprat limestone and the higher two Na_2O_e (1.0 and 1.2) had length increases after one year that exceeded the criterion established by ASTM C1293 (0.04 percent) as indicative of potential ASR reactivity. However, concrete micro-cracks and ASR gel exudate were apparent on prisms with one of the three Florida limestones and on prisms with each of the three granite coarse aggregates for mixes with $Na_2O_e = 1.2$ and no $LiNO_3$, even though length increases were less than 0.04 percent. Mixes with this Florida limestone and admixed $LiNO_3$ also exhibited micro-cracking. Criteria for qualifying coarse aggregates for use in high alkalinity concretes were developed. It is concluded that the FDOT should pursue further the use of HACs with $Na_2O_e = 1.0$ in mixes with admixed $LiNO_3$ and fly ash, provided Na_2O_e for the latter does not exceed 0.7 and the coarse aggregate contains no ASR reactive components.

17. Key Word	18. Distribution Statement
Bridges, reinforced concrete, high alkalinity cement, alkali silica reaction, aggregates, corrosion	No restrictions. This document is available to the public through NTIS, Springfield, VA 22161

19. Security Classif. (of this report)	20. Security Classif. (of this page)	21. No. of Pages	22. Price
Unclassified	Unclassified	188	

Form DOT F 1700.7 (8-72) Reproduction of completed page authorized

ACKNOWLEDGEMENTS

The authors are indebted to the FDOT State Materials Office for technical comments and guidance during the course of this project, in particular Mr. Michael Bergin, Mr. Charles Ishee, and Mr. Rodney Powers. The assistance of Mr. George Jones of this laboratory is also acknowledged.

EXECUTIVE SUMMARY

Corrosion induced deterioration of reinforced concrete bridge substructures in Florida coastal waters has been recognized for decades as a continuing maintenance problem. Such distress arises as a consequence of 1) progressive chloride intrusion into the concrete over time, 2) localized breakdown of the otherwise protective passive film upon embedded reinforcing steel once chlorides achieve a critical concentration at the steel depth, 3) corrosion of the steel at a rate controlled by oxygen and moisture availability, and 4) cracking and spalling of the concrete cover from tensile hoop stresses generated in the concrete about the reinforcement by expansive corrosion products. Unaddressed, these processes can lead to structural failure if either the reinforcement or concrete cross section (or both) become sufficiently reduced. The objective of this project was to investigate a previously unaddressed option for mitigating corrosion induced bridge substructure deterioration and thereby extend service life of new structures through improved concrete mix design and materials selection.

Previously sponsored FDOT research demonstrated that time-to-corrosion of reinforcing steel in concrete can be extended by use of high alkalinity cements. However, such cements may cause other deterioration processes, in particular, alkali-silica reaction (ASR) which is a destructive chemical reaction of alkali with aggregates. The objective of the present study was to investigate the extent to which high alkalinity cements promote ASR for materials relevant to concrete bridge construction in Florida.

Measurements of 1) concrete specimen length change for times up to two years, 2) concrete alkalinity content by both ex-situ leaching and pore water expression, 3) compression and flexural strength, and 4) concrete electrical resistivity were made on a series of, first, mortars and pastes to establish appropriate alkali dosages and, second, 55 concrete mixes that contained five candidate coarse aggregates and cements of three different alkalinities. Two additional coarse aggregates that are know from previous studies to be ASR susceptible where included for baseline purposes. Additional mix variables were inclusion of fly ash and a lithium nitrate admixture, the latter being a known ASR inhibitor. From this, criteria were establish for qualifying a particular FDOT Class V high alkalinity concrete based upon it containing 1.2 percent alkali and no lithium admixture according to the following:

- Concrete expansion after one and two years of ASTM C1293 exposure (38^{o}C and 100 percent relative humidity) should be below 0.010 percent.

- There should be no significant concrete length change between the first and second years of ASTM C1293 exposure.

- There should be a complete absence of cracking after two years of ASTM C1293 exposure, as determined by microscopic examination of molded and cast concrete surfaces.

- Petrographic examination (ASTM C295) should confirm that the fine and coarse aggregates contain no known potentially alkali-silica reactive phases (strained quartz, microcrystalline quartz, chalcedony, chert, tridymite, cristobalite, opal, and others).

- Petrographic examination (ASTM C856) should confirm absence of any microstructual features indicative of ASR activity. (alkali-silica gel, diagnostic cracking within aggregate particles and within cement paste adjacent to cracked aggregate particles, reaction rims on aggregate particles, and gel-stained cement paste adjacent to cracked aggregate particles) after two year of ASTM C1293 exposure.

- There should be a normal, expected increase in concrete flexural and compressive strengths as measured at one year compared to that at 28 days.

Based upon the above criteria, two of the five experimental concretes, both of which were fabricated with Florida limestones, were qualified for further study. It is recommended that the first ranked coarse aggregate (Rinker Materials, Miami Oolitic Limerock, Pit 87-089) be considered for further trials so that high-alkali concretes might be further qualified for use in Florida reinforced concrete bridge structures. Upon such qualification, service life of Florida coastal bridges can be significantly extended at no additional cost or construction complexity. Alternatively, the option exists to relax other design parameters, such as concrete cover over reinforcement, such that construction costs are reduced.

TABLE OF CONTENTS

TABLE OF CONTENTS (continued)

TABLE OF CONTENTS (continued)

TABLE OF CONTENTS (continued)

LIST OF FIGURES

LIST OF FIGURES (continued)

page no.

LIST OF FIGURES (continued)

LIST OF FIGURES (continued)

LIST OF FIGURES (continued)

page no.

LIST OF FIGURES (continued)

page no.

LIST OF TABLES

LIST OF TABLES (continued)

I. INTRODUCTION

Corrosion induced deterioration of reinforced concrete bridge substructures in Florida coastal waters is a pervasive problem. Such distress arises as a consequence of 1) progressive chloride intrusion into the concrete, 2) breakdown of the otherwise protective passive film upon the embedded steel once chlorides achieve a critical concentration at the steel depth, 3) corrosion of the reinforcing steel at a rate controlled by oxygen and moisture availability, and 4) cracking and spalling of the concrete cover from tensile hoop stresses generated in the concrete about the reinforcement by expansive corrosion products. Unaddressed, these processes can lead to structural failure if either the reinforcement or concrete cross section (or both) become sufficiently reduced. This deterioration process is commonly modeled in terms of three component steps: 1) time for corrosion initiation, 2) time for corrosion propagation (appearance of cracking on the external concrete surface), and 3) time for surface cracks to develop into spalls that require repair, rehabilitation, or replacement. Figure I-1 illustrates this schematically, where T_i, T_p, T_d, and T_f refer to times for initiation, propagation, continued damage (spalling), and failure, respectively. Of these, T_i is typically of greatest duration; and it is the parameter that can be most influenced by various corrosion control measures. Parameters that determine T_i are 1) properties of the component concrete materials (cement, admixtures, and aggregates), 2) concrete mix design, 3) corrosion properties of the reinforcement, 4) concrete cover, and 5) nature and severity of the exposure.

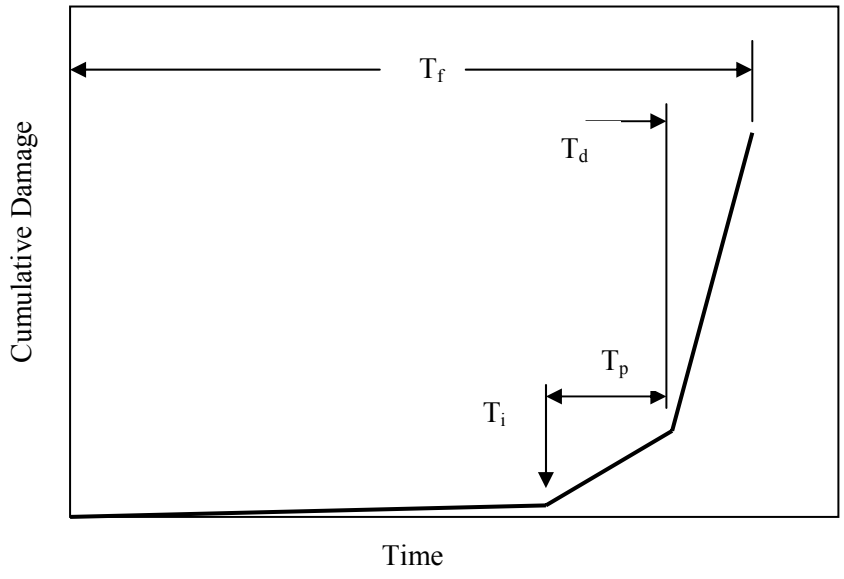

Figure I-1: Schematic illustration of the various steps in deterioration of reinforced concrete due to chloride induced corrosion (modified from Tutti).

Based upon research, testing, evaluation, and service experience, various options have been identified whereby the onset of chloride induced reinforcing steel corrosion can be controlled. For new construction, these include the following:

1. Use of a protective coating on the embedded steel.
2. Use of a protective coating on the external concrete surface.
3. Increased concrete cover over the reinforcement.
4. Use of an admixed corrosion inhibitor.
5. Use of pozzolanic admixtures.
6. Cathodic protection (alternatively termed cathodic prevention).
7. Use of corrosion resistant alloy reinforcement.

Option 1, which is exemplified by epoxy-coated reinforcing steel, is intended to isolate the steel from chlorides that have penetrated the concrete to the reinforcement depth. While this approach is relied upon for corrosion control of bridge structures throughout much of North America, it has been shown to be ineffective in Florida coastal waters.[1,2,3] Option 2 intends to provide a barrier layer at the concrete surface; however, such an approach is now recognized as not being effective in the long-term. Options 3 and 5 both delay the time for chlorides to achieve a critical concentration, designated C_T,[4] at the reinforcement depth, the former by increasing the distance over which Cl^- must diffuse and the latter by decreasing the rate of this diffusion. However, experiments in aqueous solutions have indicated that C_T increases linearly with increasing $[OH^-]$, meaning that C_T can be represented in terms of a critical ratio of Cl^--to-OH^- (Cl^-/OH^-). While such a parameter and relationship is now recognized as overly simplified in the case of actual concrete pore water, in general terms the Cl^-/OH^- term has utility. Accordingly, it has been reasoned that pozzolans should reduce C_T since they lower pore water pH. It is generally considered, however, that the reduced Cl^- diffusivity afforded by pozzolans more than offsets any C_T reduction. Option 4 normally functions by enhancing stability of the passive film in the presence of Cl^- (increased C_T). Option 6 provides an electric field that opposes the diffusion of negatively charged ions such as Cl^- into the concrete. In effect, option 7 functions similarly to option 4 in that it renders the reinforcement surface more resistant to chlorides and elevates C_T.

The approach adapted by the Florida Department of Transportation (FDOT) during the past decade-plus for new construction has been to extend time-to-corrosion initiation by a combination of 1) enhanced concrete cover (75 mm minimum for precast and 100 mm for cast in place

components) and 2) use of high performance concretes; that is, ones with permeability reducing (pozzolanic) or corrosion inhibiting admixtures (or both) and low water-to-cementiteous ratio (w/cm). Examples in the former category are fly ash and silica fume and for the latter calcium nitrite, with numerous studies having documented the benefit(s) that each provides. Limitations, however, involve concerns regarding long-term availability and material property consistency (fly ash), placeability (silica fume), and cost. The last of these factors (cost) is now commonly addressed, both nationwide and in Florida by Life Cycle Cost Analysis (LCCA) whereby both initial and maintenance expenses are normalized in terms of Present Worth. Added initial costs, as can occur in conjunction with admixtures, enhanced cover, and other options, have a negative impact on an LCCA determination.

The critical Cl^- threshold for corrosion initiation, $C_{T,}$ is particularly important to materials selection, design, and analysis for concrete structures exposed in coastal locations since knowledge of this parameter facilitates projection of T_i. This is apparent from the one-dimensional solution to Fick's second law of diffusion,

$$\frac{C_{x,T} - C_o}{C_s - C_o} = 1 - \text{erf}\left[\frac{x}{2\sqrt{D_{eff} \cdot T}}\right], \qquad (1$$

where $C_{x,T}$ is $[Cl^-]$ at depth x after time T, C_s is $[Cl^-]$ at the concrete surface, C_o is the baseline $[Cl^-]$ in the concrete, and D_{eff} is the effective Cl^- diffusion coefficient. The expression, as written, assumes that Cl^- transport is by one-dimensional Fickian diffusion. By setting x equal to the concrete cover and $C_{x,T} = C_T$, then $T = T_i$. Consequently, any factor that elevates C_T enhances T_i. However, C_T is now recognized as being dependent upon multiple factors, including 1) cement composition, 2) concrete mix design, 3) exposure conditions, and 4) reinforcing steel surface condition. Also, C_T is higher for corrosion resistant alloys, such as stainless steels, than for carbon steels. Even when each of the above factors is held constant, the value for C_T is distributed because of the heterogeneous nature of the concrete matrix, the steel surface, and the interface between the two. From literature data, Glass and Buenfeld[4] reported values for C_T in the range 0.17-2.5 (total Cl^- on a cement weight percent (w/o) basis) or, alternatively, 0.68~10 kg/m^3 (concrete weight basis assuming 400 kg/m^3 cement content).

Several recent FDOT sponsored research projects[5,6,7,8] have focused upon, first, defining C_T with regard to Florida bridge concretes, and, second, exploring the utility of high alkalinity cements in concrete as an alternative for increasing T_i. With regard to the latter, a series of experiments where steel was exposed in aqueous solutions demonstrated that C_T increases with increasing solution pH.[9,10,11,12,13,14] This occurs because Cl^- serves as a corrosion activator and OH^- as a passivator. Hausmann[15] projected a critical Cl^-/OH^- ratio of 0.6. Chloride binding renders concrete pore water more complex electrolytes than simulating aqueous solutions; however, some degree of correlation between critical $[Cl^-]/[OH^-]$ and pH still prevails over at least some pH range(s). Figure I-2[5,7] shows an example of this as a log-normal cumulative distribution plot of T_i (T_c in the figure) for a series of G109 0.50 water-to-cement ratio reinforced concrete specimens that were cyclically ponded with a 15 w/o NaCl solution. Cements of two equivalent alkalinities, Na_2O_e, as defined by the equation,

$$Na_2O_e = Na_2O + 0.658K_2O, \qquad (2$$

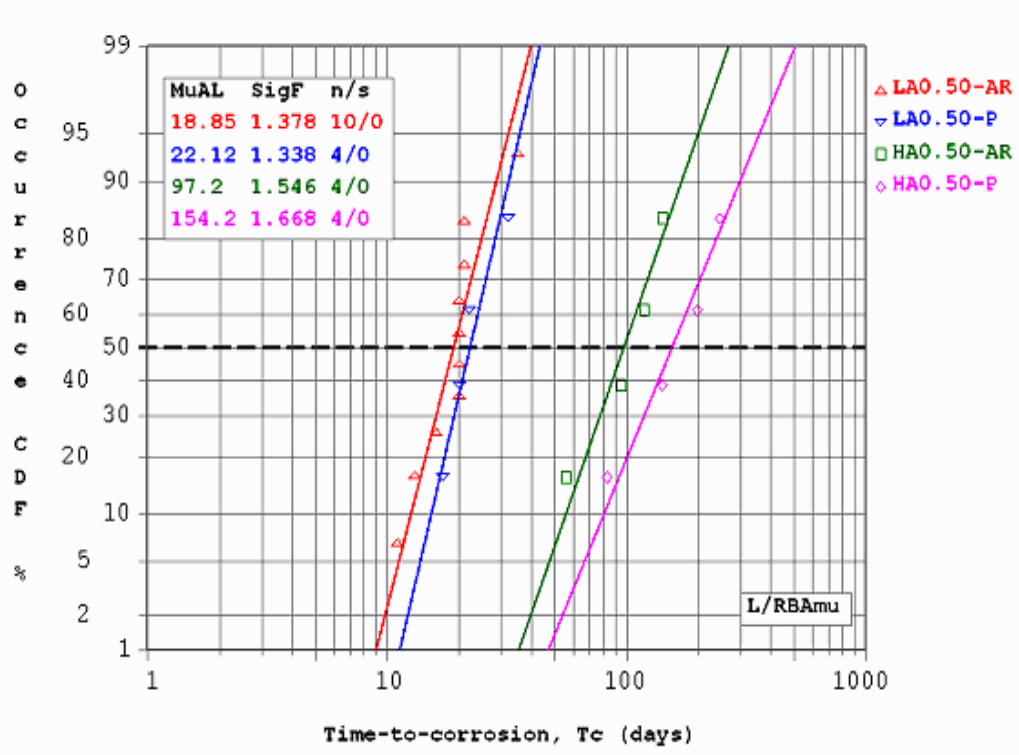

Figure I-2: Log-normal cumulative distribution plot of T_i for cements of two Na_2O_e. Specimens utilized bars with an as-received (AR) and wire brushed (P) surface finish. MuAL is the mean T_i, SigF is the slope of the best fit straight line, n is the number of specimens tested in each category, and s is the number of run outs (zero in all cases).

were employed, 1.08 (designated HA) and 0.32 (designated LA). The data indicate that the mean T_i for HA specimens was 5-10 times greater than for the LA and, consequently, that high alkalinity cements have potential as an option for extending service life of concrete structures in marine applications provided it can be demonstrated that there are no adverse effects of such cements on other concrete properties.

II. PROJECT OBJECTIVE

While it is now accepted that time-to-corrosion of reinforcing steel can be extended if concrete mix designs utilize a high alkalinity cement, the possibility arises that one or more alternative deterioration processes such as alkali-silica reaction (ASR) or alkali carbonate reaction (ACR) or both, might arise. Based upon this understanding, the present project was initiated with the objective of investigating the extent to which high alkalinity cements promote such reaction, ASR in particular. The study included aggregates that are relevant to Florida bridge construction. In addition, two aggregates that are recognized as being ASR susceptible were included for reference purposes. Additional mix design variables included 1) three cement alkalinity levels and 2) presence versus absence of fly ash and of an ASR-inhibiting admixture ($LiNO_3$). The assessment approach involved 1) measurement of concrete pore water pH, length change, resistivity, and compressive and flexural strengths, and 2) petrographic analyses with data being collected for up to two years. Based upon the results, criteria are proposed for utilization of high alkalinity cements in Florida concrete bridges.

III. NATURE AND CONTROL OF ALKALI SILICA REACTION IN CONCRETE

General

Alkali-silica reactions have been documented in portland cement concretes since around 1940. Classical ASR involves alkali cations and OH^- from concrete pore water reacting with metastable forms of SiO_2, which are present in a wide variety of igneous, sedimentary, and metamorphic aggregates used in concrete. The fundamental cause of alkali-silica attack is an elevated $[OH^-]$ in concrete pore solutions from cements rich in Na^+ and K^+ with the reaction product being a gel. Following this, the ASR gel imbibes water which causes the gel to expand. This expansion creates stresses which, in many cases, are sufficiently large and sustained to fracture both the offending aggregate particle and cement paste in contact with the particle.

During the initial stage of ASR activity, alkali-silica gel may be formed without any deleterious effects on the concrete: but subsequently, cracking may initiate within the reacting aggregate particles. The particles may be of either the coarse or fine aggregate phase in the concrete. In the early stages of destructive ASR activity, cracks in the reacting aggregate are widest in the particle interior. Frequently, a darkened rim forms along the outer edge of the reacting aggregate particle, and the cement paste in contact with the particle changes color as it becomes saturated with the ASR gel. In advanced ASR activity, the reacting particle is completely gelatinized. When concretes showing advanced ASR activity are sectioned, the soft, gelatinized interior of the reacting particles is frequently lost, leaving only a peripheral hull that is bonded to the concrete.

In general, destructive ASR expansions are expected to continue as long as ample supplies of the reacting chemical species and water are available. However, it has been recognized for many years that there is not a simple relationship between the amount of the reactive silica phase in the concrete and the alkali supply. Researchers have coined the term "pessimum" amount to indicate the "optimum" offending aggregate content with regard to the greatest potential for destructive ASR activity. If the offending aggregate content is too low, the potential for damage is also low regardless of the alkali supply. If the offending aggregate content is sufficiently high, the available alkali may become depleted before any significant damage occurs. The pessimum value is unique for different aggregates.

The primary reaction between aggregate and alkali is still not well understood; however, a simplified representation of the compounds and process involved is given by the reaction,[16]

$$4SiO_2 + 2NaOH \rightarrow Na_2Si_4O_9 + H_2O \quad \text{(Gel)}. \qquad (3$$

The driving force for ASR is provided by the concentration of alkali hydroxides, which is proportional to the equivalent alkali content of the cement (Na_2O_e) as defined by Equation 2. It has been shown that Na^+ and OH^- penetrate reactive silica more easily than Ca^{2+}.[17] Thus, cements with a Na_2O_e upper limit of 0.60 percent (low-alkali cement) are recommended and normally specified[18] for concrete construction in order to accommodate the possibility that aggregates might be reactive and minimize ASR. However, consideration of the potential for alkali migration, as well as the use of supplementary cementitious materials (SCMs) that produce more ASR-resistant concretes, can be taken into account to establish different limits.

Some investigators have suggested including the alkali content of SCMs, aggregates, and admixtures in the calculation of the Na_2O_e.[19] However, there is uncertainty regarding this approach since other guidelines recommend that the contribution of materials such as fly ash (FA) be ignored due to their action as alkali reducer.[20,21]

Silica, besides being present as a crystalline oxide such as quartz, is also found in compounds where Si and O are combined with other elements such as Ca, K, and Na. Reactive SiO_2 refers to poorly crystallized compounds of Si and O that are capable of reacting with OH^-. The more disordered the crystalline structure, the greater the surface area available for reaction and, hence, the greater the susceptibility to ASR. Most aggregates employed in concrete production are not pure but contain other mineral components including reactive SiO_2. To determine if an aggregate is reactive, a petrographic examination should be performed.[22] This identifies any potentially reactive constituents and estimates their amount. Since it is the proportion of reactive SiO_2 that determines the degree of reactivity, it is the aggregate combination (fine and coarse) that must ultimately be evaluated. Table III-1 lists known ASR aggregate constituents.[23]

Table III-1: Reactive components of ASR susceptible aggregates.

Reactive Component	Physical Character
Opal	Amorphous
Chalcedony	Microcrystalline
Cristobalite	Crystalline
Tridymite	Crystalline
Quartz	a) Microcrystalline
	b) Crystalline but intensely fractured, strained, or inclusion filled
Siliceous rhyolitic, dacitic or andesitic	Glass or cryptocrystalline

Moisture plays a dual function in occurrence of ASR. First, it serves as the medium for transport of reactive ions and, second, it reacts with the ASR gel to generate expansive stresses in the concrete. Additional factors regarding ASR are:

a) Effects of additional elements on the formation of the expansive gel,

b) Role of temperature in gel formation, and

c) Presence of ASR controlling admixtures.

Models for ASR

Several authors have proposed models for the deterioration of concrete structures by ASR. Generally, these focus on kinetics of the chemical reactions and gel expansion.[24] As noted above, ASR is thought to involve two steps where, first, ASR gel is formed from the reaction of amorphous SiO_2 and OH^- in the pore solution and, second, water is absorbed by the gel causing the latter to expand. While the former reaction rate is determined by humidity and temperature, the latter is considered to be instantaneous as a consequence of the density change of the products with respect to reactants.[25] At early stages of deterioration, the expanding gel fills the interconnected aggregate pores and the interfacial transition zones (ITZs).[26] During this phase, the ASR reaction occurs; but no change is observed in the concrete. However, once the pores become filled, further reaction causes internal stresses and concrete expansion.

Steffens et al.[24] presented a model in which ASR expansion was represented by an equation of the form,

$$\varepsilon = \alpha \cdot (1 - \exp(-b(t - \tau_f))), \qquad (4$$

where

ε is concrete strain,

α is the maximum level of expansion depending on the availability of reactants,

b is a coefficient related to the reaction kinetics,

t is time, and

τ_f is the characteristic time related to the period at which pores become filled.

On the other hand, an expression for concrete expansion with time in terms of concrete parameters has been proposed as,[24]

$$\varepsilon = \frac{\beta \cdot M}{\rho} \frac{1}{1+\gamma} \exp\left[-\frac{\tau_f}{\tau_r}(1+\gamma) \right] \left[1 - \exp\left[-\frac{(t-\tau_f)}{\tau_r}(1+\gamma) \right] \right], \qquad (5$$

where,

β is a chemical dilatation coefficient of the gel,

M is a water-gel combination coefficient,

ρ is the change in gel density,

τ_r is the reaction characteristic time between OH^- and silica compounds, and

γ is the ratio between the reaction characteristic time and the aging characteristic time.

Example concrete expansion results calculated according to this model[24] are presented in Figure III-1.

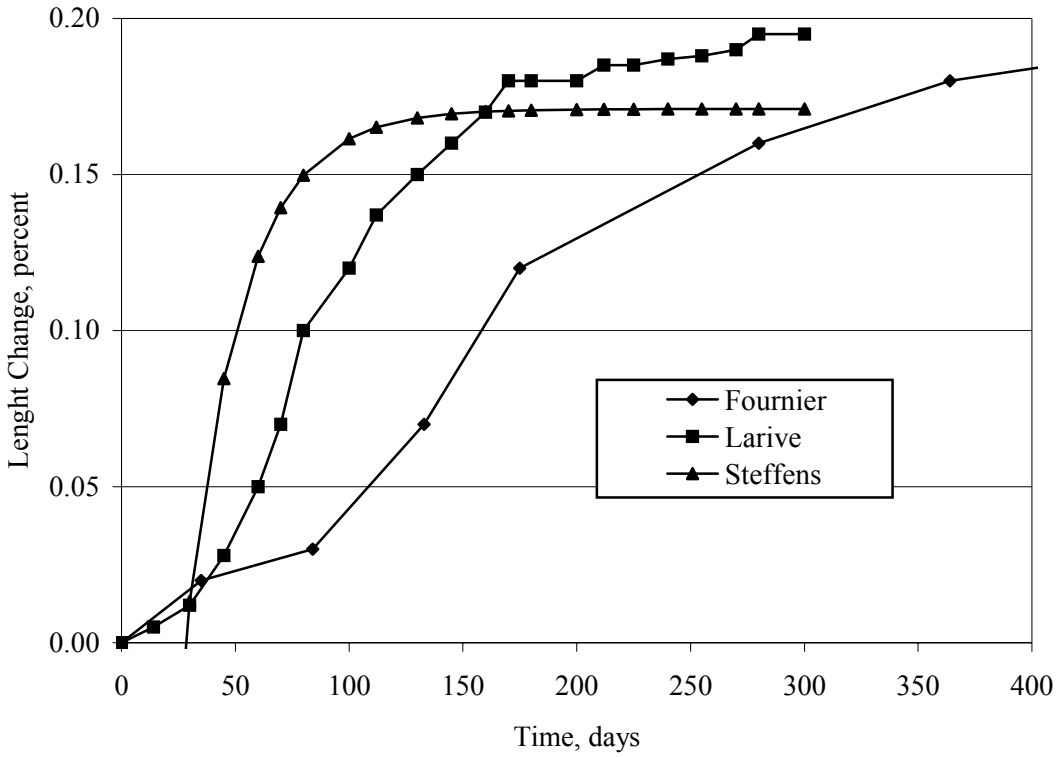

Figure III-1. Theoretical and experimental expansion results due to ASR (Fourier and Malhotra[25] (experimental), Larive (experimental, referenced by Steffen et al.[24]), and Steffen et al.[24] (analytical)).

Susceptibility of Florida Aggregates to Alkali-Silica Reaction

A Strategic Highway Research Program (SHRP) study[27] reported that potentially reactive rocks exist in every state in the US. Despite this, many state departments of transportation

(DOTs) have not reported a problem with ASR in their concretes. The authors of this SHRP report concluded that the reasons for this may include the following:

1. Historically, cements of low-alkali have been used.
2. Concretes often contain pozzolans.
3. There has been a lack of awareness by highway personnel of ASR symptoms.
4. There has been an over-reliance on inadequate ASR testing methods, which has led to an incorrect conclusion that no problem exists.

In a SHRP study questionnaire survey regarding ASR, 19 of the 44 states that responded acknowledged a problem with ASR, 23 reported no problem, while two were "uncertain". Florida was one of the states that reported "no problem". Subsequent efforts to identify occurrence of ASR activity in Florida by the present project team led to a similar finding with the single exception of anecdotal information provided by a company that markets a Li-based compound for ASR activity control. In two cases of warehouse floor distress, ASR was cited; but on-going litigation precluded identification of the structures.

Despite the fact that Florida has not reported an ASR problem, it was deemed prudent by the research team to examine this situation further. The reasons for this include the following:

1. Historically the cements available in Florida have had a low or normal alkali content.

2. Most Florida limestone aggregates contain some SiO_2-bearing compounds (including Florida limestones used in the present study).

3. Two aggregates that have been used in Florida bridge construction are siliceous rocks (granites) from Georgia and Nova Scotia.

4. The FDOT structural concrete that served as the mix design in the current study contains fly ash. It is possible that the use of this supplementary cementitious material has historically provided a safety factor in any marginal situations.

It has been known for many years that supplementary cementitious materials (SCMs), including fly ash, can mitigate or eliminate destructive ASR activity in portland cement concretes. More recently, Li compounds have been used for the same purpose.

Supplementary Cementitious Materials for ASR Control

Supplementary cementitious materials (SCMs) are widely used in many types of portland cement concretes to provide both economic and performance benefits. The most widely used SCMs include 1) fly ash, 2) silica fume (also referred to as microsilica), and 3) slag cement (GGBS – ground-granulated blast furnace slag). One of the purposes of SCM useage is to minimize or eliminate destructive ASR-activity in concrete.[28,29,30,31,32,33,34,35,36,37,38,39,40]

Control of ASR by Lithium Compound Admixtures

The use of Li compounds to control ASR expansion was reported based on a comprehensive investigation involving different chemical admixtures.[41] Among these, $LiNO_3$ is preferred since a number of studies have demonstrated that insufficient dosages of LiOH, $LiCO_3$ and LiF may actually increase ASR expansion rather than reduce it. Concerns regarding toxicity are also an issue for some of these.[41,42] Although not completely confirmed, there are several proposed mechanisms for ASR suppression by Li compounds. The most accepted considers that, since Li^+ has a smaller ionic radius and relatively high surface charge density, it is more readily incorporated into the ASR gel than Na^+ and K^+ which gives rise to a non expansive product.[42,43] Most studies performed to-date indicate that the effectiveness of Li compounds against ASR is principally determined by the concrete alkali content. These suggest that a Li/(Na+K) molar ratio between 0.6 and 1.0 is sufficient to eliminate expansion for most aggregates,[41,43] and recommended dosages are generally based on achieving this proportion.

IV. OTHER FACTORS AFFECTING DURABILITY OF REINFORCED CONCRETE

Chemical Resistance of Concrete

Although concrete performs satisfactorily in most waters and soils that contain aggressive chemicals, there are some environments in which service life is reduced unless precautions are taken. To produce significant attack on concrete itself, chemicals such as salts and acids must be in solution at above a certain concentration. The most common type of degradation by salts is sulfate attack, which leads to the formation of ettringite and gypsum which cause concrete to lose strength. Other salts, such as Na_2CO_3, have a different mechanism of attack where, once dissolved, ions migrate into the concrete, concentrate, and finally precipitate at an exposed surface. Physical deterioration includes surface scaling, which progressively damages the

exposed concrete and eventually leads to total disintegration of poor quality concrete. Acid attack, on the other hand, is the result of reaction between an acid and $Ca(OH)_2$ in the hydrated cement or other Ca compounds such as limestone in aggregates. As a consequence, water-soluble Ca^{2+} substances are formed and then leached. Protection against most types of chemical attack is generally achieved by an appropriate mix design that reduces the ingress of water. This includes the selection of an appropriate cement content, low w/cm, air entrainment, and proper placement and curing.

Chloride Permeability and Binding

The transport rate of ions or molecules as either liquids or gases in concrete constitutes a key factor affecting durability. In many cases, service life is determined accordingly. Fluid movement through concrete occurs by a) capillary suction which depends on the physical properties of the fluid and concrete pore structure, b) flow under a pressure gradient, known as the sorptivity, and c) flow under a concentration gradient, also termed diffusivity. Permeability of concrete to a particular substance depends on the pore structure, the degree of pore interconnectivity, and the water content and its composition. Generally, ions and molecules are smaller than the concrete pores; and so all concretes are permeable to some degree. Concrete permeability is principally determined by the cement paste, especially that situated at the surface and in ITZs.

Capillary pores in cement paste, which are associated with calcium silicate hydrates that form during the hydration process and have a radius of 10^{-8} - 10^{-4} m, are generally recognized as being particularly influential with regard to transport. Because hydration of cementitious grains continues in the water filled capillary pores with time, a continuous reduction of net porosity results. The transport mechanisms most studied for concrete applications are gaseous diffusion, ionic diffusion, and liquid flow under pressure, especially the first two since they account for carbonation and chloride ingress, the principal causes of corrosion of concrete reinforcement.

As noted above, chloride ions are the primary cause of loss of reinforcing steel passivity in concrete. Identification of the sources and distribution of chlorides is then relevant to understanding durability. Chlorides in concrete may be either dissolved in the pore water as free ions or chemically bound to cement hydrates. Binding capacity is the capability of a material to bind ions. Mechanisms of Cl^- binding include formation of Friedel's salt ($3CaO\ Al_2O_3\ CaCl_2$

$10H_2O$) and calcium chloroferrite ($3CaO\ Fe_2O_3\ CaCl_2\ 10H_2O$).[23] It is generally recognized that only free chlorides are involved in the corrosion process; however, some authors consider that there is corrosion risk from bound chlorides as well since, under certain circumstances, these may become liberated.[44,45] In a general sense, Cl^- intrusion involves both absorption and ionic diffusion; however, in circumstances where the depth to which the former occurs is relatively superficial compared to the reinforcement cover, only the latter is included in modeling and analysis efforts. Diffusional ingress of chlorides and time-to-corrosion were discussed above in conjunction with Equation 1.

Electrical Resistivity of Concrete

Electrical resistivity is a bulk material property that represents the resistance of a material to current flow. In response to an applied electric field, current is initially carried by the free migration of ions through the cement pore system. However, anions accumulate on one side of a pore and cations on the other, which creates an opposing electric field and contributes to a current decrease. Magnitude of the electric field and the mobility of ions in the pore water solution control the conduction process.[46] Electrical resistivity of concrete depends on microstructure of the cement paste and concentration and mobility of ions in the pore solution, as determined in part by water content. Cement chemistry and content, w/cm, and presence of admixtures and SCMs are factors that influence cement paste microstructure, pore solution composition, and, hence, electrical resistivity.[47]

Although there have been only limited studies of the effect of aggregates upon resistivity, it is recognized that electrical resistivity of cement paste is generally much smaller than that of aggregate, with values for the former being on the order of 1.5 kΩ·cm and for the latter 100 kΩ·cm. Thus, in terms of electrical properties, concrete can be regarded as comprised of distributed insulating particles embedded in the conducting cement paste matrix.[48] It follows then that resistivity is a function of the volume fraction and distribution of aggregates throughout the system. Also apparent is that Cl^- penetration varies with concrete resistivity according to an inverse power law relationship.[49] However, modeling analyses have not been able to predict the full range of measurement results found in field tests.[50]

Concrete resistivity and reinforcement corrosion rate subsequent to depassivation have been shown to be interrelated. Potential monitoring of steel reinforcement can identify anodic regions

of active metal dissolution and cathodic regions of oxygen reduction. A low resistance path between such macro-anode and cathode sites is normally associated with a higher rate of corrosion, and so electrical resistivity measurements can be used to evaluate the risk of corrosion at any given time.[51]

In principle, resistivity can be determined by placing an electrode at each end of a concrete member and measuring the potential drop, P, between the electrodes upon application of a current, I. However, given the size, shape, and non-uniformity of concrete members in the field, as well as the variable geometry of laboratory specimens, such an approach is generally impractical. Instead, the four-probe Wenner type method, similar to what has been employed to measure soil resistivity, is generally used. Here, current is applied between the two outer probes, and the resulting potential between the two center probes is measured. For this approach, the relationship between I, P, and bulk resistivity, ρ, has been derived as,

$$\rho = 2\pi a \frac{P}{I}, \qquad (6$$

where a is the probe spacing. Because of concerns regarding possible polarization of the concrete, alternating rather than direct current is normally employed. Also, the probe tips are moistened wood in order to minimize contact resistance. Issues regarding concrete non-homogeneity are minimized by averaging multiple readings. The FDOT has developed a standard method for resistivity measurements on concrete.[52] Classification of concretes into five categories depending on the resistivity has been proposed, as indicated in Table IV-1. A concern in the case of field measurements, however, is that reinforcing steel in the potential/current field of the probes can short-circuit the cement paste conduction path, in which case an incorrect low resistivity reading may result.

V. EFFECT OF HIGH ALKALINITY ON ENGINEERING PROPERTIES OF CONCRETE

Although the effects of high alkalinity upon cement hydration and microstructure have been studied,[53,54,55] resultant changes in the engineering properties of concrete are not fully understood. Enhancement of alkali by addition of NaOH to mix water and exposure of concrete to alkaline solutions have been the preferred methods for accelerating ASR.[56] However, some studies have

indicated that such treatments do not result in the expected increase of [OH^-] pore water. Irrespective of this, NaOH admixing is considered more practical than comparing cements with different alkali content and composition; and it continues to be widely used.[57] Smaoui et al.[55] concluded that addition of alkali in the form of NaOH causes a reduction of compressive, splitting tensile, and flexure strength of concrete because a more porous cement paste results, although the nature of the hydrates apparently remains the same. It has also been shown that low-alkali concretes undergo less shrinkage than high-alkali ones, even if both are based upon the same w/cm.[53] Another investigation found that addition of alkali generated a hydration rate increase during the first hours of setting but that this subsequently moderated.[58] As noted above, previous FDOT sponsored research has shown that elevated cement alkalinity increases C_T and, hence, the time for reinforcing steel depassivation and onset of active corrosion.[5,6,7,8]

Table IV-1: Concrete permeability classifications based on resistivity.[52]

Concrete Ion Permeability	Resistivity, kOhm·cm
High	> 12
Moderate	12 – 21
Low	21 – 37
Very low	37 – 254
Negligible	< 254

VI. PROJECT MORTARS AND CONCRETES

Mix Design

General: To accomplish the overall project objective of evaluating use of high alkalinity cements (HACs) in concrete for bridge construction in Florida, a series of mortars were initially prepared in order to establish admix NaOH dosages for achieving target Na_2O_e values. Once these were defined, the results were extended to mix designs for concrete specimens.

Mortars and Pastes: Seven mortar mixes and two cementitious pastes were prepared using one of three Type II Portland cements, the first with Na_2O_e = 0.40, designated Na; a second with Na_2O_e = 0.54, designated F1; and the third with Na_2O_e = 1.00, designated HA. All of the mortars and one of the pastes had 19 percent cement replacement with fly ash (FA), and w/cm in all cases was 0.41. Fine aggregate was silica sand of fineness modulus 2.22 from a local source. Some series

were admixed with NaOH to elevate alkalinity. The mortar series designs were the same as for the concretes (see below) but without coarse aggregate. Thus, it was intended that the cement paste would be the same for all series (mortars and concretes). Individual mortar series were designated according to the materials and admixtures using the convention:

M#/XX/YY,

where,

M# number of the mortar/paste batch,
XX indicates the cement type (Na, F1, or HA), and
YY indicates the target Na_2O_e of the series.

Mix designs for the individual paste and mortar series are provided in Appendix A. Three 15.2 cm (6.0 in.) diameter by 30.5 cm (12.0 in.) high cylinders of each series were cast, as listed in Table VI-1.

Table VI-1: List of mortar and paste mixes for alkalinity determination.

Mix Designation	Target Na2Oe
M1/Na/0.4	0.4
M2/F1/0.6	0.6
M3/F1/1.0	1.0
M4/HA/1.0	1.0
M5/F1/1.2	1.2
M6/F1/1.5	1.5
M7/F1/1.5	1.5
Plain cement paste (C+W)	0.5
Cement paste with FA (C+FA)	0.5

Concretes: Specimens of this type were prepared using either the Type II Portland cement designated F1 (Na_2O_e = 0.54) or HA (Na_2O_e = 1.00) that were employed for the mortars (see above). In each case, the mix was based on the FDOT Class V design; and volume fraction of coarse aggregate and w/cm were maintained constant, the latter being 0.41 as for the mortars. Either NaOH or $LiNO_3$ (or both) was admixed in some cases, the purpose of the former being to elevate concrete pore water alkalinity and of the latter to inhibit any ASR. Most series contained fly ash at a cement replacement of 19 percent. Also, the concretes utilized the same silica sand as

the mortars (fineness modulus 2.22) and one of seven coarse aggregates (maximum nominal size 25 mm in most cases) which encompassed a range of ASR susceptibilities, as inferred in some cases by past experience in Florida bridge construction and in others by previous research studies. For all mixes, aggregates were saturated surface dry (SSD). Table VI-2 shows the general mix design, and Appendix B provides the design for each of the 55 series that were prepared. Individual series were designated according to the materials and admixtures using the convention,

##/XX/YY/ZZ/WW,

where,

is an identification number of the batch,
XX indicates the cement type (F1 or HA),
YY indicates the aggregate type as defined subsequently,
ZZ shows the target Na_2O_e of the series, and
WW is the dosage of lithium-based ASR preventing admixture (1 for the manufacturer's recommended dosage and 1.5 for 1.5 times the recommendation).

Series without FA had the added notation NF at the end.

Table VI-2: General mix design.

Material	Content, kg/m^3	Specific gravity	Volume, percent
Portland cement	363	3.15	11.5
Fly Ash	83	2.22	3.8
Water	178	1	17.9
Fine aggregate	607	2.65	22.9
Coarse aggregate	1100	2.45 - 2.70	40.9
Air	-	0.01	3
		cm content, kg/m^3	446
		w/cm	0.41

Cement, Fly Ash, and Aggregates

As noted above, three different Type II Portland cements were employed. The NA cement (Na_2O_e = 0.40) was provided by the Cemex Brooksville Plant in Brooksville, Florida, the F1 (Na_2O_e 0.54) by Eastern Portland Cement Corp. from Port Manatee, Florida (producer Volorantim Cimentos, Brazil), and the HA (Na_2O_e 1.00) by Hercules Cement Company. The fly

ash (FA) was Class F with a total alkali content (Na_20_e) of 2.03 percent and was supplied by Boral Material Technologies from the Crystal River Unit 4 and 5 source. Available alkalis (water soluble) were reported as 0.60 percent. As such, this was a low-alkali fly ash. Table VI-3 lists the composition for each cement and the FA.

Table VI-3: Chemical composition of cements and FA.

MaterialDesignation	SiO_2	Al_2O_3	Fe_2O_3	CaO	SO_3	Na_2O	K_2O	Na2Oe
F1	19.09	5.59	4.17	63.87	3.55	0.148	0.6	0.544
HA	20.08	4.95	3.05	61.98	4.2	0.278	1.15	1.037
NA	21.66	4.82	3.8	63.53	2.97	0.08	0.47	0.386
FA	52.82	21.9	6.06	4.92	0.27	0.284	1.49	1.267

Mix designs for the different concrete series were based upon coarse aggregates from seven different sources, as listed in Table VI-4. Three of these, designated FPL-1, FPL-2, and FPL-3, are Florida limestones from FDOT approved quarries about the state, whereas GG and NG are granites from out-of-State sources (Georgia and Nova Scotia, respectively) but are sometimes utilized for Florida bridge construction. Coarse aggregate H1 (Sprat limestone) is a fine grained argillaceous limestone that is characterized based upon previous research studies as being highly ASR reactive, and H2 (Sudbury gravel) has a complex silica/silicate lithology and is characterized as being moderately reactive.[25] Both are supplied by the Ontario Ministry of Transportation specifically for use as standards in ASR studies. For this reason, there is considerable information on the performance of these aggregates in concretes.

For each series, material contents were adjusted depending on properties of the specific aggregate and admixtures with the goal of achieving constant coarse aggregate volume percent in all cases. Table VI-5 lists the different combinations of cement type, target Na_2O_e, presence versus absence of FA, coarse aggregate type, and $LiNO_3$ dosage (if any). All batches with F1 cement with a target Na_2O_e of 1.0 or 1.2 were NaOH admixed. Lithium nitrate (Eucon Integral Arc manufactured by the Euclid Chemical Co.) was admixed either at the manufacturer's recommended dosage (designation 1) or at 150 percent of this recommendation (designation 1.5), as noted above. An air entraining agent (Air Extra, the Euclid Chemical Co.) was added to each concrete batch. Air content, slump, and unit weight were measured according to ASTM C231.[59] Table VI-5 lists the 55 individual batches that were prepared along with the materials involved for each, the date poured, specific gravity, slump, and air content.

Table VI-4. Designation and physical properties of aggregates.

Aggregate Type	Designation	Supplier	Pit Number	Specific Gravity	Absorption, percent	Generic Name	ASR Reactive
Silica sand	Silica sand	Florida Rock Industries Interlachen, FL	76-137	2.65	1.00	-	-
Florida limestone	FPL-1	Rinler Materials Miami, FL	87-089	2.46	3.26	Oolitic limerock #57 and #89	-
Florida limestone	FPL-2	Vulcan Materials, Brooksville, FL	08-005	2.43	3.50	Brooksville limerock #57 and S1B	-
Florida limestone	FPL-3	Aggrisource, LLC Naples, FL	2.24	-	9.00	-	-
Nova Scotia granite	NG	Martin Marietta Materials Mulgrave, NS	NS-315	2.65	0.76	Nova Scotia granite #57 and #89	-
Georgia granite	GG	Rinker Materials, Macon, GA	GA-178	2.65	0.76	Georgia granite #57 and #89	-
Sudbury gravel	H2	Ontario Ministry of Trans., Canada	Ontario, Canada	2.72	0.46	Sudbury gravel	Moderate
Sprat limestone	H1	Ontario Ministry of Trans., Canada	Near Ottawa	2.70	0.46	Sprat limestone	High

Table VI-5. List of concrete mixes.

Cement Type and Alkalinity	Coarse Aggregate							
	Mortar	FPL-1	FPL-2	FPL-3	GG	NG	H1	H2
NA	X							
F1	X	X	X	X	X	X	X	X
F1-Na2Oe=1.0	X	X	X	X	X	X	X	X
F1-Na2Oe=1.2	X	X	X	X	X	X	X	X
F1-Na2Oe=1.0-Li1	-	X	X	X	X	X	X	X
F1-Na2Oe=1.0 - Li1.5	-	X	-	-	X	X	X	-
F1-Na2Oe=1.2-Li1	-	X	X	X	X	X	X	X
F1-Na2Oe=1.2-Li1.5	-	X	-	-	X	X	X	-
HA	X	X	X	X	X	X	X	X
F1-NFA	-	X	-	-	-	-	X	X

Table VI-6: Materials and properties of individual concrete batches.

Batch No.	Coarse Aggr. Type	Cement Type	Target Na2Oe	LiNO3	Date Poured	Specific Gravity	Slump, mm	Air content, percent
0	FPL-1	F1	0.5	0	03/25/04	2.26	165	3.2
1	NG	F1	0.5	0	04/08/04	2.34	159	3.5
2	NG	HA	1.0	0	04/08/04	2.34	146	3.4
3	FPL-1	HA	1.0	0	04/13/04	2.26	140	3.5
4	GG	HA	1.0	0	04/15/04	2.37	184	3.6
5	GG	F1	0.5	0	04/15/04	2.37	191	3.2
6	F2	F1	0.5	0	04/22/04	2.27	121	3.6
7	F2	HA	1.0	0	04/22/04	2.27	146	3.6
8	FPL-1	F1	1.0	0	05/05/04	2.27	165	3.6
9	FPL-1	F1	1.2	0	05/05/04	2.26	165	3.9
10	FPL-1	F1	1.0	1	05/13/04	2.23	171	3.9
11	FPL-1	F1	1.2	1	05/13/04	2.26	133	3.8
12	FPL-1	F1	1.0	1.5	06/02/04	2.26	159	3.5
13	FPL-1	F1	1.2	1.5	06/02/04	2.26	140	3.7
14	GG	F1	1.0	0	06/04/04	2.36	178	4.0
15	GG	F1	1.2	0	06/04/04	2.38	146	3.7
16	GG	F1	1.0	1	06/08/04	2.37	165	4.0
17	GG	F1	1.0	1.5	06/10/04	2.42	140	3.0
18	GG	F1	1.2	1	06/10/04	2.42	114	3.0
19	GG	F1	1.2	1.5	06/10/04	2.40	146	3.3
20	NG	F1	1.0	0	06/15/04	2.34	146	3.4
21	NG	F1	1.2	0	06/15/04	2.36	121	3.0
22	NG	F1	1.0	1	06/17/04	2.34	152	3.7
23	NG	F1	1.0	1.5	06/17/04	2.34	171	3.5
24	NG	F1	1.2	1	06/22/04	2.34	171	3.6
25	NG	F1	1.2	1.5	06/22/04	2.36	121	3.0
26	FPL-2	F1	1.0	0	06/22/04	2.27	121	3.4
27	FPL-2	F1	1.2	0	06/24/04	2.26	133	3.7
28	FPL-2	F1	1.0	1	06/29/04	2.27	165	3.9
29	FPL-2	F1	1.2	1	06/29/04	2.27	146	3.5
30	H1	F1	0.5	0	07/01/04	2.35	133	3.5
31	H1	F1	1.0	0	07/01/04	2.34	152	4.0
32	H1	F1	1.2	0	07/13/04	2.38	146	3.4
33	H1	F1	1.0	1	07/06/04	2.35	146	3.2
34	H1	F1	1.0	1.5	07/08/04	2.38	159	3.0
35	H1	F1	1.2	1	07/08/04	2.38	159	3.2
36	H1	F1	1.2	1.5	07/13/04	2.37	127	3.4
37	H1	HA	1.0	0	07/13/04	2.37	133	3.0
38	H2	F1	0.5	0	07/15/04	2.37	95	3.0
39	H2	F1	1.0	0	07/15/04	2.37	127	3.7

Table VI-6: Materials and properties of individual concrete batches (continued).

Batch No.	Coarse Aggr. Type	Cement Type	Target Na2Oe	LiNO3	Date Poured	Specific Gravity	Slump, mm	Air content, percent
40	H2	F1	1.2	0	07/27/04	2.37	146	3.7
41	H2	F1	1.0	1	07/27/04	2.36	133	3.6
42	H2	F1	1.2	1	07/29/04	2.37	152	3.4
43	H2	HA	1.0	0	07/29/04	2.36	133	3.3
44	FPL-3	F1	0.5	0	08/05/04	2.21	64	3.5
45	FPL-3	F1	1.0	0	08/05/04	2.22	83	3.1
46	FPL-3	F1	1.2	0	08/10/04	2.22	70	3.2
47	FPL-3	F1	1.0	1	08/10/04	2.22	108	3.4
48	FPL-3	F1	1.2	1	08/12/04	2.21	102	3.5
49	FPL-3	HA	1.0	0	08/12/04	2.18	108	3.5
53*	FPL-1	F1	1.0	0	03/01/05	2.67	152	4.8
54*	H1	F1	1.0	0	03/01/05	2.80	191	4.5
55*	H2	F1	1.0	0	03/01/05	2.79	171	5.5

* No fly ash.

Mixing Procedure

Mortar batches were mixed in a 19 liter mixer during March 4-15, 2004 and concrete ones in a 57 liter mixer between April 8, 2004 and March 1, 2005. The mixing procedure was as follows:

1. Fine and coarse aggregates in the SSD state were introduced in the mixer with some of the water containing the air-entraining admixture.

2. The mixer was turned on for approximately one minute, after which cement and FA were added.

3. Water containing the rest of the admixtures was progressively introduced.

4. The mixing procedure continued for three minutes followed by a three-minute pause and another three minutes of mixing.

5. Tests for fresh concrete slump, unit weight, and air content were performed according to the applicable ASTM standard. Target ranges for concrete slump and air content were 0.075 to 0.150 m and 3 to 4 percent, respectively.

For each mortar mix, three 100 mm (4.0 in.) diameter by 200mm (8.0 in.) high cylinders were cast, as noted above. In the case of concrete mixtures, four 76 mm (3.0 in.) square by 300 (12.0 in.) mm long prisms and eight 100 mm (4.0 in.) diameter by 200 mm (8.0 in.) high cylinders were cast into molds in two and three layers, respectively, and consolidated by rodding according to ASTM C192.[60] A hardened steel stud was mounted in each end face of the steel prism molds to facilitate subsequent length measurements. Cylinders were sealed and prisms covered with plastic wrap for the initial 24 hours subsequent to casting. Concrete specimens were demolded after that time and maintained subsequently in sealed 21 liter plastic containers at 95 percent relative humidity and 38˚C. Mortar specimens were kept in similar containers but at 20˚C.

VII. EXPERIMENTS AND ANALYSES

Length Change

The length of concrete prisms was measured at 1, 7, 14, 28, 56, and 90 days and monthly thereafter. Specimens were stored in groups of three in 21 liter plastic containers with sealable lids, as shown in Figure VII-1, and maintained at 38˚C and 95 percent relative humidity. Figure VII-2 shows a photograph of the container storage room which had two space heaters and a fan that maintained temperature control. At specified times, individual containers were removed from the room and allowed to cool to ambient temperature over a 16-24 hour period.

Figure VII-1: Storage container and concrete prism specimens.

Figure VII-2: Storage room for concrete specimens.

Subsequently, the prisms were taken from their container; and the length of each was measured, first, using both a pair of calipers with a resolution of 0.02 mm and, second, a length comparator with a resolution of 0.002 mm, as shown in Figures VII-3 and VII-4, respectively. The procedure generally conformed to that specified by ASTM C1293.[61]

Petrographic Analyses

General

The overall objective of the petrographic examinations was to provide an assessment and characterization of, first, the individual bulk aggregates and, second, the effect of the one-year ASTM C1293 exposure on the mineralogy and microstructure of the concretes. It was expected that the high alkali contents of the concretes and the high temperature and humidity exposure would initiate ASR activity in those concretes that contained potentially reactive forms of SiO_2. The petrographic examinations were intended to identify the presence, source, and extent of any ASR activity in the concretes; and resulting information was used to assess the risk associated with use of high alkalinity cements in Florida bridge construction. ASR activity is a concern for

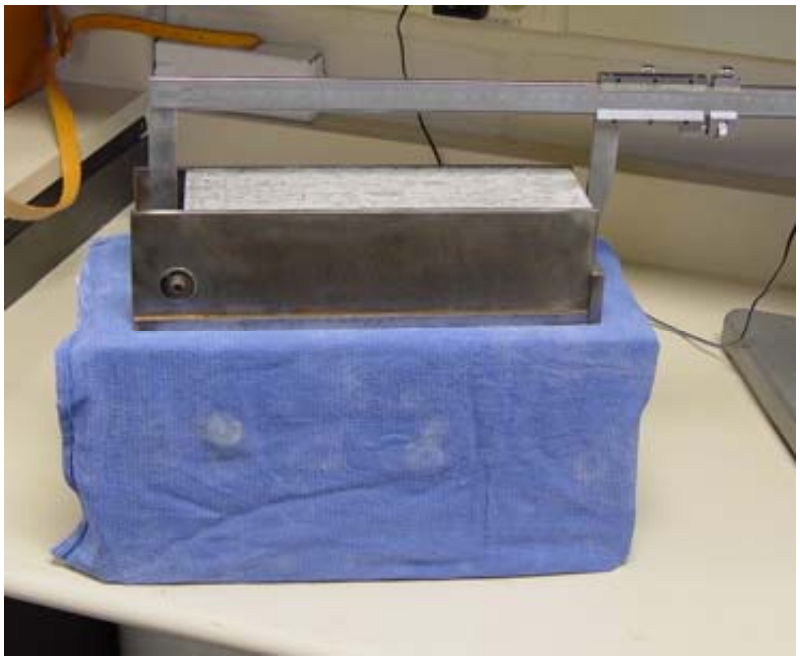

Figure VII-3: Photograph showing prism length measurement with calipers.

Figure VII-4: Photograph showing prism length measurement with digital comparator.

the concretes used in the present study due to the intentional elevation of the alkali content for purposes of suppressing initiation of embedded reinforcing steel corrosion.

Petrographic examinations were conducted on 1) bulk samples of the fine and coarse aggregates used in the study and 2) prism specimens following one year of ASTM C1293 exposure. Examination procedures and guidelines were in accord with ASTM C856,[62] ASTM C295,[63] and ASTM C294.[64]

Petrographic Examination of Fine and Coarse Aggregate Samples

General: The bulk aggregate samples were initially examined visually using a hand lens. This facilitated classification of the lithologic types of the different aggregates on the basis of 1) color, 2) texture, and 3) type and amount of porosity. Detailed examinations were then conducted on each identified lithologic phase to provide qualitative and semi-quantitative information on chemical and mineralogical content and information regarding microstructure.

Characterization of Aggregate Particle Color: Aggregate particles from the Florida limestones were classified simply on the basis of the four distinctive color groups found in samples from these, which collectively include off-white (termed white) and various shades of tan, gray, and orange.

Characterization of Textural Features: The three Florida limestones were described on the basis of their depositional texture. The terms used include "packstone," which describes a rock that is grain supported but which also contains a small percentage of micritic or sparite mud. In those instances where the limestone is mud-supported but contains more than ten percent grains, it is termed a "wackestone".

The term "micrite" describes a calcareous mud (often calcitic) that is present as a very fine grained matrix phase in many limestones. The individual grains in a micrite are ≤ 4 μm in size. The term "sparite" describes a calcareous mud in which the individual grain size is 4 to 10 μm.

The "grains" referred to in the above discussion are allochems, which is a collective term used to describe carbonate "aggregates" embedded in a calcareous mud matrix (micrite/sparite) in a limestone. In the Florida limestones that comprised the present study, the principal allochems include silt and sand sized intraclasts, pellets, and fossils and fossil fragments.

Characterization of Porosity: Porosity of the limestone aggregate samples was characterized using both reflected light microscopy on lapped surfaces and thin section transmitted light microscopy. The types of porosity encountered in the Florida limestones include 1) moldic, 2) vuggy, 3) interparticle, and 4) intraparticle. Each of these is described below.

Moldic porosity refers to pores formed in the limestones by the selective removal of a former grain in the rock, such as a fossil grain. The removal, typically occurring through a solution reaction, leaves behind a pore that is shaped like the grain that was removed.

Vuggy porosity is pores in any sedimentary rock (most typically limestones) resulting from selective dissolution of the rock are in this category. The pores thus formed are often lined with crystalline material, have irregular shapes, and a wide range in size.

Interparticle porosity refers to the void space that is present between individual allochems or grains in the rock. This type of porosity can be moderately large in size.

Intraparticle porosity occurs as voids within an individual allochem particle are in this category. These voids can be spherical or irregular in shape and are typically less than 100 μm in size.

Characterization of Limestone Aggregate Hardness: Relative to the global carbonate rock suite in Florida, the three limestone aggregate sources are on the high end of the hardness scale. Individual aggregate particles from the three sources were assessed as "soft", "moderately hard", or "hard". The degree of hardness was estimated on the basis of probes made with a steel needle on lapped surfaces of individual particles. A "soft" particle is one in which the surface could be easily penetrated with light hand pressure to produce powdered material. A "hard" particle, on the other hand, resisted penetration with moderate hand pressure.

Chemical Analysis: A measurement was made of the elemental chemical species present in the aggregate samples using energy dispersive x-ray spectroscopy (EDX) in conjunction with a scanning electron microscope (SEM) examination (Japan Electrooptical Lab (JEOL) Model JSM-820 microscope). These analyses were conducted at low magnifications (≤ 50X) on aggregate samples that had been pulverized to pass a 50 mesh sieve. The elemental data were converted to oxide analyses by assuming stoichiometric cation/oxygen ratios for various compounds. Quantitative chemical analyses using this EDX procedure were compared with measurements

made on the same materials using conventional quantitative chemical analyses procedures such as X-Ray Fluorescence. These chemical analyses were made on individual aggregate particles that were selected on the basis of color, hardness, and microstructural features representative of the bulk sample.

X-Ray Diffraction (XRD) Examinations: This method provided qualitative and semi-quantitative information on the crystalline phases present in a material. For this examination, samples of the various lithologic species identified in the preliminary examination were pulverized in a mortar and pestle to pass a 200 mesh sieve.

Thin Section Examinations: Standard 25 to 30 μm thin sections of fine and coarse aggregate samples were prepared for examination using an Olympus CX-31 polarizing optical microscope at magnifications from 40 to 400X. This provided information on 1) identification of mineral phases and allochems, 2) shape and distribution of the mineral phases and allochems, and 3) microstructural features, including aspects of porosity and the nature and condition of grain boundaries.

Research dating to the 1940's has identified the various forms of silica (SiO_2) that are potentially alkali-silica reactive. They include microcrystalline quartz (particles less than 20 μm in size), chert, chalcedony, opal, tridymite, and cristobalite. Also included is crystalline quartz that has crystal lattice defects or is in a strained condition as a result of exposure to metamorphic activity. So-called strained quartz can include particles that are medium to coarsely crystalline. Rocks containing large strained quartz particles such as these tend to be very slowly expansively reactive. The examination of rock particles in the polarizing microscope in thin sections can verify the presence and distribution of any of these SiO_2 minerals. In addition, strained quartz grains exhibit unique optical behavior in polarizing microscope examinations that confirms their presence as well (this is referred to as undulatory extinction in which the extinction front moves through the grain in a wavy manner as the microscope stage is rotated).

Various forms of SiO_2 and silicates are present as mineral phases in all seven of the coarse aggregates and the fine aggregate used in the present study. Included here are forms of SiO_2 that are known to be potentially deleteriously reactive including microcrystalline quartz, strained quartz, chert, and chalcedony. Thin section examinations were used to characterize the silica

minerals in the aggregates from the point of view of 1) mineral type, 2) grain size, 3) abundance, 4) extinction behavior, and 5) distribution within the microstructure.

These examinations provided more detailed information on the mineralogical make-up of the aggregates; particularly with regard to ASR proneness of the siliceous aggregate components. In those instances where ASR activity was indicated by observations made on the concrete prism specimens, thin section examinations of the aggregates provided further verification of the presence and nature of this phenomenon in these concretes.

Petrographic Examination of the Concrete Prism Specimens

General: For each concrete series, one of the four prism specimens was removed from the ASTM C1293 test after one year and subjected to a detailed petrographic examination. The procedures included 1) reflected light microscopy and 2) scanning electron microscopy (SEM) in conjuction with EDX.

Reflected Light Microscopy: Reflected light microscopic examinations were made using a stereomicroscope at magnifications of 10 to 100X on 1) molded surfaces of the prisms as-cast, 2) fracture surfaces, 3) saw-cut surfaces, and 4) lapped surfaces. The fracture surfaces included 1) fractures that were formed in prisms due to exposure and 2) fractures that were intentionally created.

Surfaces for lapping (polishing) were created by diamond saw-cutting perpendicular to a cast prism face. Saw-cut surfaces were lapped according to the procedure described in ASTM C856.[62] At least 1,300 cm^2 of concrete prism surface were examined.

The stereomicroscopic examinations provide opportunities for 1) further characterization of the aggregates in the concretes, 2) observation, identification, and collection of exudate materials on the molded and cast prism surfaces, 3) observation and characterization of microstructural features indicative of ASR activity, and 4) observation and characterization of cracking distress in the prisms. Reflected light microscope examination also provided an opportunity to diagnose very early reaction activity that had not yet created distinctive microstructural features.

Scanning Electron Microscope Examinations and EDX Analyses: The SEM/EDX examinations were made on material collected from molded, lapped, and fresh fracture surfaces of prism

specimens during the reflected light microscopy examinations. The collected material, typically suspected of being a form of ASR product, was excavated from prism surfaces in areas of interest using steel probes. This material was collected 1) from fresh fracture surfaces of aggregate particles suspected of participation in ASR activity, 2) as exudate present as streaks and patches on lapped and molded concrete prism surfaces, and 3) as secondary deposits present on free surfaces in the concrete, such as surfaces of entrained and entrapped air voids. Results of elemental chemical analyses are reported as oxide constituent analyses by assuming stoichiometric cation/oxygen ratios for the oxides. This provided direct chemical verification of material that was suspected on the basis of optical microscope examinations as being ASR gel.

Alkalinity

Concrete alkalinity can be expressed either as weight percent of Na equivalent of unhydrated cement (Na_2O_e) or OH^- concentration in the pore solution, $[OH^-]_{pore}$. While some argue that all materials in the concrete should be taken into account to express alkalinity, no consensus has been reached, particularly in cases when a SCM is present. Consequently, Na_2O_e continues to serve as the most quoted indicator of concrete alkalinity.[19] Although a number of assumptions are involved in the Na_2O_e parameter, it is considered appropriate for studies of alkali effects on permeability and ASR reactivity since it reflects the effective concentration of ions available in concrete that can react with other compounds.

Assuming that all cement alkali enter the pore water, $[OH^-]_{pore}$ can be theoretically calculated from the cement Na_2O_e using the expression,[67]

$$[OH^-]_{pore} = \frac{C \cdot Na_2O_e \cdot h}{50M\rho}, \qquad (7$$

where,

C is the cement content of the mix in kg/m^3,
h is the degree of cement hydration,
M the molecular weight of Na_2O, and
ρ is the capillary porosity.

Hydroxyl concentration in the pore water is typically measured by titration with HCl of samples obtained by pore water expression (PWE),[65] in-situ leaching (ISL),[66] or ex-situ leaching (ESL).[67] The ESL method was used in this study by analyzing powder samples after 7, 28, and 500 days subsequent to mortar or concrete casting. In addition, PWE was performed at 550 days. The PWE method consisted of placing 200g of crushed concrete in a steel vessel and applying a pressure in the range of 200 to 500 MPa, at which water was expressed and collected with a syringe. Figure VII-5 shows a photograph of the test system. The expressed water was titrated for $[OH^-]$ in the same way as in the ESL method but with no subsequent adjustment for Ca^{2+} since its concentration in the actual pore water is negligible. Expression was performed at Purdue University with participation by personnel from this project.

Figure VII-5: Test system for concrete pore water expression.

Compressive Strength

Compressive strength of three cylinders of each concrete mix design was measured at 28 and 365 days according to ASTM C39.[68] For the 365 days measurements, one of the cylinders was unloaded after the maximum load was reached but before the specimen was completely crushed for the purpose of analyzing the type of fracture and further studying the possibility of ASR occurrence.

Flexural Strength

Four-point bend tests were performed on two concrete prisms of several mixes according to ASTM C78.[69] approximately two years after casting. The purpose was to assess any effects of ASR on concrete mechanical properties that might not be revealed from compression testing. Figure VII-6 shows a photograph of the experimental setup for these tests.

Figure VII-6: Photograph of the experimental setup for flexural strength tests.

Resistivity

Resistivity measurements were made on three cylinders of each mix (concretes and mortars) at approximately 14, 180, 360, and 500 days using a four-point Wenner probe and standardized procedures.[52] Specimen handling was essentially the same as for length change measurements (see above) except that cylinders rather than prisms were involved. The protocol consisted of 1) removing the 21 liter plastic container with the specimens of interest from the 38°C room and allowing it to cool overnight with the lid in-place so that saturation was maintained, 2) removing

individual specimens from the container the next day and measuring resistivity, and 3) returning specimens to the container, replacing the lid, and returning the container to the 38°C room. The meter was calibrated according to the manufacture's directions prior to making each set of measurements. Figure VII-7 shows a photograph of measurements being made on a concrete cylinder.

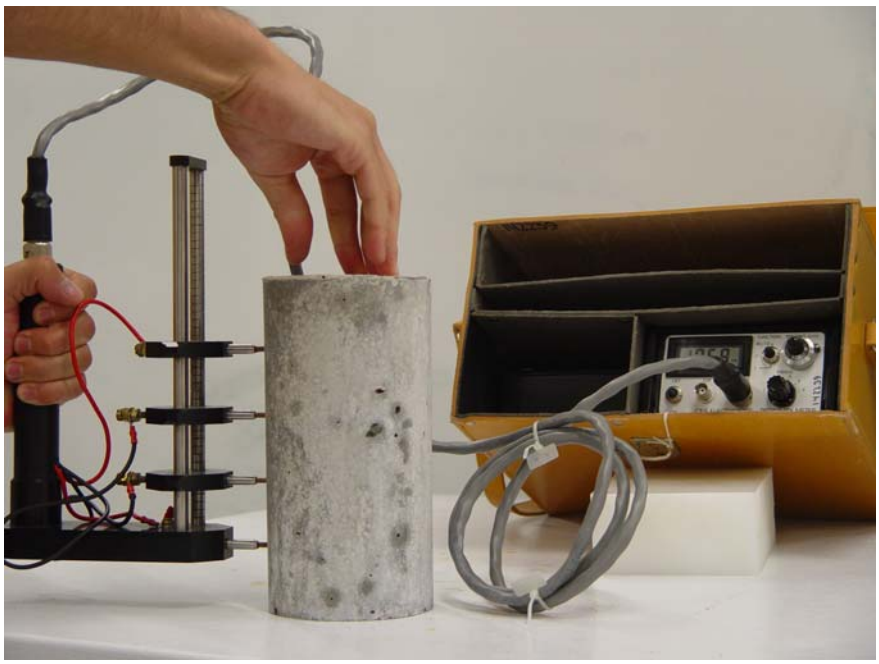

Figure VII-7: Photograph of four point probe resistivity measurement being made on a concrete cylinder.

VIII. EXPERIMENTAL RESULTS AND DISCUSSION

Effectiveness of Sodium Hydroxide for Enhancement of Concrete Alkalinity

Values for $[OH^-]_{pore}$ of the seven mortar and two cement paste mixes were initially estimated using Equation 7 based on the measured hardened material densities and porosities reported in the literature for similar mixes as listed in Table VIII-1 and shown in Figure VIII-1.[70,71] Results obtained by ESL at 7, 60, and 500 days and PWE at 550 days are shown in Table VIII-2; and Figure VIII-2 plots these versus Na_2O_e. Also shown are other results from the literature and theoretical values

Table VIII-1: Density of cement pastes and mortars.

Material	Density, g/cm^3
Cement paste	1.92
C+FA paste	1.84
Mortar	2.2

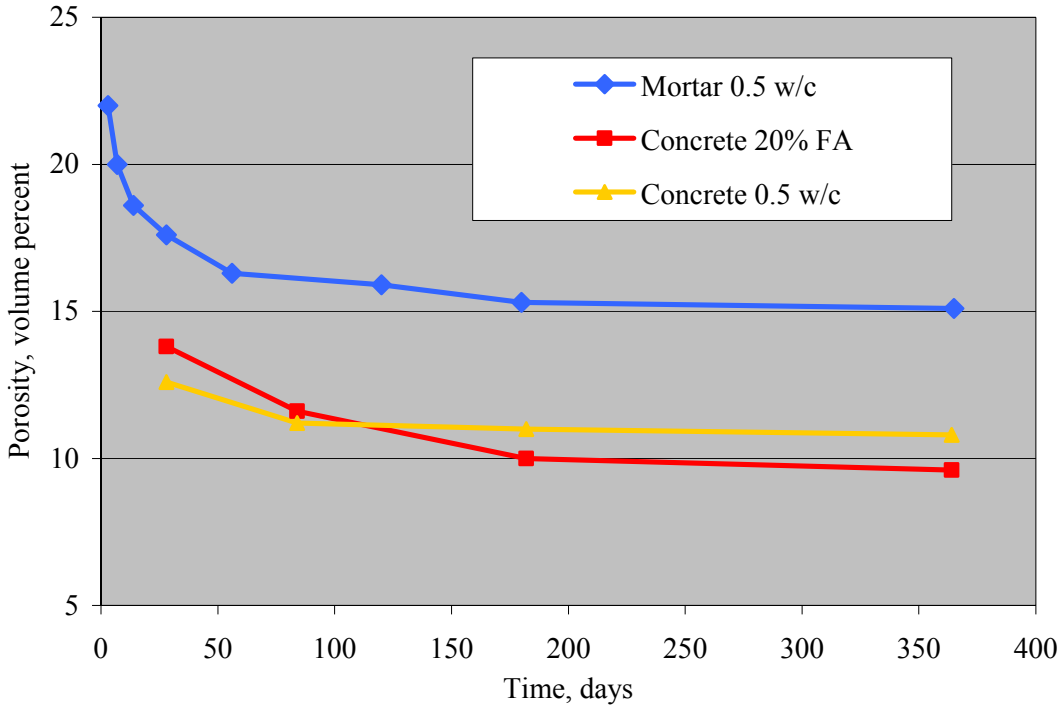

Figure VIII-1: Porosity of mortar and concrete.

Table VIII-2: Pore water $[OH^-]_{pore}$ of mortar and cement pastes.

Mortar	$[OH^-]_{pore, M}$			
	7 days	60 days	500 days	550 days PWE
C+W	0.62	0.65	0.55	0.33
C+FA	0.61	0.94	0.98	0.26
M1/NA/0.4	0.55	0.62	0.71	-
M2/F1/0.6	0.72	-	0.87	0.32
M3/F1/1.0	1.05	-	1.27	-
M4/F1/1.2	1.06	-	1.42	0.39
M5/F1/1.5	1.44	1.72	1.77	0.41
M6/F2/1.0	1.28	-	-	0.27
M7/HA/1.0	1.31	1.33	1.29	-

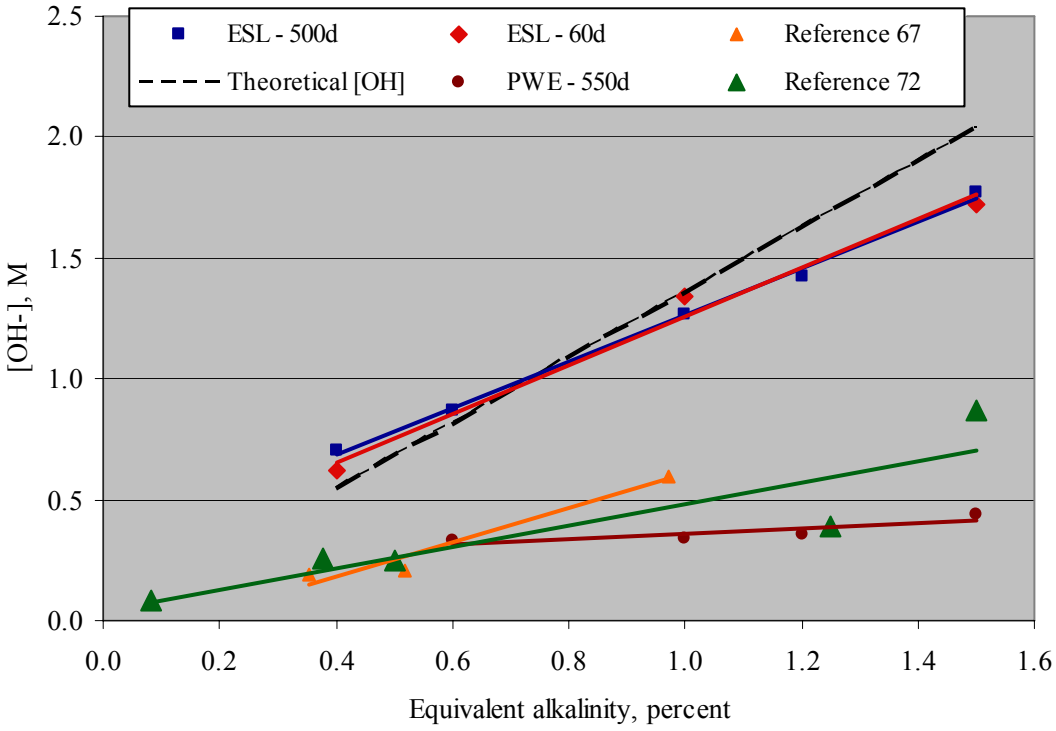

Figure VIII-2: Plot of hydroxyl concentration in pore solution versus cement Na_2O_e.

calculated using Equation 7. These indicate that the experimental, literature, and theoretical results exhibit a similar trend in that $[OH^-]_{pore}$ increases with increasing Na_2O_e. However, $[OH^-]_{pore}$ determined by ESL exceeded that of the other methods and was even greater than the theoretically calculation value, albeit by a relatively small amount, in those cases where Na_2O_e was below 1.0 percent. This may have been a consequence of the ESL method,[72] since during

any leaching process alkali that are trapped by cement hydrates may be released and thereby increase [OH^-] and result in an overestimation of this concentration. Equation 7 projects a direct proportionality between $[OH^-]_{pore}$ and cement content, such that, other factors being the same, pastes are calculated to have a relatively high $[OH^-]_{pore}$ followed by mortars and the concrete. Also, no change was observed in the ESL alkalinity measurements between 7 and 500 days, as would be expected as cement continues to hydrate and the pore water content reduced with a consequent increase in alkali concentration. While as much as 90 percent of the total cement alkali may be released into the pore solution and remain available, alkali from FA and other SCMs, though eventually released to the pore solution momentarily, may become entrapped by reaction with secondary hydrates and thereby contribute negatively to pore water alkalinity.[72,73,74,75] Finally, the PWE results indicate a relatively small increase in pore water alkalinity from addition of NaOH in the presence of FA, in accord with expected behavior for this type of mix.

Figure VIII-3 presents [OH^-] data for cementitious paste pore waters obtained in the present study by ESL and PWE and by ISL and PWE from previous research. The ESL result shows that $[OH^-]_{pore}$ of paste containing FA exceeded that of the plain cement pastes; however, the opposite

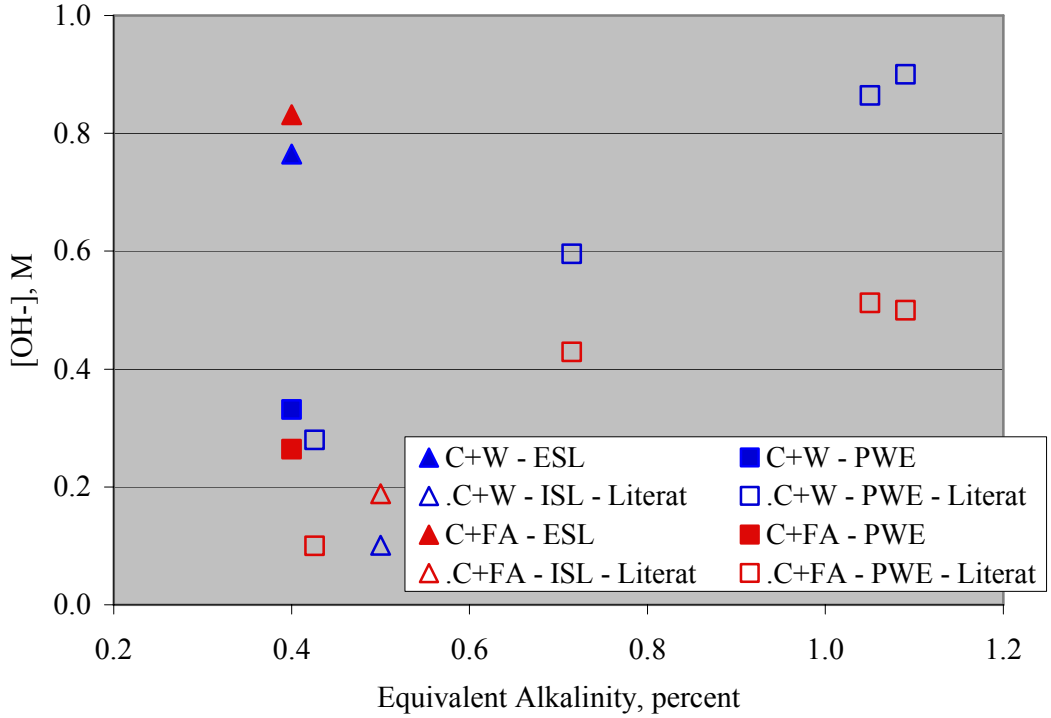

Figure VIII-3: Hydroxyl concentration of plain cement and FA pastes.[65,66,67]

occurred when the determination was by PWE. This was probably a consequence of the leaching issue addressed above and the Equation 7 limitation. Based upon these results, it was concluded that the target elevated Na_2O_e values were being achieved by the present mix designs and that these could be applied to the concretes.

Concrete Prism Specimen Length Change

General

Length of prisms of each of the 55 concrete series (Table VI-6) was measured at times up to two years and normalized relative to the initial length to provide a measure of length change. The results were organized according to coarse aggregate type. In each case, results from the study by Fourier and Malhotra[25] for concrete with a moderately ASR reactive siliceous/argillaceous coarse aggregate and no FA are shown for comparison.

Coarse Aggregate FPL-1

Figure VIII-4 shows the average length change versus time for the different concrete series with this aggregate, and Table VIII-3 lists expansions at one and two years of exposure. Prisms

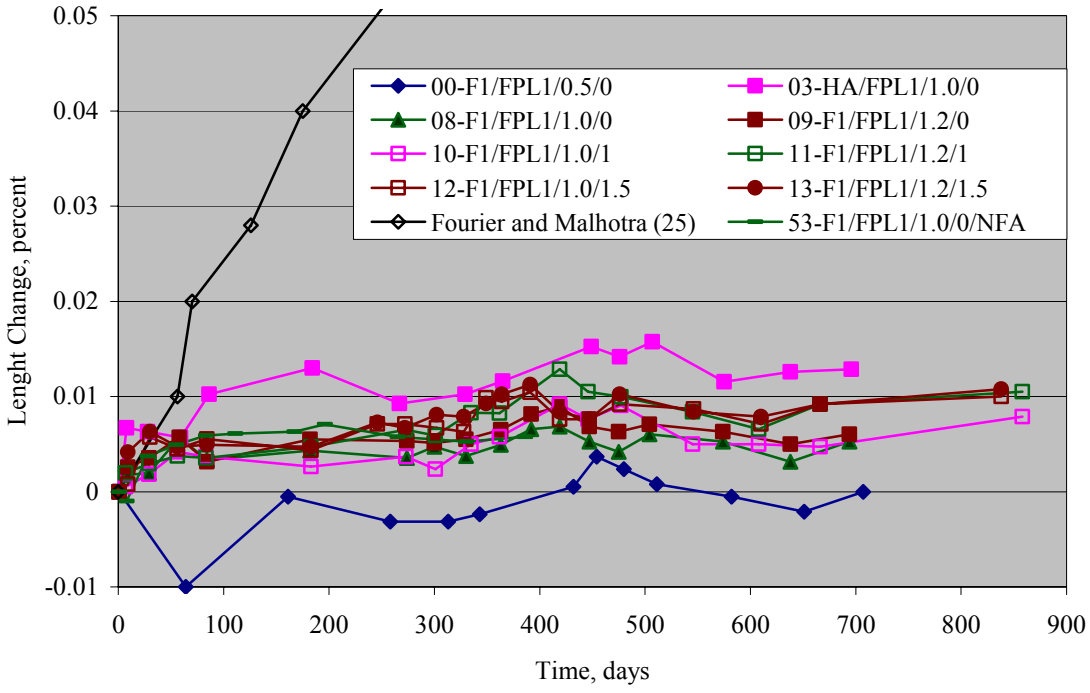

Figure VIII-4: Length change of specimens containing coarse aggregate FPL-1.

Table VIII-3: Listing of concrete series with FPL-1 coarse aggregate and length change after one and two years.

Concrete Series No.	Cement Type	Na20e, percent	LiNO3 Dosage	Expansion, percent	
				One Year	Two Years
0	F1	0.5	0	-0.0024	-0.0021
3	HA	1.0	0	0.0116	0.0129
8	F1	1.0	0	0.0049	0.0053
53*	F1	1.0	0	0.0058	-
9	F1	1.2	0	0.0065	0.006
10	F1	1.0	1	0.0058	0.0047
11	F1	1.2	1	0.0083	0.0092
12	F1	1.0	1.5	0.0095	0.0092
13	F1	1.2	1.5	0.0102	0.0092

* Year two data not yet available.

with Na_2O_e = 0.5 exhibited contractions (average 0.0024 percent at one year and 0.0021 percent at year two). For all other FA specimens the average one year expansion was 0.0083±.0038 percent and for the second year 0.0088±0.0040 percent. As such, expansions for each series were relatively modest, as were variations between the different series, the latter probably being within the range of normal measurement scatter. In most cases, no significant length change occurred between years one and two. The one concrete series without FA (series 53) had an average one year expansion comparable to the series with FA.

Coarse Aggregate FPL-2

Figure VIII-5 shows length change versus time for the concrete series with FPL-2 coarse aggregate, and Table VIII-4 lists expansions at one and two years of exposure. Prisms with Na_2O_e = 0.5 had essentially no length change (average 0.0000 percent at one year and 0.0002 percent at year two). For all other specimens the average one year expansion was 0.0127±0.0025 percent and for the second year 0.0176±0.0060 percent. Expansions for the HAC cement series exceeded those with the F1 (Na_2O_e = 1.0 and no $LiNO_3$) over much of the monitoring period, although they remained will below the ASTM C1293 threshold (0.04 percent after one year). Length increases between years one and two were nil or modest except for concrete series 27 (Na_2O_e = 1.2 and no $LiNO_3$), which had a 55 percent increase.

Coarse Aggregate FPL-3

Figure VIII-6 presents length change versus time data for the concrete series with FPL-3

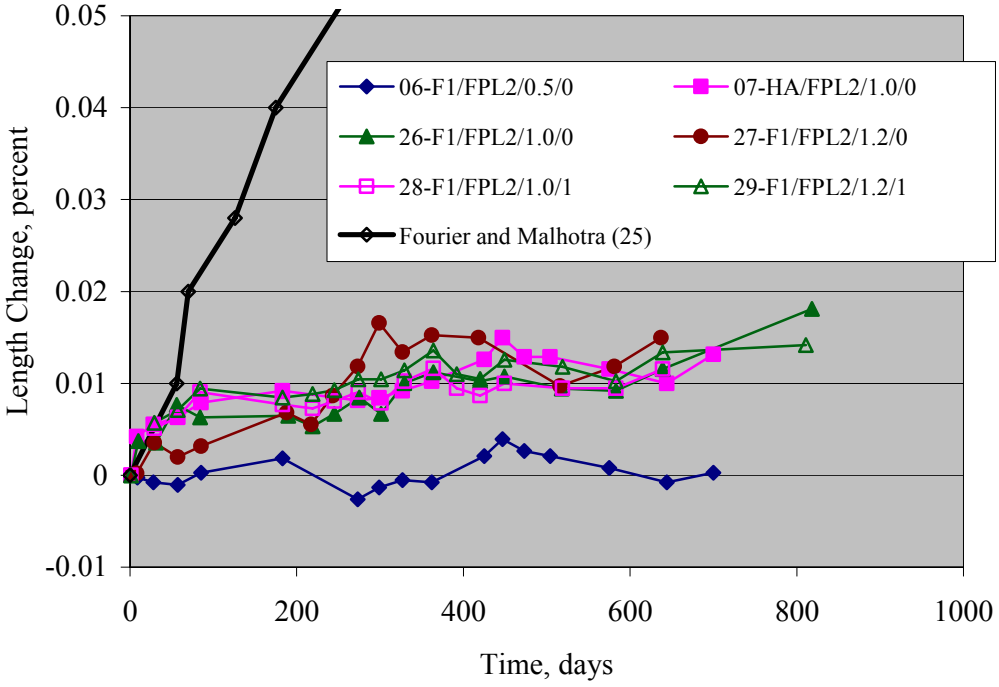

Figure VIII-5: Length change of specimens containing coarse aggregate FPL-2.

Table VIII-4: Listing of concrete series with FPL-2 coarse aggregate and length change after one and two years.

Concrete Series No.	Cement Type	Na_2O_e, percent	$LiNO_3$ Dosage	Expansion, percent	
				One Year	Two Years
06	F1	0.5	0	0	0.0002
07	HA	1.0	0	0.0102	0.0130
26	F1	1.0	0	0.0112	0.0115
27	F1	1.2	0	0.0152	0.0236
28	F1	1.0	1	0.0116	0.0116
29	F1	1.2	1	0.0136	0.0134

coarse aggregate, and Table VIII-5 lists expansions at one and two years of exposure. This shows that prisms with Na_2O_e = 0.5 had some length increase (average 0.0020 percent at one year and 0.0008 percent at year two). For all other specimens the average one year expansion was 0.0099±0.0010 percent and for the second year 0.0105±0.0029 percent. As for FPL-1 and FPL-2, expansions remained will below the ASTM C1293 threshold (0.04 percent after one year). Length increases between years one and two, where these occurred, were modest which suggests that the reaction that gave rise to expansions during year one had subsided or ceased.

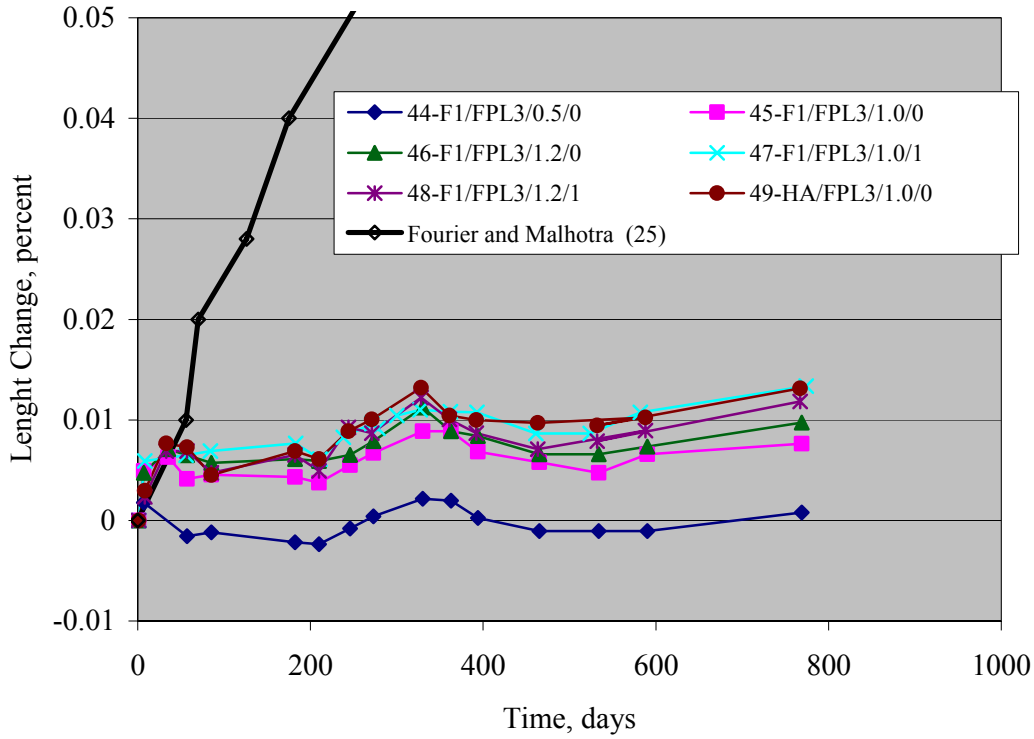

Figure VIII-6: Length change of specimens containing coarse aggregate FPL-3.

Table VIII-5: Listing of concrete series with FPL-3 coarse aggregate and length change after one and two years.

Concrete Series No.	Cement Type	Na_2O_e, percent	$LiNO_3$ Dosage	Expansion, percent	
				One Year	Two Years
44	F1	0.5	0	0.0020	0.0008
45	F1	1.0	0	0.0089	0.0076
46	F1	1.2	0	0.0089	0.0097
47	F1	1.0	1	0.0108	0.0134
48	F1	1.2	1	0.0100	0.0118
49	HA	1.0	0	0.0104	0.0131

Coarse Aggregate GG

Figure VIII-7 shows length change versus time data for the concrete series with GG coarse aggregate, and Table VIII-6 lists expansions at one and two years exposure. Prisms with Na_2O_e = 0.5 showed some length increase at year one (average 0.0047 percent) but a small contraction (0.0005 percent) after year 2. For all other specimens, the average one year expansion was 0.0100±0.0059 percent and for the second year 0.0188±0.0101 percent. The highest average

expansion (0.0289 percent for concrete series 15 (Na_2O_e = 1.2 and no $LiNO_3$) after two years) was 72 percent of the ASTM C1293 threshold (0.04 percent after one year). The average prism length increase and rate of increase were greater for the HAC series (Na_2O_e = 1.0 and no $LiNO_3$) than any of the other series beyond about 400 days.

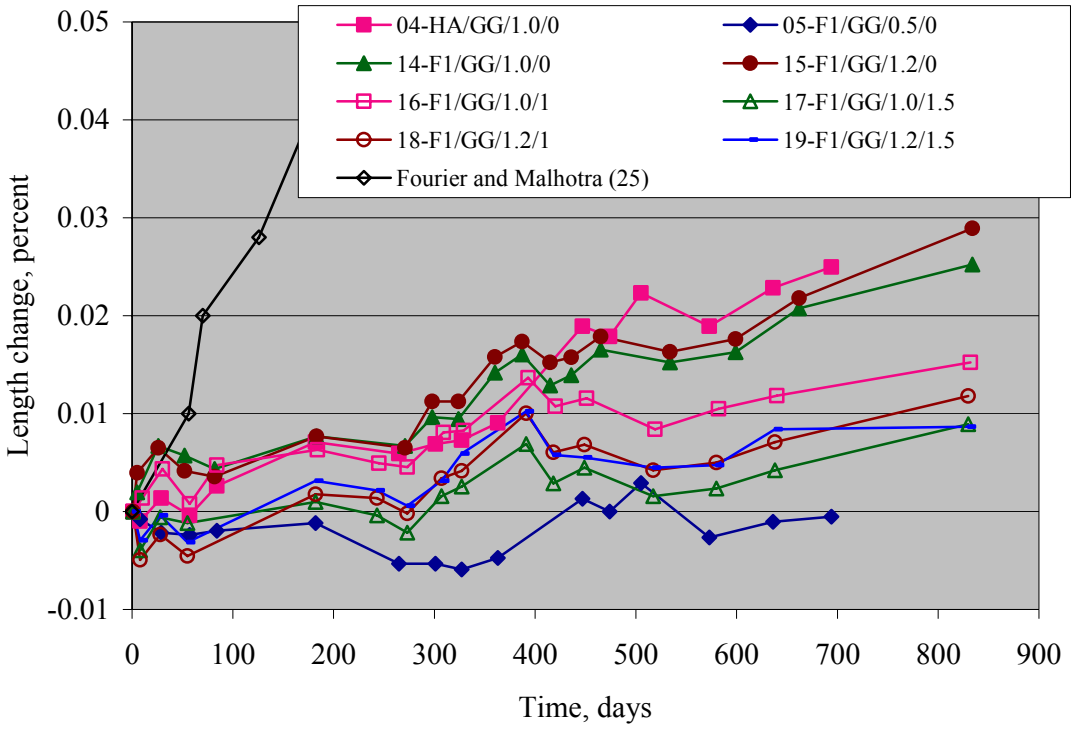

Figure VIII-7: Length change of specimens containing coarse aggregate GG.

Table VIII-6: Listing of concrete series with GG coarse aggregate and length change after one and two years.

Concrete Series No.	Cement Type	Na_2O_e, percent	$LiNO_3$ Dosage	Expansion, percent	
				One Year	Two Years
04	HA	1.0	0	0.0091	0.025
05	F1	0.5	0	0.0047	-0.0005
14	F1	1.0	0	0.0142	0.0252
15	F1	1.2	0	0.0158	0.0289
16	F1	1.0	1	0.0083	0.0152
17	F1	1.0	1.5	0.0026	0.0089
18	F1	1.2	1	0.0041	0.0118
19	F1	1.2	1.5	0.0059	0.0087

Coarse Aggregate NG

Figure VIII-8 shows length change versus time data for the concrete series with NG coarse aggregate, and Table VIII-7 lists expansions after one and two years exposure. Prisms with Na_2O_e = 0.5 had contracted at the end of both years one and two (average expansions -0.0008 and -0.0003 percent, respectively). For all other specimens, the average one year expansion was

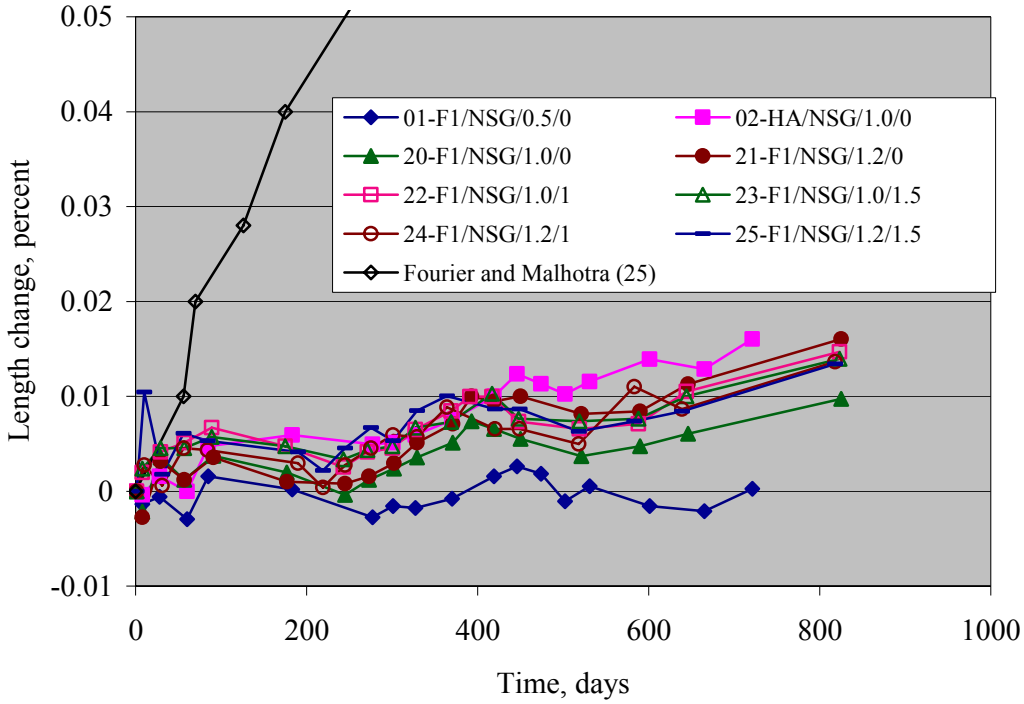

Figure VIII-8: Length change of specimens containing coarse aggregate NG.

Table VIII-7: Listing of concrete series with NG coarse aggregate and length change after one and two years.

Concrete Series No.	Cement Type	Na_2O_e, percent	$LiNO_3$ Dosage	Expansion, percent	
				One Year	Two Years
01	F1	0.5	0	-0.0008	-0.0003
02	HA	1.0	0	0.0075	0.0160
20	F1	1.0	0	0.0051	0.0097
21	F1	1.2	0	0.0071	0.0160
22	F1	1.0	1	0.0085	0.0192
23	F1	1.0	1.5	0.0073	0.0163
24	F1	1.2	1	0.0089	0.0137
25	F1	1.2	1.5	0.0100	0.0134

0.0076±0.0025 percent and for the second year 0.0145±0.0048 percent. The highest average expansion (0.0192 percent for concrete series 22 (Na_2O_e = 1.0 and no $LiNO_3$) after two years) was 48 percent of the ASTM C1293 threshold (0.04 percent after one year). The average prism rate of length increase and rate of increase for the HAC cement (series 02) was higher than for the other series beyond year one.

Coarse Aggregate H1

Figure VIII-9 shows length change versus time data for the concrete series with H1 coarse aggregate, and Table VIII-8 lists expansions at one and two years exposure. All prisms exhibited expansions with the Na_2O_e = 0.5 ones having the least of this group (one and two year values of 0.0018 and 0.0034 percent, respectively). For all other specimens with FA the average one year expansion was 0.0445±0.0352 percent and for the second year 0.0475±0.0318 percent. The highest average expansion for these (0.0801 percent for concrete series 32 (Na_2O_e = 1.2 and no $LiNO_3$) after two years) exceeded the ASTM C1293 threshold (0.04 percent after one year) by a factor of two. For the specimens without FA, the average one year expansion was over nine times greater than the ASTM C1293 threshold. Also, expansion of all specimens of this series continued between years one and two.

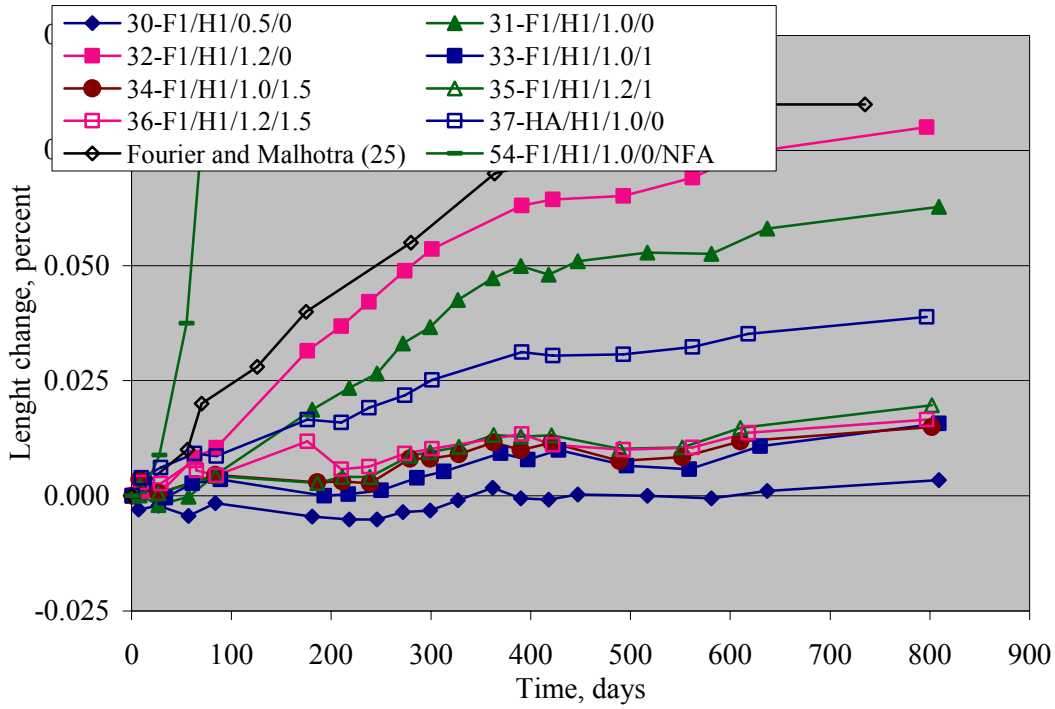

Figure VIII-9: Length change of specimens containing coarse aggregate H1.

Table VIII-8: Listing of concrete series with H1 coarse aggregate and length change after one and two years.

Concrete Series No.	Cement Type	Na_2O_e, percent	$LiNO_3$ Dosage	Expansion, percent	
				One Year	Two Years
30	F1	0.5	0	0.0018	0.0034
31	F1	1.0	0	0.0473	0.0688
32	F1	1.2	0	0.0796	0.0801
33	F1	1.0	1	0.0093	0.0157
34	F1	1.0	1.5	0.0116	0.0149
35	F1	1.2	1	0.0132	0.0176
36	F1	1.2	1.5	0.0142	0.0166
37	HA	1.0	0	0.0322	0.0389
54*	F1	1.0	0	0.346	-

* Year two data not yet available.

Coarse Aggregate H2

Figure VIII-10 shows length change versus time data for the concrete series with H2 coarse aggregate, and Table VIII-9 lists expansions at one and two years exposure. All prisms exhibited expansions, with concrete series 41 (41/F1/H2/1.0/1) having the least at one year (0.0045 percent

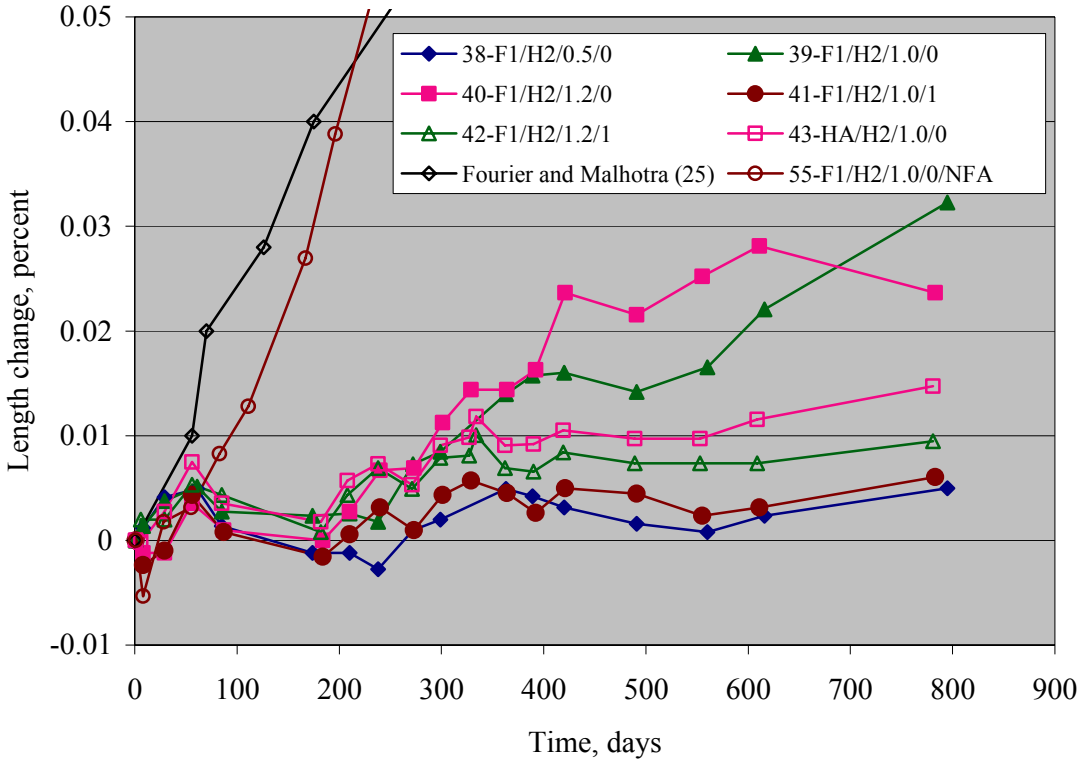

Figure VIII-10: Length change of specimens containing coarse aggregate H2.

which is slightly less than the Na_2O_e = 0.5 series) but the Na_2O_e = 0.5 series having the least expansion at two years (0.0050 percent). For all other specimens with FA, the average one year expansion was 0.0095±0.0050 percent and for the second year 0.0192±0.0131 percent. The highest average expansion of these (0.0323 percent for concrete series 39 (Na_2O_e = 1.0 and no $LiNO_3$) after two years) is 81 percent of the ASTM C1293 threshold (0.04 percent after one year). Also, the average prism length for all specimens of this series with FA increased between years one and two. The greatest expansion occurred for series 54 (no FA) with the average being over twice the ASTM C1293 threshold.

Table VIII-9: Listing of concrete series with H2 coarse aggregate and length change after one and two years.

Concrete Series No.	Cement Type	Na_2O_e, percent	$LiNO_3$ Dosage	Expansion, percent	
				One Year	Two Years
38	F1	0.5	0	0.0049	0.0050
39	F1	1.0	0	0.0139	0.0323
40	F1	1.2	0	0.0144	0.0240
41	F1	1.0	1	0.0045	0.0060
42	F1	1.2	1	0.0069	0.0095
43	HA	1.0	0	0.0090	0.0147
55*	F1	1.0	0	0.0852	-

* Year two data not yet available.

From these results, the following conclusions were reached:

1. Fly ash in the present specimens had a relatively strong inhibiting effect upon prism expansion, as seen by comparing, first, data for non-fly ash specimens (Figures VIII-4, VIII-9, and VIII-10 and Tables VIII-3, VIII-8, and VIII-9) with comparable concrete series with FA from these same figures and tables and, second, the Fournier and Malhotra data[25] with specimens without FA in Figures VIII-4 to VIII-10.

2. Specimens with the Na_2O_e = 0.5 cement had the lowest expansions in almost all cases. For some concrete series (FPL-1, GG, and NG, these concretes contracted.

3. All of the Na_2O_e = 1.0 and 1.2 specimens exhibited expansions. For specimens with coarse aggregate H1, length increase for the Na_2O_e = 1.2 series was greater than for Na_2O_e = 1.0 (Figure VIII-9 and Table VIII-8); however, for other series expansion of

concretes with these two Na_2O_e levels are comparable. The general trend is one where expansion was greatest during the initial year but moderated thereafter. However, prism length for all specimens of these series continued to increase between years one and two.

4. Only one specimen series 32-F1/H1/1.2/0 had a one year expansion that exceeded the ASTM C1293 criterion of 0.04 percent (non-fly ash specimens excluded), although series 31-F1/H1/1.0/0 expansion was close to this value. However, as discussed in the subsequent section (Petrographic Analyses), some of the concrete series with expansions below threshold are probably not suitable for long-term structural service.

5. For most series with Na_2O_e = 1.0 and 1.2, presence of admixed $LiNO_3$ reduced expansion. The effect was most significant for the H1 and H2 coarse aggregates, which exhibited the largest expansions and was minimal or nil for series with relatively small expansions.

6. Generally, the concretes ranked according to the year two average expansion of Na_2O_e = 1.0 and 1.2 as (greatest to least expansion) H1 > H2 > GG > NG > FPL-2 > FPL-3 > FPL-1.

Accuracy of the length change measurements was verified as satisfactory according to the ASTM C1293 criterion. As such, the difference in expansion of any given specimen from the average of its group did not exceed 0.003 percent when the average was below 0.020 percent and was within 15 percent when the average was above 0.020 percent. Figure VIII-11 shows the average of the four length change measurements along with the maximum and minimum values (black markers) at the time of each measurement for mixes containing the H1 aggregate (Spratt Limestone).

The length change trends detailed above are best explained in terms of ASR being nil for the Na_2O_e = 0.5 cement and having occurred for the Na_2O_e = 1.0 and 1.2 ones. The basis for this is the known effect of elevated cement Na_2O_e as an ASR promoter and of FA and $LiNO_3$ as inhibitors. As noted above, three criteria must be met for ASR to occur: a) a reactive form of SiO_2 must be present, b) alkali ions must be available, and c) sufficient moisture must be present. Relatively few concrete aggregates are entirely void of SiO_2, and so most are susceptible to ASR activity to some degree. In this regard, most natural sands, nearly all gravels, and many

limestones have a SiO_2 component that includes reactive phases such as chert and strained crystalline quartz. Thus, given the widespread nature of potentially reactive forms of SiO_2 in natural aggregate sources, there is a potential for ASR activity in almost all concretes. However, ASR is not necessarily found because the alkali content of the concrete is sufficiently low. In other cases, ASR occurs; but because of the use of an ASR-preventing admixture or a SCM (or both), damage is not significant.

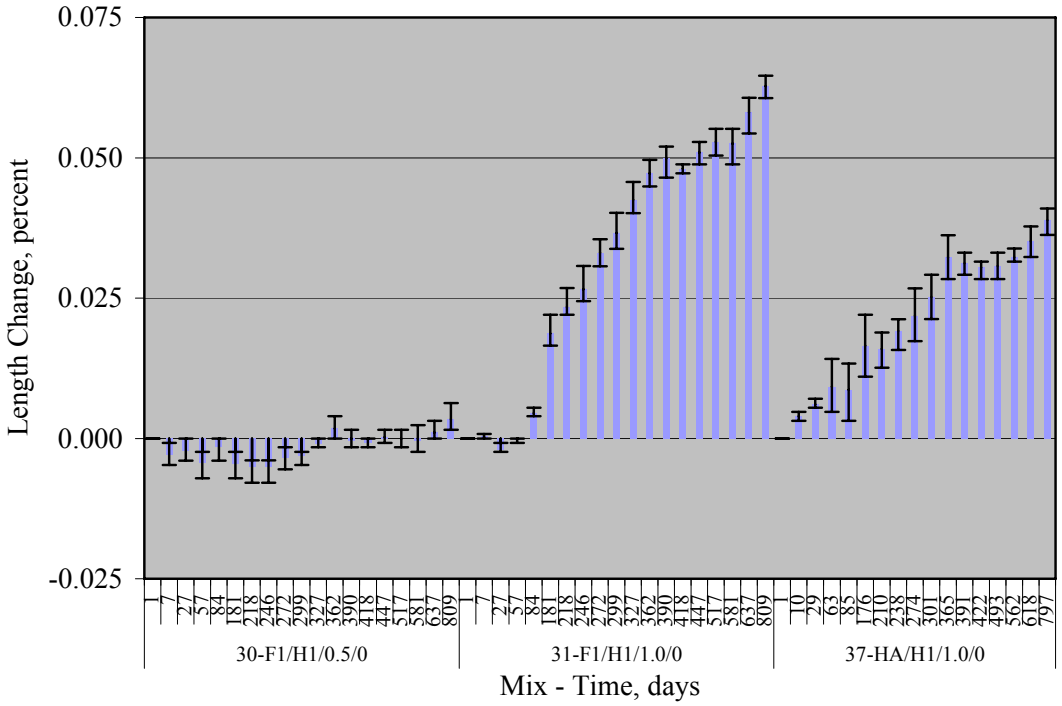

Figure VIII-11: Average expansion and range of length change at different times for three series containing H1 coarse aggregate.

As noted in ASTM C33, there is no general agreement between results from standardized tests that quantify ASR and long-term service durability.[76] To illustrate the difficulty in determining such a correlation, Figure VIII-12 shows the different trends followed by several of the present mixes with one year length changes in the range of 0.007-0.013 percent. Mix 14 expanded continuously and was considered ASR affected, whereas length change for mixes 03, 27, 36, and 46 appears to have stabilized after about one year. However, prisms of these latter four mixes exhibited cyclic behavior (periods of expansion and contraction), making it unclear as to whether or not ASR would be an issue in the long-term. Thus, interpretation of length change results should be complemented by not only how length change varies over time but also

microscope examination, first, to determine the extent of any cracking and, second, petrographic analysis to disclose other possible ASR-related indicators.

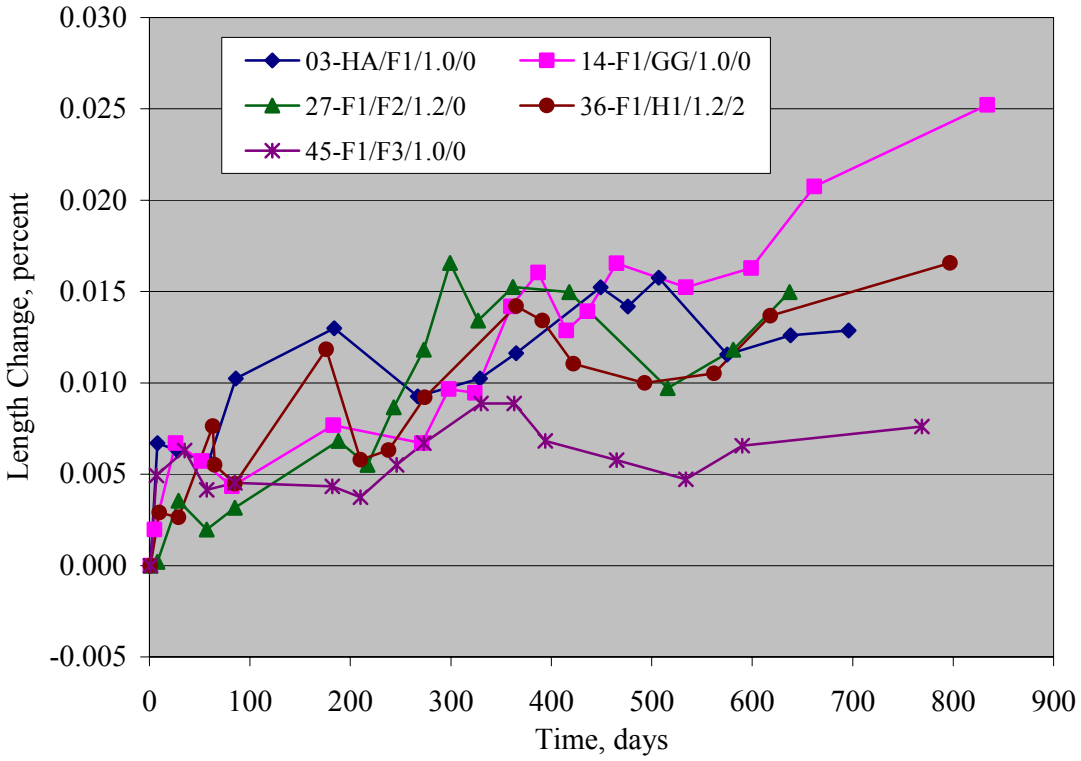

Figure VIII-12: Behavior of mixes with different aggregates and admixtures.

The long-term expansion for one concrete series was estimated utilizing the model represented by Equation 4. From the expansion data at 100 days, values for α, b, and τ_f were calculated and the expansion at 1,000 days projected. Table VIII-10 lists these results, and Figure VIII-13 graphically compares the calculated and experimentally measured expansion trend for series 54/F1/H1/1.0/0/NF and indicates good agreement between the two. The model projects continued expansion in the long-term but at a decreased rate.

On the basis of the above, consideration was given to rate of expansion between years one and two serving as an indicator as to whether or not significant ASR induced distress will occur in the long-term. This point is discussed in detail subsequently.

Table VIII-10: Calculated Equation 4 parameters and projected expansion at 1,000 days for different mixes.

Mix	τ_f	α	b	Expansion at 1000 Days, percent
54/F1H1/1.0/0/NoFA	28	0.369	0.010	0.369
15/F1/GG1.2/0	82	0.018	0.007	0.017
27/F1/F2/1.2/0	182	0.012	0.007	0.011
32/F1/H1/1.2/0	29	0.065	0.010	0.065
40/F1/H2/1.2/0	184	0.024	0.009	0.023

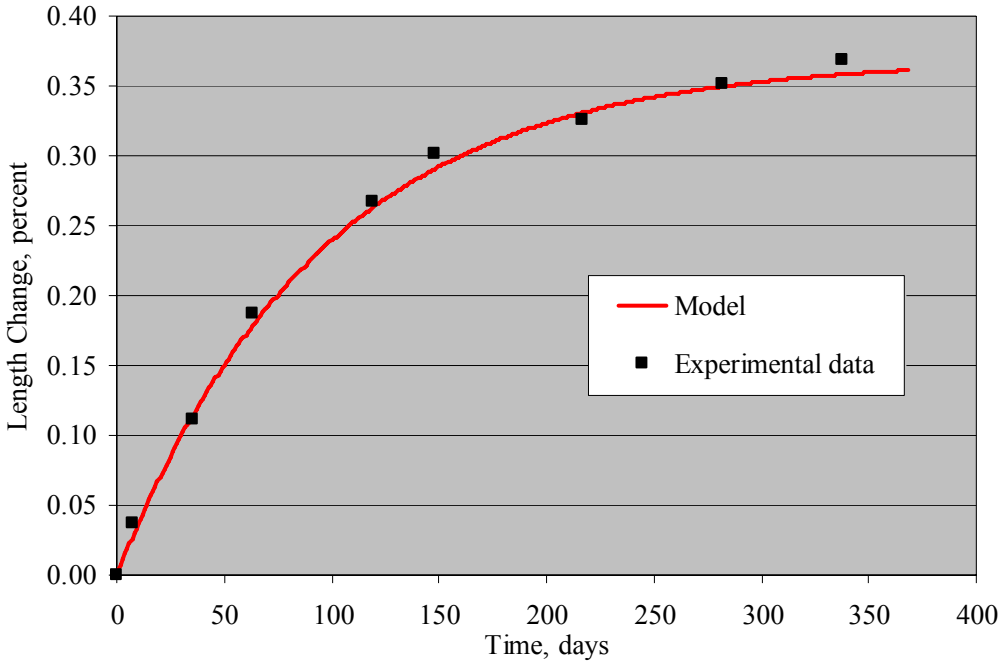

Figure VIII-13: Comparison of measured and calculated expansion for concrete series 54/F1/H1/1.0/0/NF specimens.

Petrographic Analyses – Silica Sand

As noted earlier, the fine aggregate used in the mortars and all of the concretes is a natural Florida silica sand. Crystalline quartz is the predominant component of the sand, with the majority of quartz particles ranging in size from 8 mesh (2.4 mm) to 100 mesh (0.15 mm). The crystalline quartz phase represents over 99 percent of the mineral phases passing an 8 mesh sieve and retained on a 100 mesh sieve. The minor and trace mineral phases in the sand include limestone particles (the most abundant), quartzites, mudstones, sandstones, feldspar, and magnetite. Most of the minor mineral phases were present as particles in the minus 4 mesh (4.8 mm) - plus 8 mesh (2.4 mm) size range. The fineness modulus of the sand is 2.22.

Although this is a crystalline quartz, 15 to 20 percent of the quartz particles showed some degree of undulatory extinction, which indicates that the quartz is strained and, therefore, may be susceptible to ASR activity. The majority of quartz particles showing this extinction behavior have a particle size in the 1.0 to 2.5 mm size range. Despite this condition, this Florida sand has no reported history of ASR activity in service.

Petrographic Analyses - Concrete Series with Coarse Aggregate FPL-1 (Florida Limestone, Source 1)

Physical Features: Lapped section views of concrete prism 9b are shown in Figure VIII-14. Enlarged views of the aggregate particles are shown in Figure VIII-15.

Color: The FPL-1 aggregate particles exhibit three distinctive colors: 1) off-white, 2) gray, and 3) tan. The overall makeup of the aggregate is approximately 90 percent white particles, 8 percent tan, and 2 percent gray. All three are identified in Figure VIII-14.

Shape and Angularity: The FPL-1 particles are sub-angular to angular, with a shape that tends from compact to platy.

Hardness: The great majority of particles of all three colors are moderately hard to hard.

Chemistry and Mineralogy: The two dominant mineral species in this rock are a major phase, calcite ($CaCO_3$), and a minor phase, crystalline quartz (SiO_2). There is also a low clay mineral content and trace amounts of plagioclase feldspar.

A representative white FPL-1 white aggregate particle was selected for an EDX chemical analysis. The results, presented in Table VIII-11, show a CaO content of 91.6 percent, a SiO_2 content of 7.2 percent, and trace amounts of MgO (probably as dolomite) and Al_2O_3. The XRD data show calcite as the major phase and crystalline quartz as the minor. Optical microscope examination revealed a similar texture and mineral content for the white and orange particles. Together the white and orange particles account for approximately 98 percent of the FPL-1 coarse aggregate.

The gray particles, which represent around two percent of the FPL-1 aggregate, show different mineral phases relative to the white/orange particles. The EDX analysis of a

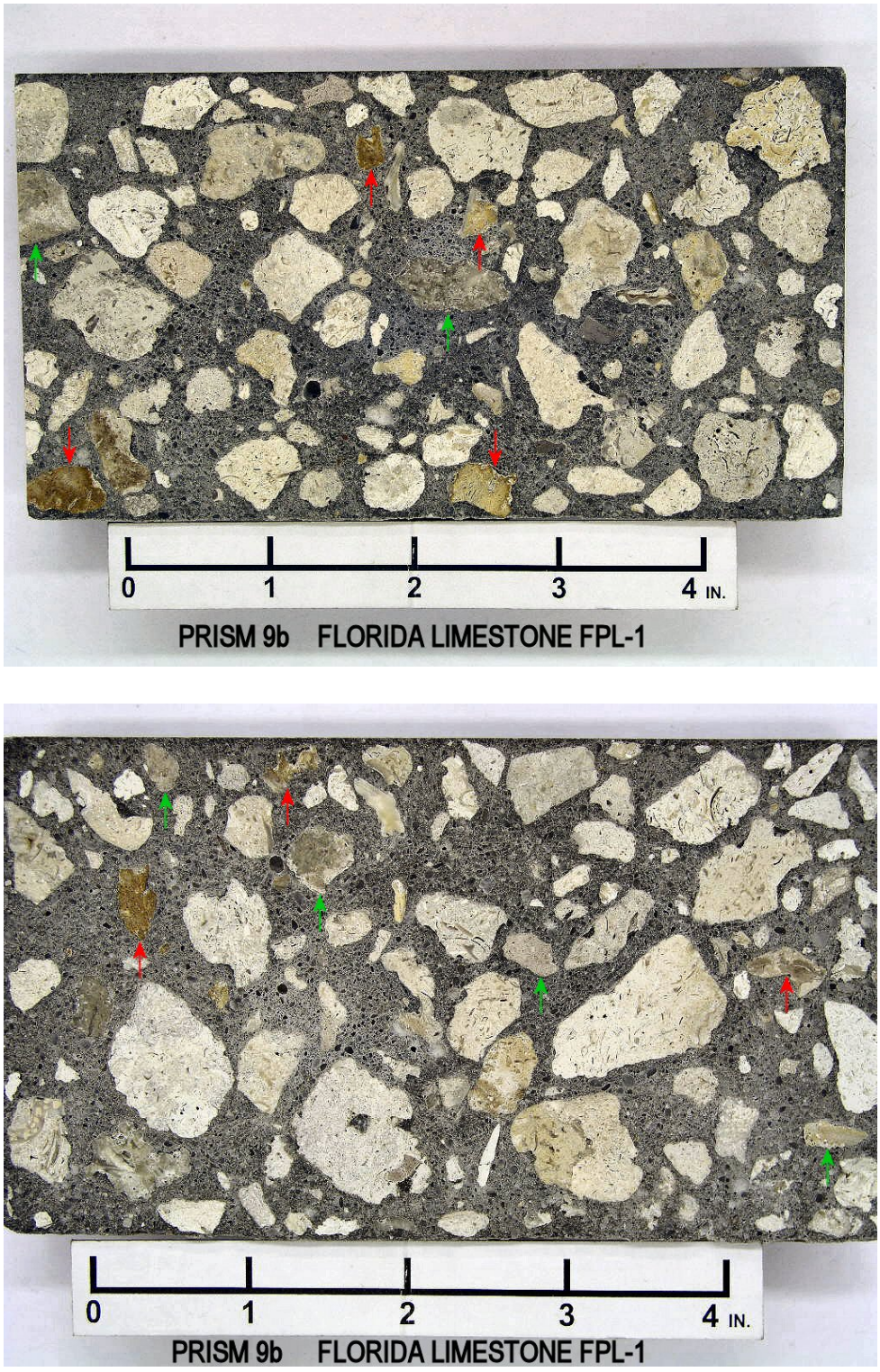

Figure VIII-14: Lapped section views of Prism 9b (09-F1/FPL-1/1.2/0). The red arrows point to tan-colored aggregate particles and the green to gray-colored ones. The majority of aggregate particles are white in color.

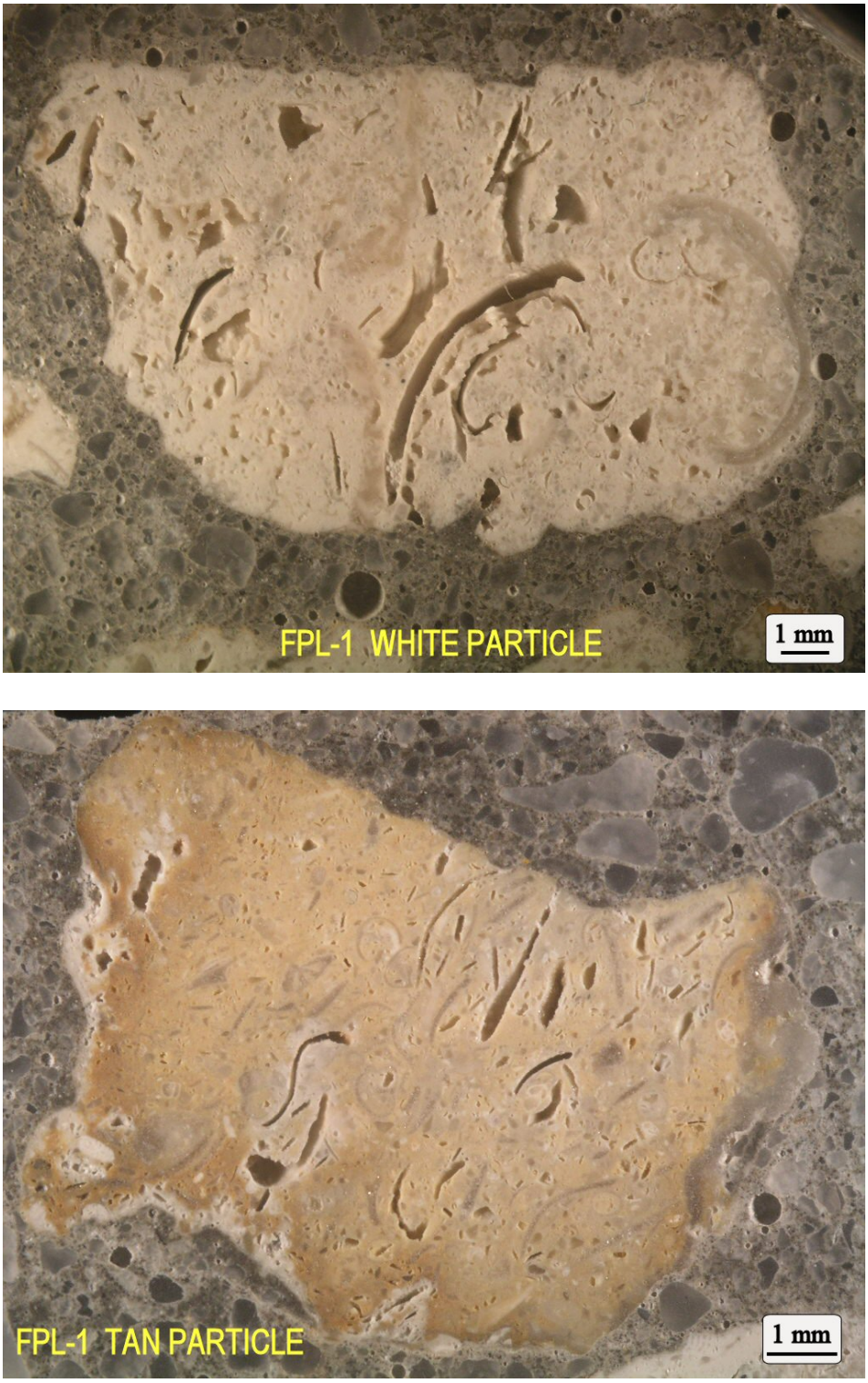

Figure VIII-15: Lapped section views of prism 9b showing enlarged views of a typical white limestone coarse aggregate particle (7X) and a typical tan limestone coarse aggregate particle (10X). The tan coloration is due in part to a clay component in some of the limestone particles. The visible porosity in the aggregate particles is primarily of the moldic variety.

Table VIII-11: Chemical Composition (EDX Analysis) of the FPL-1 Coarse Aggregate (Rinker Materials Oolitic Limerock).

Oxide Constituent	White Particle	Gray Particle
CaO	91.55	83.59
MgO	0.81	0.67
SiO_2	7.17	12.05
Al_20_3	0.47	2.03
Na_20	0	0.25
K_20	0	0.39
Fe0	0	1.01
P_20_5	0	0
$S0_3$	0	0

representative gray particle is also shown in Table VIII-11 and indicates a CaO content of 83.6 percent and a SiO_2 content of 12.05 percent. Also shown is an alumina (Al_2O_3) content of 2.03 percent and a small amount of Na_2O, K_2O, and iron oxide. These latter constituents indicate the presence of a clay mineral although the XRD analysis, which identified only calcite (major) and quartz (minor), did not pick this up. As is shown in the bottom photograph of Figure VIII-16, subsequent thin section examinations did confirm the presence of small amounts of clay in the gray and tan FPL-1 aggregate particles. At least some of the SiO_2 component of these particles (as indicated in the chemical analysis of Table VIII-11) can be attributed to the silicate component of the clay constituent.

Microstructural and Textural Features: The dominant texture in the FPL-1 limestone aggregate particles is a matrix supported structure (wackestone). Occasional individual aggregate particles show small regions of grain-supported structure (packstone). Micrite is the dominant matrix material in this rock. The allochem content varies from sparse to packed in all three colors of the rock. The dominant allochems are intraclasts and fossil fragments. The intraclasts are present as particles of varying shape but are often rounded and comprised of calcite crystals ranging from sparite size to as large as 200 μm. Individual quartz grains are common, and occasional quartz grains are embedded as a discrete phase in the calcite intraclasts (indicating that the calcite and quartz came from the same sediment).

Porosity in this aggregate includes moldic, vuggy, and intraparticle; however, the dominant

type is moldic porosity formed from the dissolution of fossil allochems. Examples are shown in Figure VIII-15, which presents photographs of enlarged views of the lapped surface of a white and a tan aggregate particle. The void surfaces are commonly lined with a calcitic micrite or sparite coating, much like the crystal lining in vuggy pores. This latter feature can be seen in Figure VIII-16, which shows crossed polars thin section views (100X) of two of the FPL-1 limestone aggregate particles.

The moldic pores range in shape from spherical to elongate (crescent). As measured in two dimensions on a lapped surface, the length of the elongated pores ranges from 0.5 to 6 mm. The width is typically less than 0.3 mm.

Intraparticle porosity is common in the intraclast particles in which the pore size is typically less than 100 μm. The less common vuggy pores are irregular in shape and have a maximum dimension of ca. 2 mm. These pores lie within the micritic matrix of the limestone particles and they commonly have a crystalline sparite lining.

Type and Distribution of the Silica Phase**:** The XRD analyses indicated the presence of the silica phase in this limestone rock as crystalline alpha quartz. These are present most typically as discrete particles embedded within the micritic matrix. Remnants of the calcitic intraclast material are often adhered to these quartz particles. Less commonly, quartz particles are completely embedded in an intraclast particle.

Examples of quartz particles in this aggregate are shown in the top photograph of Figure VIII-16. The content of these is variable from one aggregate particle to another. There are very low to moderate numbers of quartz particles in white, gray, and tan. As noted previously (Table VIII-11), the silica content of the white particles is around seven percent with most being present as quartz. These are present primarily as subangular to subrounded particles ranging in size from 0.05 to 0.3 mm. A small number of quartz particles fall within the size range of 0.3 to 0.5 mm.

As noted above, it has been demonstrated that crystalline quartz that has been fractured or strained may be vulnerable to attack by alkali hydroxide solutions, leading to ASR activity. When examined in thin sections, strained quartz particles show undulatory (wavy) extinction behavior when rotated on the microscope stage under crossed polars. Very few of the quartz particles examined here showed this type of extinction behavior, strongly indicating that they are

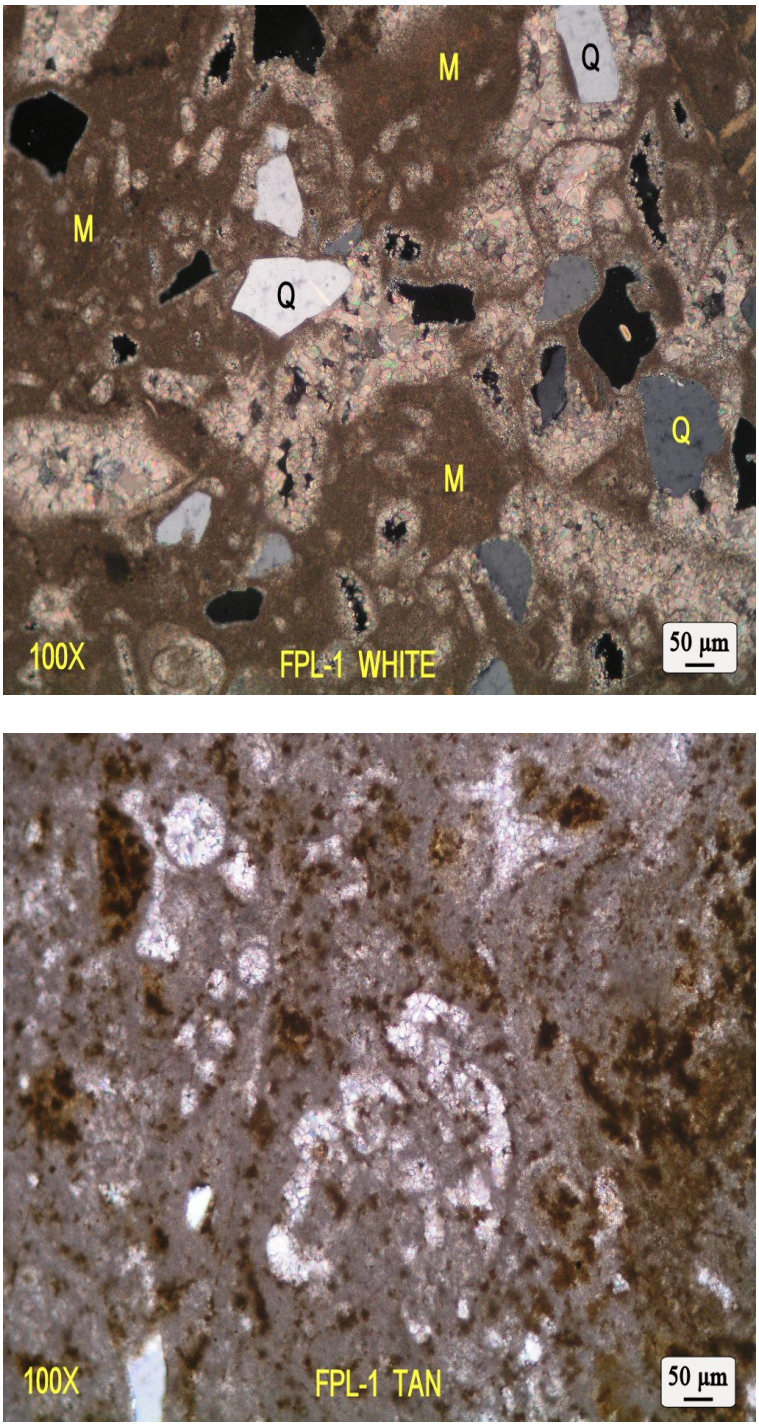

Figure VIII-16: Thin section views (crossed polars) of a white limestone aggregate particle and a tan limestone aggregate particle. The white particle shows a micritic calcite matrix (M) surrounding discrete quartz particles (Q) and fine-grained calcite intraclasts. Occasional quartz particles are a component of the intraclasts. The tan limestone particles derive coloration from streaks and veins of clay particles (dark material in the bottom photo).

not expected to be involved in ASR activity. In addition, none of the potentially deleterious silica minerals (chert, chalcedony, or opal) was found in this limestone aggregate.

Behavior of FPL-1 Concretes in the ASTM C1293 Test: As discussed in the preceding section, nine concrete series were prepared using the FPL-1 Florida limestone coarse aggregate, and prisms from each were subjected to the ASTM C1293 test procedure with expansions being summarized in Table VIII-3. It was concluded that expansions for these prisms were well below the 0.04 percent threshold. Petrographic examinations after the one and two year exposure revealed no cracking distress and no evidence of ASR activity. Photographs of prisms 9d and 13d after one year exposure are shown in Figure VIII-17. Prism 9d was prepared with the FPL-1 concrete having the highest alkali content (1.2 percent) and no lithium admixture. This concrete would be expected to have the greatest potential for ASR activity. Prism 13b, on the other hand, had the same alkali content as prism 9d but with the higher level of the lithium admixture (1.5 designation). The one year expansion was low in both concretes ($\leq$ 0.01 percent) and was actually slightly higher in the concrete containing the lithium admixture (0.0102 compared to 0.0065 percent).

Examination of lapped surfaces of these prisms showed no evidence of ASR gel (as exudate, pore fillings, or paste stains) and no cracking or reaction rims in any of the fine or coarse aggregate particles. As shown in Figure VIII-17, the molded and cast surfaces are smooth and clean and free of any exudate material. This condition was seen following both one and two years of ASTM C1293 exposure for all of these concretes.

Effect of Alkali on Expansion: As noted previously, the length change of the concrete prisms containing the normal alkali content of 0.5 percent (series 00) was a slight shrinkage (0.002 percent) at both one and two years. All concretes containing elevated alkali (1.0 and 1.2 percent) exhibited a slight expansion (0.0083 percent at one year and about the same at two years). This poses two questions: first, is this expansion due to a mild form of ASR activity in this concrete, despite the fact that the quartz in this coarse aggregate is not expected to be susceptible and, second, could limited ASR cause some expansion in thermodynamically stable quartz if the alkali content were sufficiently high? The significant observations relating to these questions are:

- The magnitude of the expansion was not significantly affected by the alkali content at the elevated levels (1.0 or 1.2 percent).

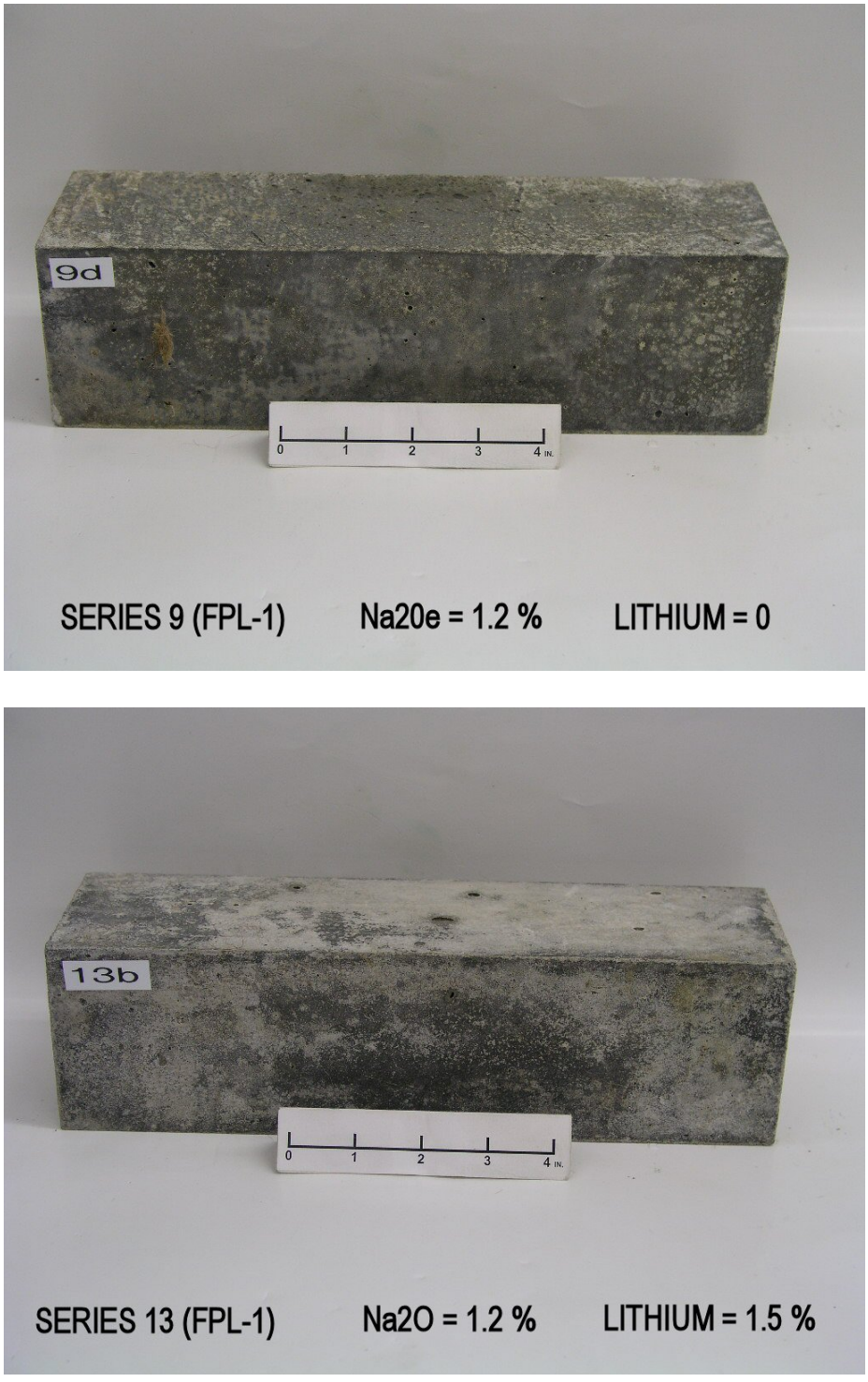

Figure VIII-17: Photographs of prisms 9b and 13b following one year exposure in the ASTM C1293 test.

- The magnitude of the expansion was not significantly affected by the presence or amount of the lithium admixture.

- The expansion did not increase from year one to year two.

- No petrographic evidence was found for any ASR activity in these concretes.

It does appear that the alkali content of the concrete is involved in some way in this phenomenon. At 0.5 percent alkali, the concrete experienced a slight shrinkage in the ASTM C1293 test. At the two elevated alkali contents, a slight expansion occurred. At this point, it can not be said with certainty that the alkali involvement in this matter is due to classic ASR activity. The question, however, may be academic as 1) none of the FPL-1 concretes show any evidence of distress after the one or the two year exposures and 2) the expansions ceased after the first year. It is of interest to note that all six of the other concretes evaluated in the present study also showed these features.

Effect of Fly Ash on Expansion: As indicated by the expansion data, FA in the concretes significantly limited the magnitude of length increases in concretes for which ASR activity was suspected. One of the FPL-1 concretes (series 53) contained no fly ash. The data in Table VIII-3 permit a comparison of expansion behavior in which the only intended difference between mixes 53 and 8 is presence versus absence of FA. The expansion at one year is virtually identical for the two concretes. This is perhaps further evidence that the alkali involvement in expansions in the FPL-1 concretes was not due to classic ASR activity.

Summary: The FPL-1 coarse aggregate contains a crystalline quartz phase; however, petrographic evidence indicates that this component should not be susceptible to ASR activity. In fact, no evidence of ASR activity was found in any of these concretes. Also, none of the FPL-1 concretes showed any evidence of cracking or other distress after two years of ASTM C1293 exposure.

All of the FPL-1 concretes except the one with normal alkali content (0.5 percent Na_2O_e) did show a slight expansion following one and two years exposure in the ASTM C1293 test. The expansion values, which ranged from 0.0049 to 0.0116 percent and averaged 0.008 percent, are well below the ASTM C1293 threshold value of 0.04 percent. Also, expansions did not increase

from between the first and second years of exposure, indicating that whatever caused the expansion had ceased by the end of the one year. Although an alkali involvement is indicated for this expansion, there is no conclusive evidence on which to base the claim that it is a mild and non-destructive form of classic ASR activity.

On the basis of the results obtained here, it is judged that the Florida FPL-1 limestone is suitable as the coarse aggregate phase in FDOT Class V concretes intended for use in possible further study and field trials to evaluate the utility of high-alkali concretes to increase time-to corrosion in reinforced concrete Florida bridge structures.

Petrographic Analyses - Concrete Series with Coarse Aggregate FPL-2 (Florida Limestone, Source 2)

Physical Features: Examples of the FPL-2 limestone coarse aggregate are shown Figures VIII-18 and 19, which are lapped section views of prism 27d.

Color: The FPL-2 aggregate particles exhibit three distinct colors including 1) off-white, 2) pale orange, and 3) gray. The white and orange particles, which are lithologically similar, account for approximately 98 percent of the coarse aggregate. As seen in the top photograph of Figure VIII-19, the matrix phase of some of the off-white particles also exhibits the pale orange color. Some of the aggregate particles display separate regions of material reflecting two of the colors.

Shape and Angularity: These coarse aggregate particles are angular to sub-rounded, primarily compact in shape, and tending to a platy shape.

Hardness: The great majority of all three colors of the FPL-2 aggregate are moderately hard to hard. The gray particles are very hard in that they can not be scored with a steel probe.

Chemistry and Mineralogy: The dominant mineral species in this rock are calcite ($CaCO_3$), which is the major phase, and quartz (SiO_2), which is the minor phase. Other silica minerals detected in particles of this aggregate include chert and chalcedony. Both are described as cryptocrystalline or microcrystalline quartz, which means that the crystals can only be observed microscopically. The maximum crystal size in the chert is placed at around 20 μm. Chalcedony is commonly observed microscopically in a fibrous form. Both chert and chalcedony are classified as potentially deleterious as regards ASR activity.

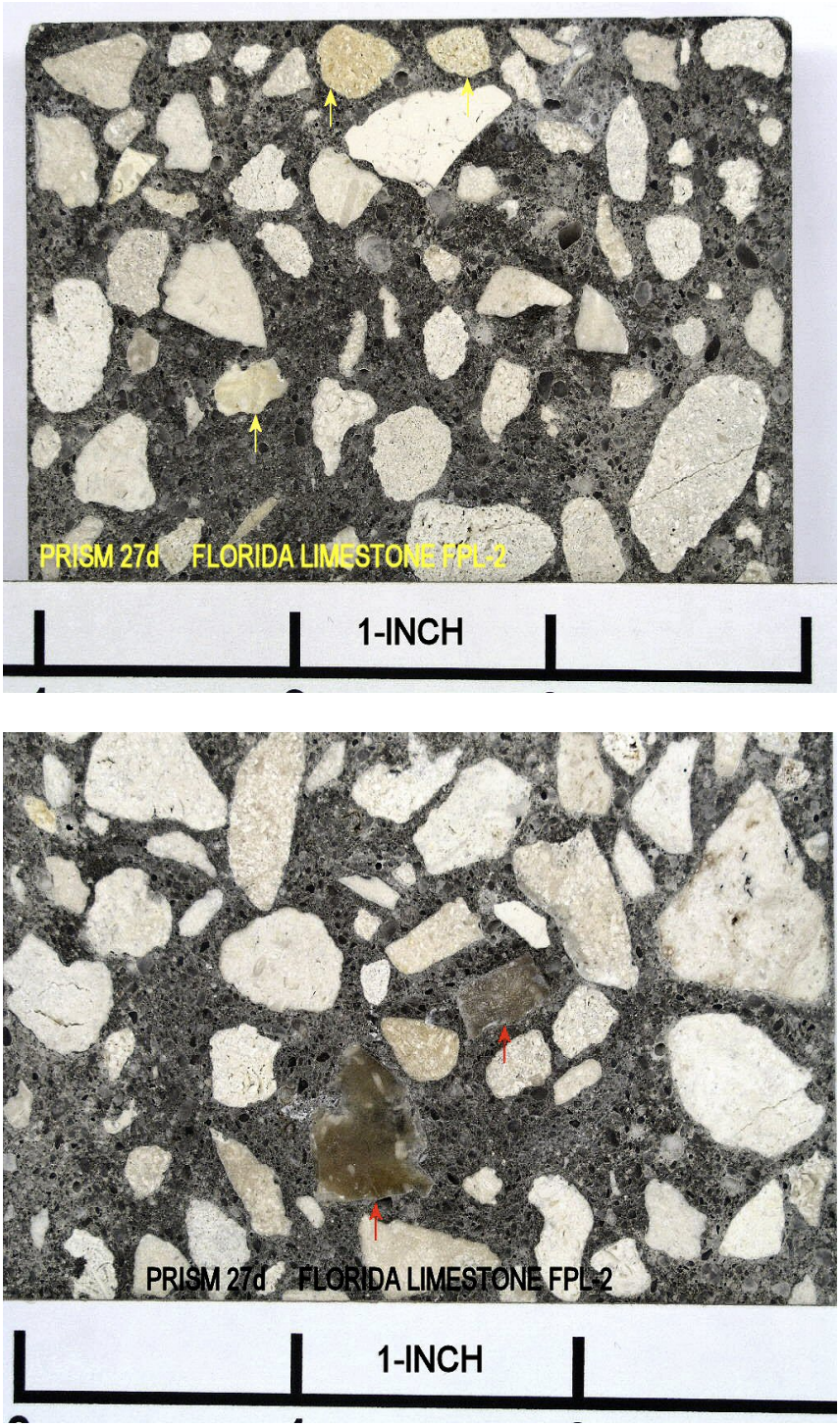

Figure VIII-18: Lapped section views of prism 27d, which contains the FPL-2 Florida limestone coarse aggregate. This concrete contains an alkali content of 1.2 percent and no lithium admixture. The majority of aggregate particles are characterized as "white limestone particles". Yellow arrows in the top photograph point to pale orange limestone particles. Red arrows in the bottom photograph point to gray chert particles.

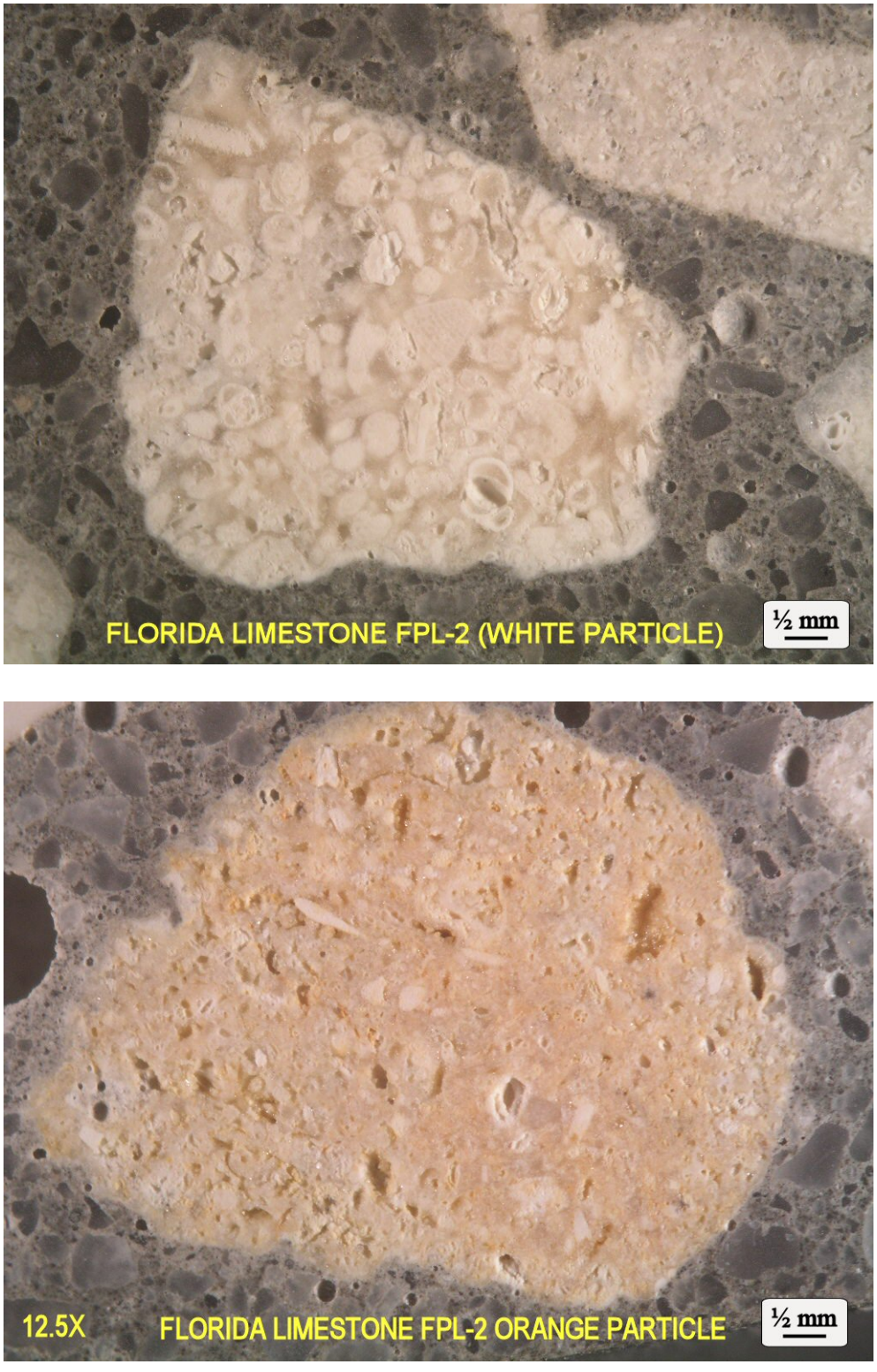

Figure VIII-19: Lapped section views (12.5X) of prism 27d showing coarse aggregate particles that are typical of the white and pale orange colors p dominant in p FPL-2.

Table VIII-12 presents the chemical analysis (EDX) results obtained on a white and an orange FPL-2 aggregate particle. The particles were selected as being representative of particles with these two colors on the basis of an optical petrographic examination. This is a very pure limestone with a CaO content of 98.3 percent and an MgO content of 0.3 percent. These limestone particles contain SiO_2 phases which range from 1.0 to 1.5 percent. The XRD data for the white and orange particles show calcite as the major phase and crystalline quartz as a minor phase. Thin section examinations established that the SiO_2 phase in the white and orange particles is crystalline alpha quartz (see Figure VIII-19). The microscopic examination indicated that the quartz content of the gray particles is higher relative to the white and orange particles and that the silica is present as chert and chalcedony.

Table VIII-12. Chemical Composition (EDX Analysis) of the FPL-2 coarse aggregate.

Oxide Constituent	White Particle	Pale Orange Particle
CaO	98.27	98.36
MgO	0.26	0.39
SiO_2	1.48	1
Al_20_3	0	0.25
Na_20	0	0
K_20	0	0
Fe0	0	0
P_20_5	0	0
$S0_3$	0	0

Microstructural and Textural Features: The white and orange limestone particles, which dominate the FPL-2 aggregate, show a matrix-supported structure (wackestone) with a moderate to abundant allochem content. The matrix is composed primarily of calcite crystallites within the sparite size range, although crystals in the size range 10 to 30 μm are also present. The primary allochems include fossil shells, fossil fragments, and peloids. The typical size of the allochems ranges from 0.05 to 0.8 mm. These features are shown in the top photograph of Figure VIII-20, which is a thin section view (plane polarized light) of a white FPL-2 limestone particle.

Sub-angular quartz grains, which range in size from 25 to 120 μm, are present as discrete grains embedded in the calcite matrix of the white and orange FPL-2 particles. Some particles show only a few quartz grains (top photograph of Figure VIII-20), while they are common in

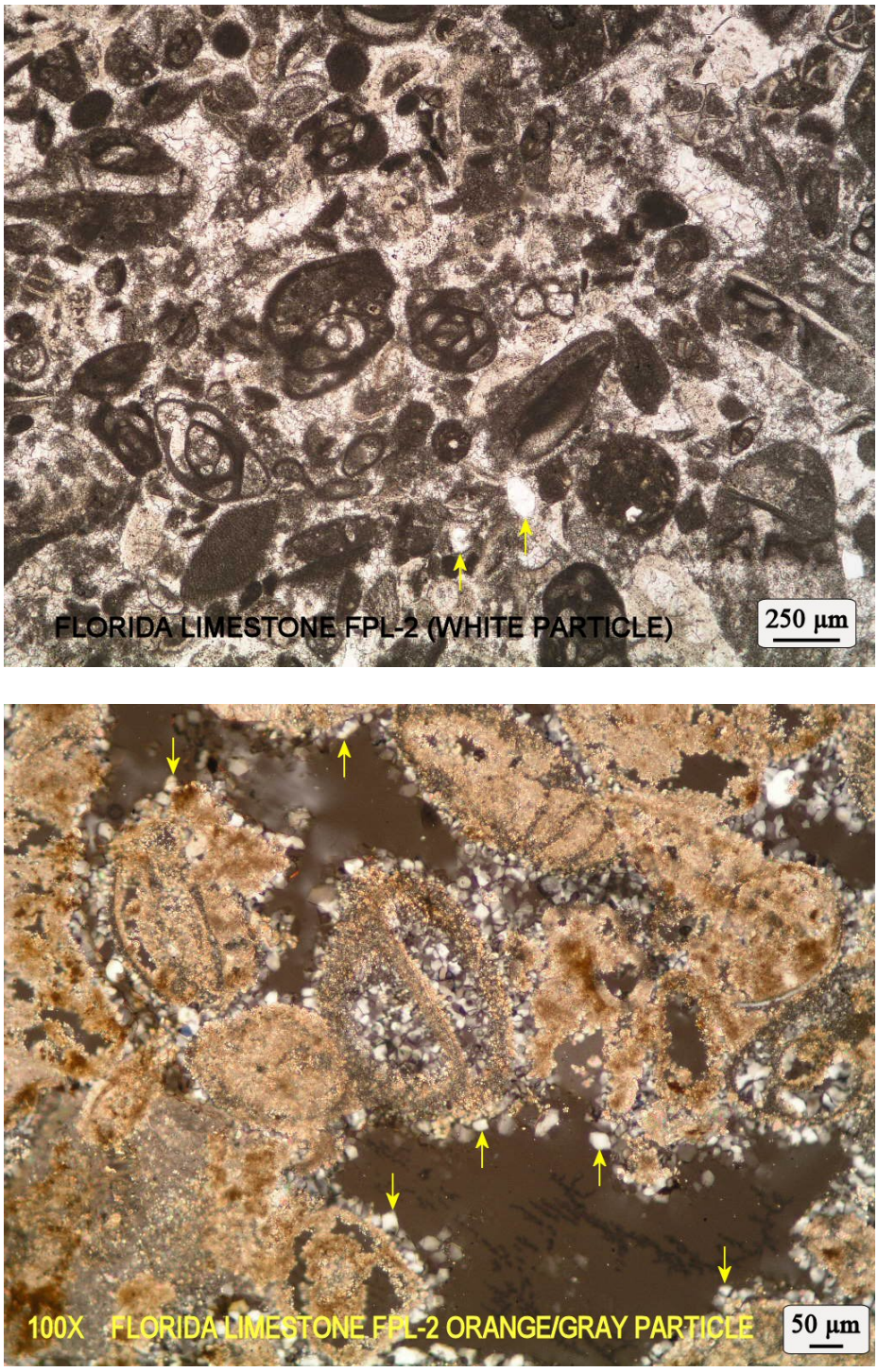

Figure VIII-20. Thin section views of FPL-2 limestone aggregate particles in prism 27d (40X and 100X). The top photograph (40X) shows a plane-polarized light view of a typical white limestone aggregate particle and a packed allochem distribution. The arrows point to small quartz particles. The bottom photograph (100X) shows a crossed-polars view of an orange/gray particle where microcrystalline quartz particles (arrows) line void cavities.

others. In the thin sections examined here, the quartz grains typically showed uniform extinction behavior in the polarizing microscope examination. No chert (microcrystalline quartz) or chalcedony was detected as a SiO_2 phase in the white or orange limestone aggregate particles examined.

The amount of porosity in the FPL-2 limestone white particles is low at both the micro- and macro-levels, as seen in Figures VIII-19 and VIII-20. The primary forms of this porosity include vuggy and intraparticle, typically having a maximum dimension ranging from 25 to 250 μm. Moldic porosity is present, but not common, in some of the rock particles.

The gray particles are present in the FPL-2 aggregate as discrete particles and also as a component of a white or orange particle. Examples of these forms of gray particles are shown in Figure VIII-18 and VIII-20. The gray particles examined in thin section show a higher level of SiO_2 relative to the white and orange particles; and in addition, much of this phase is in the form of chert and chalcedony. These forms of SiO_2 comprise the matrix phase in the gray particles. The quartz crystals in this chert are smaller than 20 μm and often are less than 1 μm. As shown in the thin section views (crossed polars) of Figure VIII-21, chalcedony is present as the microscopically fibrous form.

Figure VIII-22 shows lapped section views of two FPL-2 aggregate particles which contain both an orange component (which is principally calcite), and a gray component (which is principally chert). The chert is very hard and can not be scratched with a steel probe. Note the white exudate deposit around the perimeter of the aggregate particles, which was identified in the SEM/EDX examination as alkali-silica gel.

A thin section view (crossed polars) of the transition region between the calcite and chert components of the aggregate particles in Figure VIII-22 is shown in the bottom photograph of Figure VIII-21. In this example calcite forms the matrix phase of the particle. Numerous microcrystalline quartz particles, which range in size from less than 1 μm to 20μm, line the surfaces of pore cavities. In-filling of the intraparticle porosity with the small quartz crystals is common.

The predominantly gray coarse aggregate particles (such as in the bottom photograph of Figure VIII-18) are composed mainly of SiO_2 in the form of chert and chalcedony. Examples are shown in the thin section views (crossed polars) of Figure VIII-21. The SiO_2 phases in the chert

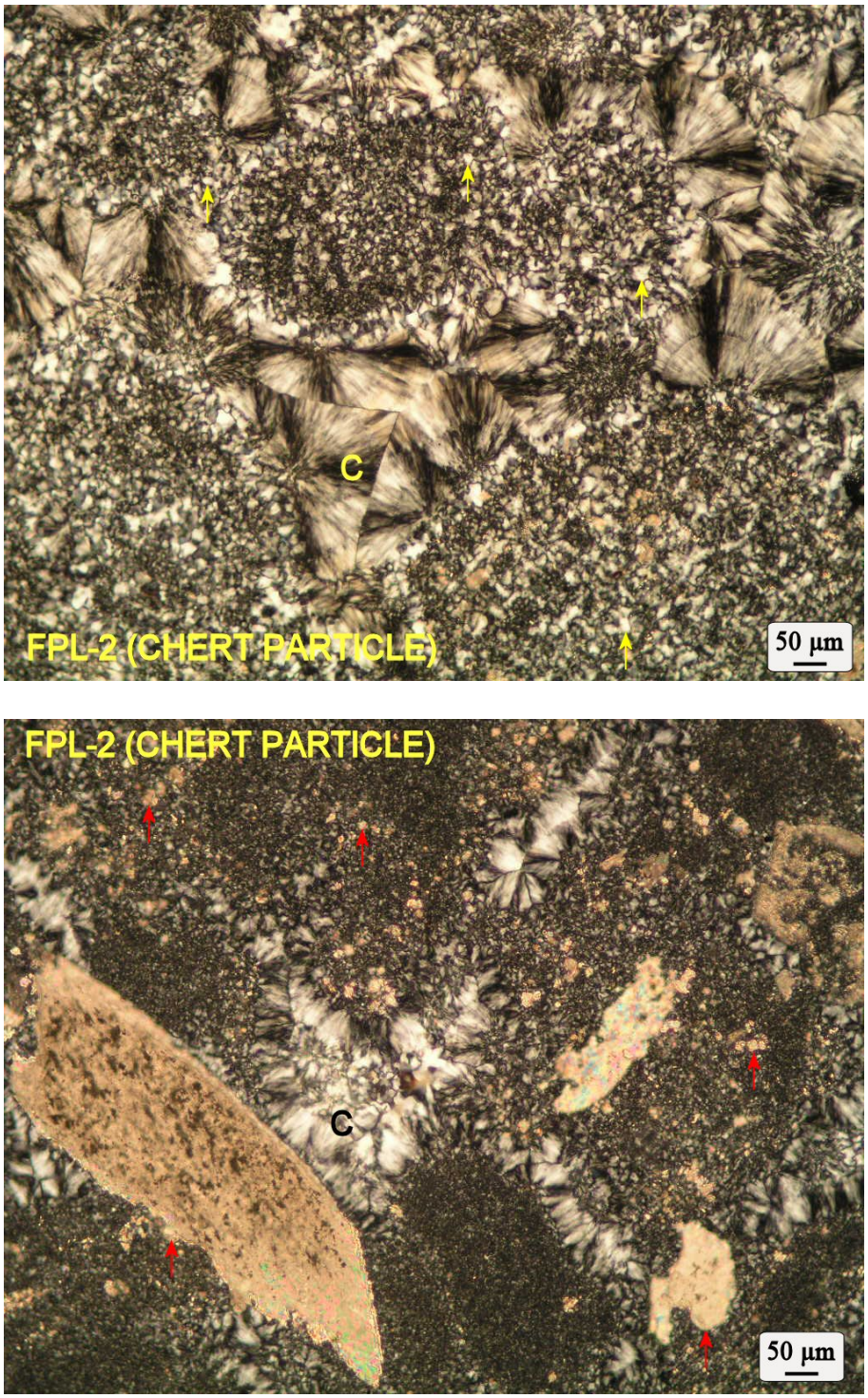

Figure VIII-21: Crossed polar thin section views (100X) of a gray FPL-2 chert aggregate particles in prism 27d. Silica phases in the chert include microcrystalline quartz particles (yellow arrows) and chalcedony (C). The red arrows point to irregularly shaped particles of micritic calcite embedded in the silica matrix.

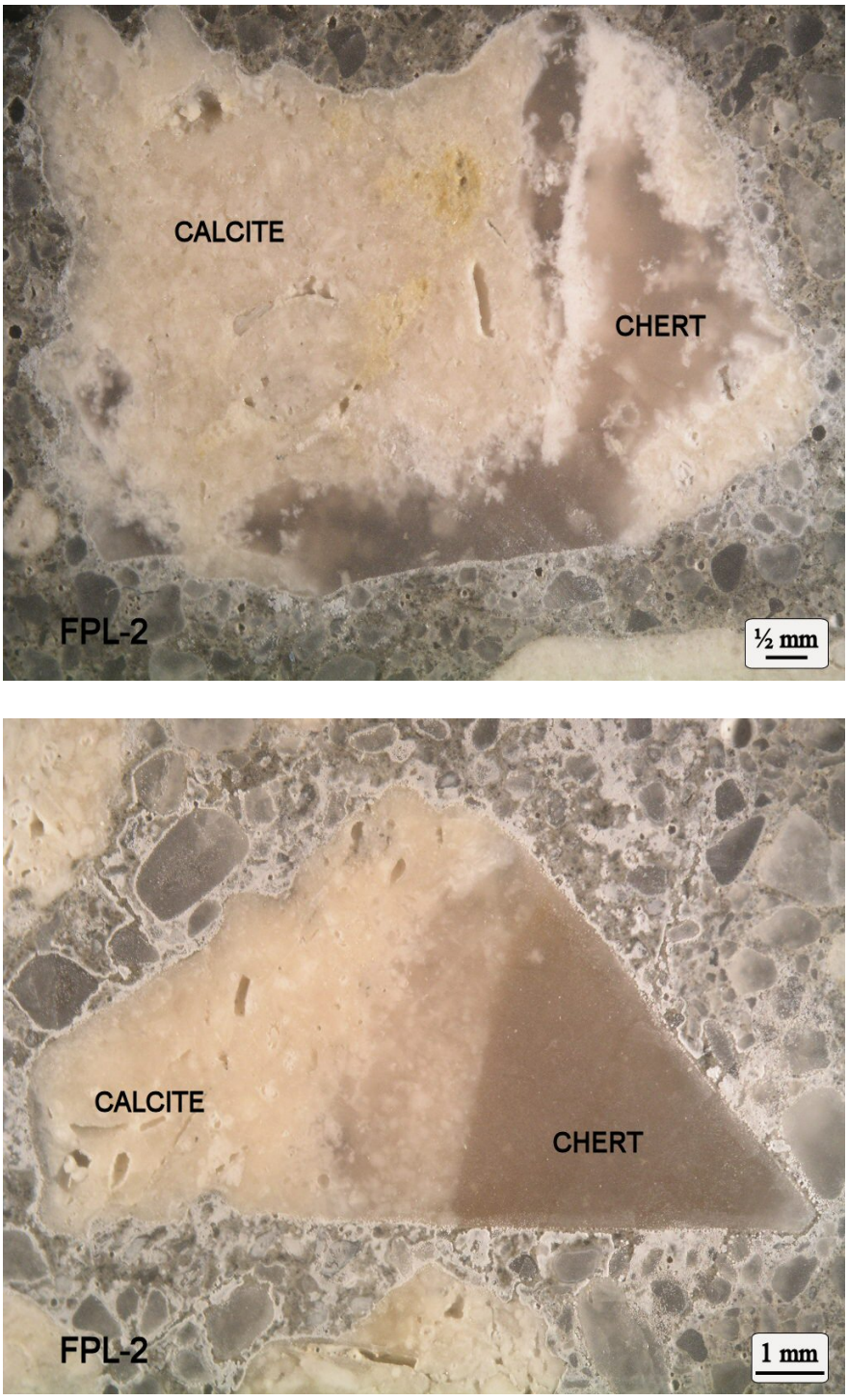

Figure VIII-22. Lapped section views (12.5X and 10X) of prism 27d showing FPL-2 coarse aggregate particles which contain discrete regions of both the calcite and chert phases within the same particle. Note the white exudate on the concrete surface adjacent to the particles which is alkali-silica gel.

include microcrystalline quartz with particles mainly less than 10 μm in size and fibrous chalcedony. As can be seen in the bottom photograph of Figure VIII-21, small micritic calcite intraclasts are embedded within the SiO_2 matrix. Most of the gray aggregate particles contain some of these micrite particles.

The chert and chalcedony in the FPL-2 aggregate have been involved in ASR activity, and this has resulted in some cracking in the FPL-2 concrete containing the highest Na_20e level (1.2 percent) with no lithium admixture (concrete series 27). Direct evidence of the presence of ASR gel from the SEM/EDX examination was also obtained. Figure C-1 (Appendix C) is an EDX spectrum of alkali-silica gel, which was collected as a white, opaque exudate on one of the molded surfaces of prism 27d at one year. None of the other concrete series containing the FPL-2 coarse aggregate showed any cracking, although ASR gel was detected in some of these high-alkali concretes.

Behavior of FPL-2 Concretes in the ASTM C1293 Test: Six concrete series were prepared using the FPL-2 coarse aggregate, and expansions for these concretes were summarized in Table XII. These data indicated an average expansion for the HAC concretes (Na_2O_e = 1.0 and 1.2 percent) of 0.0123 percent after one year. The concrete series containing the normal alkali content of 0.5 percent (series 06) showed no length change at one year and virtually no change at two years.

All examples of concrete and aggregate features in Figures VIII-18-VIII-22 are from prism 27d (Na_20e = 1.2 percent and no $LiNO_3$ admixture). Alkali silica reaction gel and associated cracking distress were observed in this prism. Examples of former which are associated with aggregate particles that contain a chert component are shown in Figure VIII-22 (lapped surfaces of prism 27d). As the samples dried from the lapping operation, water containing the soluble ASR gel evaporated on the surface leaving behind deposits of gel as exudate.

Figure VIII-23 shows photographs of prism 27d following the one year ASTM C 1293 exposure. The molded surfaces of the prism are streaked with a white deposit that subsequent chemical analysis showed to include ASR gel, and two cracks are also apparent. An enlarged view of one of the cracks is shown in Figure VIII-24. The bottom photograph here shows a small patch of ASR gel exudate on a molded surface.

The prisms of series 27 concrete had an average one year expansion of 0.015 percent and a two year expansion of 0.024 percent. This is the only FPL-2 concrete to show a continuing

Figure VIII-23: Prism 27d at after 362 days of ASTM C1293 exposure. The expansion is 0.015 percent. The arrows point to cracks. White streaks include exudates of ASR gel.

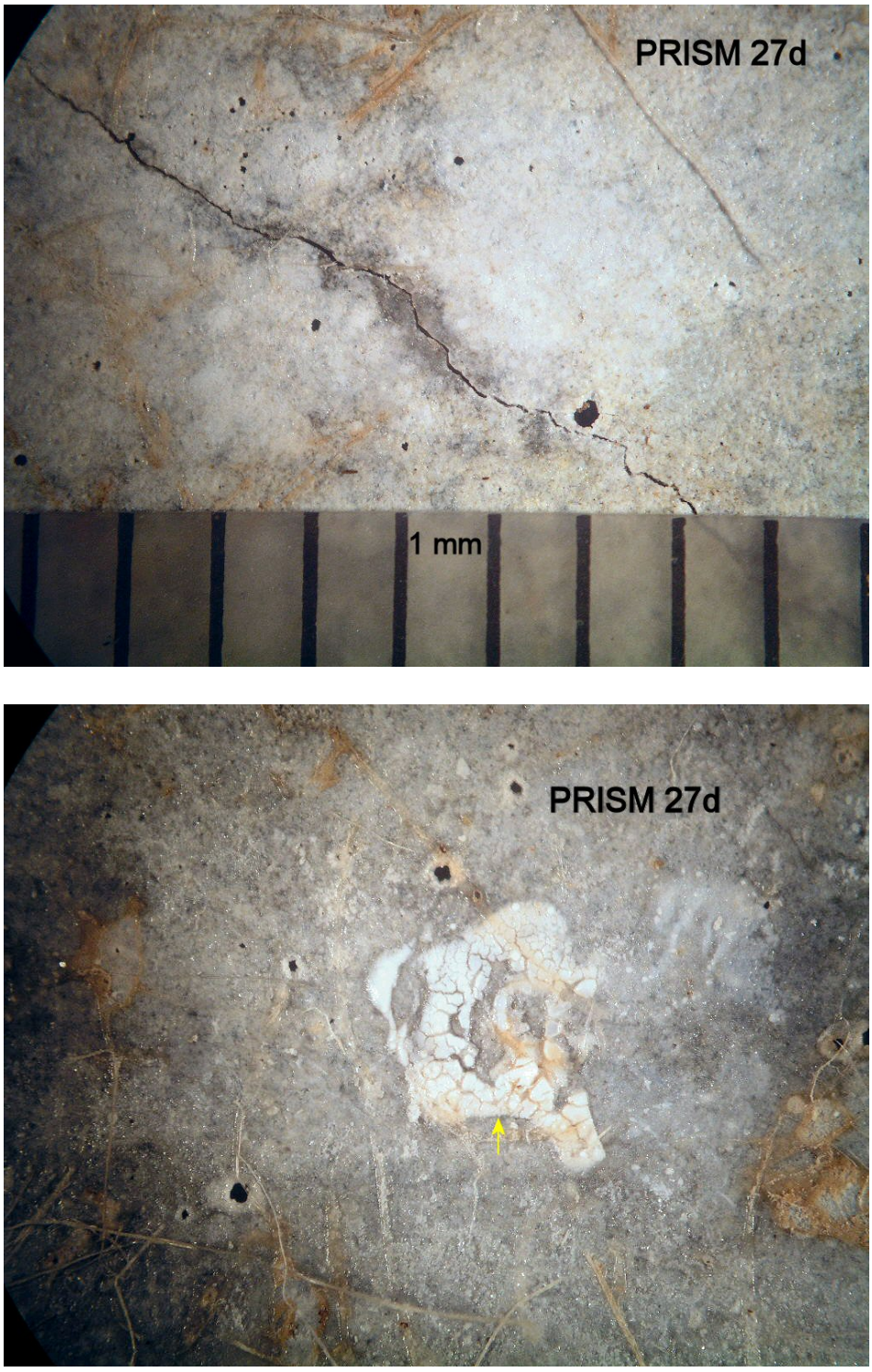

Figure VIII-24: Enlarged views of molded surfaces of prism 27d. The bottom photograph shows a small patch of ASR exudate (arrow) that was present on the molded surface of after one year of ASTM C1293 exposure.

expansion during the second year of exposure. Also, it is also the only series of the six to show any cracking distress (Figure VIII-24).

With the exception of concrete series 27, all FPL-2 prism specimens showed virtually no change in length from the first to the second year of exposure. This indicates that whatever caused the slight expansion during the first year ceased to be operative during the second year. As discussed previously, this phenomenon was also observed in the Florida limestone FPL-1 concretes as well.

Effect of Alkali on Expansion: Alkali-silica reaction activity was confirmed in the series 27 FPL-2 concrete, which contained the highest alkali content (1.2 percent) and no lithium admixture. This is consistent with presence of microcrystalline quartz (chert) and chalcedony as a minor phase in this coarse aggregate. The series 27 FPL-2 concrete is expected to be the most susceptible to ASR activity for mixes with this coarse aggregate, as it has the highest alkali content and no lithium admixture.

ASR gel was observed in prism 27d as 1) exudate on the molded surface, 2) secondary deposits on air void surfaces, and 3) exudate associated with reactive chert aggregate particles on lapped surfaces. Examples of the ASR gel associated with aggregate particles that contain a chert component are shown in Figure VIII-22. As the samples dried subsequent to the lapping operation, water containing the soluble ASR gel evaporated on the surface leaving behind deposits of the gel as exudate.

Figure VIII-23 shows photographs of prism 27d (Na_2O_e = 1.2 percent and no $LiNO_3$) following the one year ASTM C1293 exposure where ASR activity in this concrete resulted in cracking. The molded surfaces are streaked with deposits of white exudate material, which was shown to be ASR gel. Figure VIII-24 shows a close-up view of a molded surface and crack that can be seen in Figure VIII-23 (top) and of a patch of ASR exudate (bottom). An EDX analysis of this exudate is shown in Figure C-1 (Appendix C), revealing a typical fingerprint of ASR gel where cation species include Ca, Na, and K. It is not uncommon to find Al as a constituent of ASR gel, and that is the case here. There are only two cracks in this prism, but these are relatively long and wide. The presence of only a few large cracks is consistent with the fact that the chert/chalcedony was heavily concentrated in a few particles rather than as smaller amounts in a larger number of particles. In the latter case, it is expected that cracking would be ubiquitous.

The FPL-2 concretes containing 1.0 percent alkali all showed very little evidence of exudate material on molded prism surfaces or secondary deposits on air void surfaces (concrete series 07, 26 and 28). None of these concretes showed any cracking distress.

Effect of the Lithium Admixture on Expansion and ASR Activity: The length change behavior of concrete series 29 during the ASTM C1293 exposure and the effect of the lithium admixture on ASR activity in the high-alkali FPL-2 concrete were summarized in Table XII. This concrete showed no cracking through two years of testing but did exhibit exudate material on molded surfaces which EDX analyses confirmed to be alkali silica gel. Relative to the exudate gel on Prism 27d, this gel on had a much lower silica content. Prism 29d showed no expansion over the between years one and two and had no cracking distress after two years. Thus, presence of the lithium admixture suppressed expansion and cracking distress in the FPL-2 concrete at the highest alkali level. Comparison of the expansion behavior of concrete series 26 and 28 prisms shows that the lithium admixture had no effect on either the magnitude or the rate of expansion in these concretes at the 1.0 percent alkali level.

Summary: The FPL-2 Florida limestone aggregate is relatively pure with a CaO content over 98 percent and SiO_2 around 1 to 1.5 percent. In the majority of aggregate particles, the SiO_2 is present as relatively large crystalline quartz grains which are not expected to be prone to ASR activity. In less than 2 percent of the FPL-2 aggregate particles, the SiO_2 is present in large concentrations as microcrystalline quartz and chalcedony; and in the highest alkali FPL-2 concretes, these aggregate particles were involved in ASR.

The significant observations relating to the performance of the six FPL-2 concretes in the ASTM C1293 test are summarized below:

- At the normal alkali content (0.5 percent) the FPL-2 concrete showed no expansion or ASR activity through two years of ASTM C1293 exposure.

- The three 1.0 percent alkali FPL-2 concretes showed a slight expansion during the first year of test exposure (ca. 0.01 percent). The expansion did not increase during the second year of exposure. The presence of the lithium admixture had no effect on expansion. No ASR activity was confirmed in these concretes, and none showed any cracking distress after the one or two year exposure period.

- The only FPL-2 concrete that showed cracking distress in the ASTM C1293 test was series 27, which has the highest alkali content (1.2 percent) and no lithium admixture. The cracks were present after one year exposure despite the fact that the average prism expansion was only 0.0152 percent. The cracking occurred as a few relatively wide and large cracks, in contrast to the more typical ASR-related crack morphology in which cracks are ubiquitous. This condition is likely related to the fact that only a small portion of the FPL-2 limestone aggregate particles contain the form of silica that is alkali-silica reactive. Also, some of the microcrystalline quartz is present as in-fill in the intraparticle porosity of the FPL-2 rock. This microstructural arrangement may shelter this form of SiO_2 from participation in ASR. However, the increase in expansion of concrete series 27 from one to two years indicates that ASR is ongoing and that continued cracking distress should be expected with continued exposure.

- Presence of the lithium admixture at the recommended dosage level suppressed ASR activity in the FPL-2 concrete containing 1.2 percent alkali (concrete series 29). Although ASR activity was confirmed in this concrete, it showed no increase in expansion from year one to year two; and it did not exhibit any cracking through the two year exposure.

Based on the above analyses, it is judged that the Florida FPL-2 limestone is not a suitable candidate as coarse aggregate in FDOT Class V concretes intended for use in further study or field trials to evaluate the utility of high-alkali concretes to increase time to corrosion of reinforced concrete Florida bridge structures. At the highest alkali level (1.2 percent), the FPL-2 concrete exhibited ASR activity and related cracking distress.

Petrographic Analyses - Concrete Series with Coarse Aggregate FPL-3 (Florida Limestone, Source 3)

Physical Features: Figure VIII-25 is a photograph of lapped sections of prism 46d which contains the FPL-3 coarse aggregate, 1.2 percent alkali, and no lithium admixture. Enlarged views of the aggregate particles are shown in Figures VIII-26 and VIII-27. The nominal maximum size of the aggregate is 25 mm.

Color: The FPL-3 aggregate particles exhibit three distinct colors, which include 1) off-white, 2) pale orange, and 3) black. The white and orange particles are indicated in Figure VIII-25. The

Figure VIII-25: Lapped section views of prism 46d. The arrows point to pale orange-colored particles. The majority of the aggregate particles in FPL-3 are white.

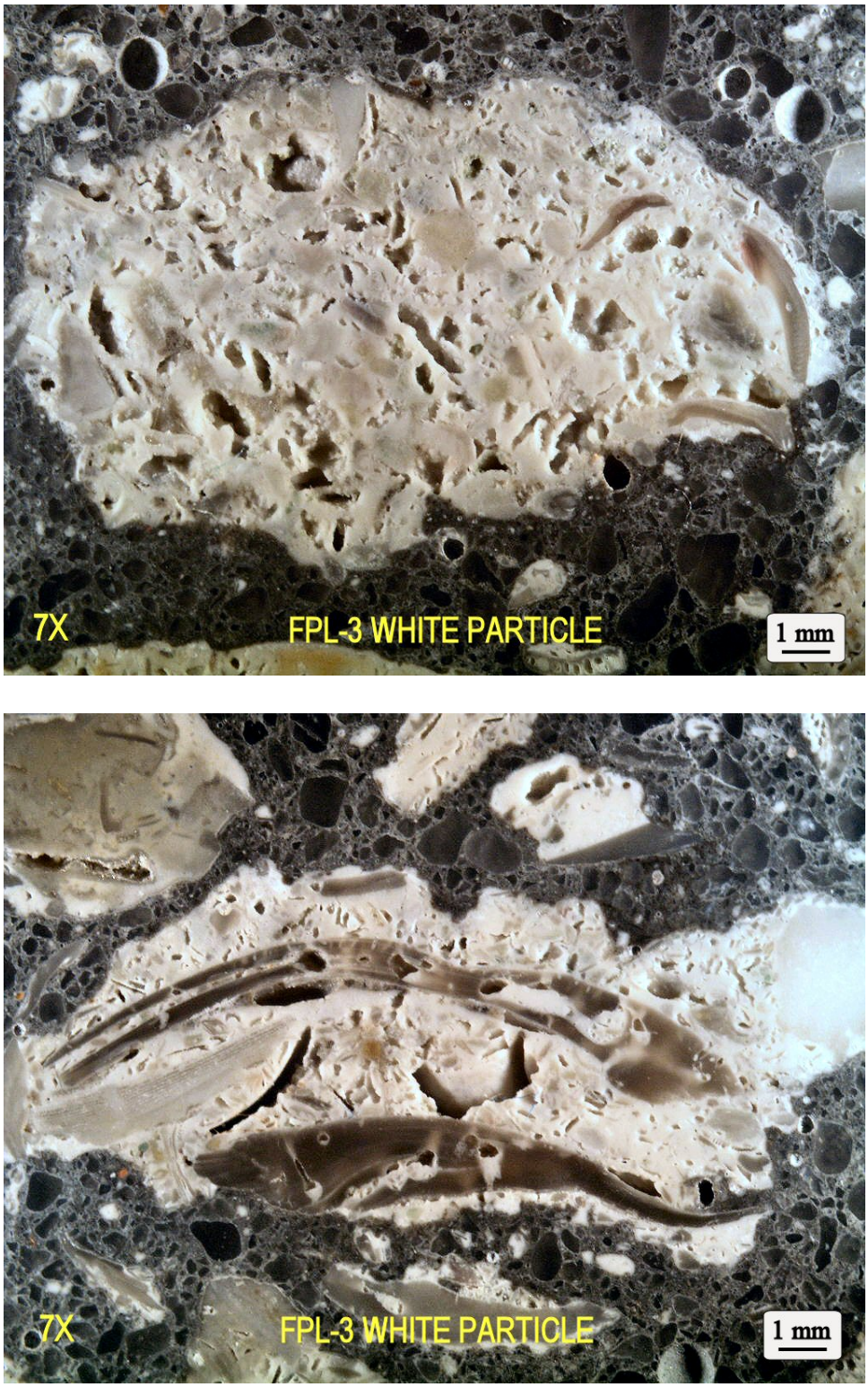

Figure VIII-26: Lapped section of prism 46d showing enlarged (7X) views of typical white FPL-3 limestone coarse aggregate particles.

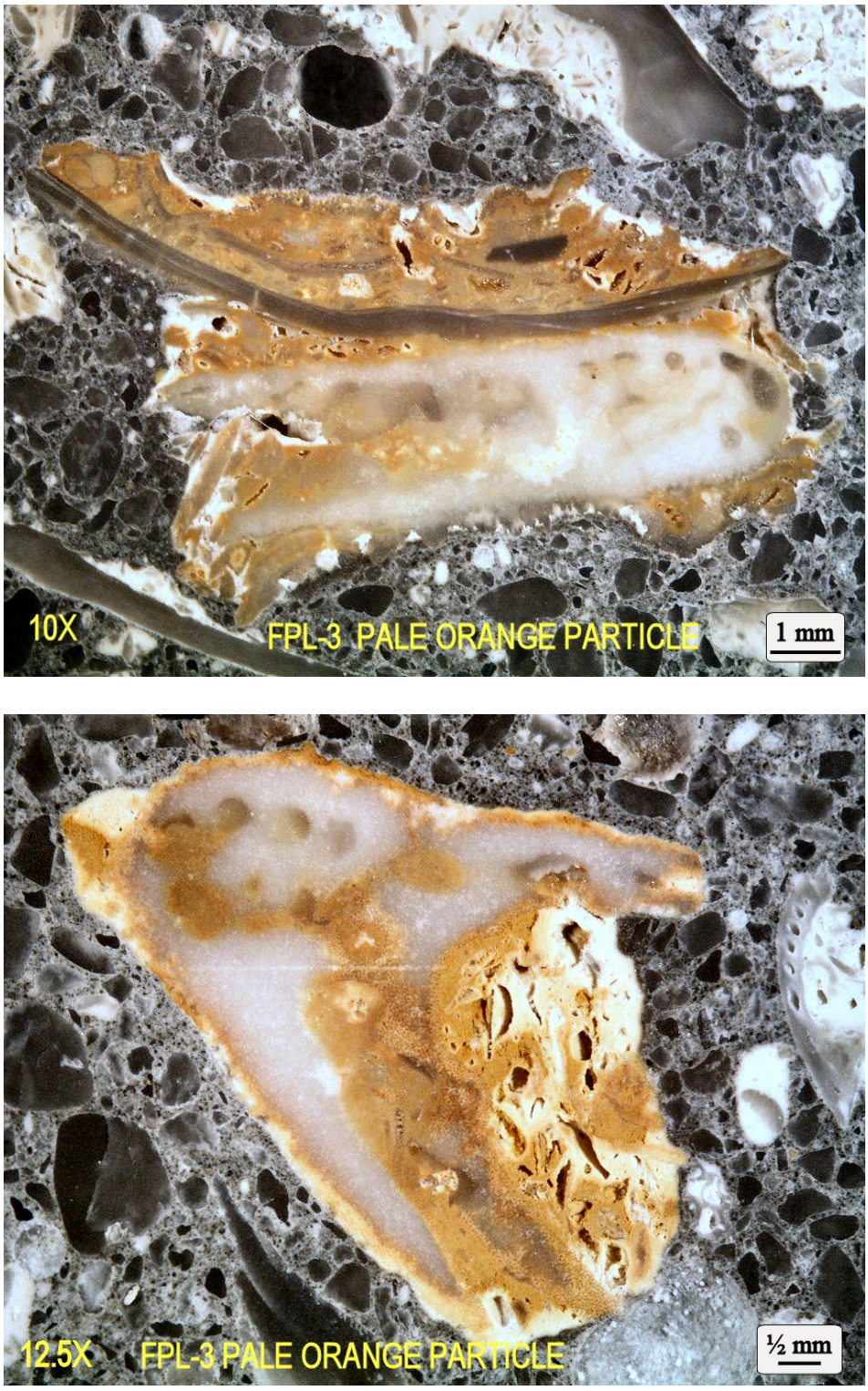

Figure VIII-27: Lapped section of prism 46d showing enlarged (7X and 12.5X) views of typical pale orange FPL-3 limestone coarse aggregate particles.

white particles make up around 85 percent of the coarse aggregate particles. The inclusion of large fragments of gray fossil shells within the white aggregate particles is a common feature (see Figures VIII-26 and VIII-27). Black particles are present in trace amounts (≤ 0.1 percent).

Shape and Angularity: The FPL-3 particles are very angular to angular; and the majority have a platy shape, tending to a bladed form. The largest particles are more compact. The presence of numerous free-standing complete fossil shells contributes to the domination of the platy shape of this aggregate.

Hardness: With reference to Figures VIII-26 and VIII-27, the large fossil fragments in the aggregate particles are quite hard. Overall, the matrix phase in the particles is characterized as soft (easily scored with a steel probe). This is the softest matrix material of the three Florida limestone aggregates in this study. In many of the aggregate particles, the large fossil fragments form a substantial portion of the exterior surface; providing a de-facto high level of hardness to the particles.

Chemistry and Mineralogy: The XRD analyses of the white particles of this aggregate showed calcite ($CaCO_3$) as the major phase and quartz (SiO_2) as a minor phase. These phases are also present in the orange particles along with goethite, a hydrated form of iron oxide, as a second minor phase. Trace amounts of mica are present in the finest size fractions of the bulk sample of this aggregate.

Chemical analyses (EDX) of a white and an orange FPL-3 aggregate particle (selected to show the most common microstructure based on the microscopic examination) are given in Table VIII-13. In both particles a relatively pure limestone is indicated with a CaO content of ca. 94 percent. A SiO_2 content of two percent is indicated for the white particle with no SiO_2 in the orange particle.

Both particles types contain Al_2O_3 at around one percent (contributed in part by the mica phase). The orange particle shows an iron oxide content of 4.5 percent, due in large part to the goethite phase. The one percent iron oxide in the white particle is likely due in part to this same source. In all of the chemical analyses conducted on the three Florida limestone aggregate particles, only the white FPL-3 particles showed a small amount of a P_2O_5-bearing phase and a sulfate (SO_3) mineral.

Table VIII-13: Chemical composition (EDX analysis) of the FPL-3 coarse aggregate.

Oxide Constituent	White Particle	Orange Particle
CaO	93.81	94.5
MgO	0.91	0
SiO_2	2.07	0
Al_20_3	1.29	1.03
Na_20	0	0
K_20	0	0
Fe0	1.05	4.47
P_20_5	0.29	0
$S0_3$	0.39	0

Two small (≤ 12 mm) black particles were found among the hundreds making up the 1.8 kg bulk FPL-3 sample that was examined. One of these was composed completely of microcrystalline quartz (chert), and the second was primarily chert. On a weight basis, the chert particles account for less than 0.1 percent of this coarse aggregate.

Microstructural and Textural Features: The dominant texture in the FPL-3 limestone aggregate particles is a matrix supported structure (wackestone) with micrite being the dominant matrix material. The allochems content typically varies from moderate to abundant, primarily as fossil shells and fragments. In many of the particles, a single large fossil fragment makes up one half to two-thirds of the entire particle volume. Less common allochems include rounded micritic intraclasts and pellets.

Small quartz grains are most common in the white FPL-3 limestone particles where they are present as discrete grains embedded within the micrite matrix. The grains range in size from 0.05 to 0.2 mm with most in the 0.1 to 0.15 mm range. The great majority of quartz grains show normal extinction behavior. These grains are less common in the orange FPL-3 aggregate particles, where they also are present as discrete particles within the micrite matrix. Mica is another mineral grain that is present in very small amounts within the micrite matrix of the orange particles.

The dominant form of porosity in the FPL-3 aggregate particles is of the moldic variety, which can be readily seen with the unaided eye in the aggregate particles shown in Figures VIII-

26 and VIII-27. Intraparticle porosity is a much less common type in this limestone.

Type and Distribution of the Silica Phase: Silica is present in the FPL-3 aggregate in three forms, including 1) discrete crystalline quartz particles in the white limestone particles, 2) a matrix of microcrystalline quartz in the black particles, and 3) a silicate in mica particles. The primary form is grains of crystalline quartz that range in size from 0.5 to 0.2 mm. These quartz grains typically show uniform extinction behavior when examined in thin sections in the polarized light microscope. In the FPL-3 concretes examined, there was no evidence of any ASR activity in this quartz phase.

Mica is an aluminosilicate mineral that is present in trace amounts as small flakes embedded in the matrix of the white and orange limestone particles and as free grains in the finest material of the bulk aggregate. This silicate material is not susceptible to alkali-silica activity.

Two chert particles were found in the bulk sample of the FPL-3 aggregate that was examined. This component constitutes around 0.1 percent (weight basis). It is expected that chert particles such as these would be susceptible to ASR activity. The small number of these and the expected lack of widespread distribution of the reactive SiO_2 species in a concrete comprised of the aggregate strongly suggest there should not be a significant problem for these concretes in service. The worst case scenario is a popout if one of the chert particles were located near a free concrete surface.

Behavior of the FPL-3 Concretes in the ASTM C 1293 Test: Six concrete series were prepared with the FPL-3 limestone coarse aggregate, and one and two year expansions were listed in Table VIII-5. These results indicate that the five FPL-3 concretes that contained elevated alkali (1.0 and 1.2 percent) showed a slight expansion during the first year of the ASTM C1293 exposure. Expansion for the different concrete series ranged from 0.0089 to 0.0108 percent, thus indicating little variability. The average expansion at one year was 0.0098 percent. Also, there was no significant increase in expansion between years one and two (average of 0.0111 percent after two years). Also, expansion behavior was essentially the same for both high alkali contents (1.0 and 1.2 percent), with and without presence of the lithium admixture. Whatever caused the slight expansion of these concretes during the first year of the ASTM C1293 test ceased during the second. This phenomenon was also observed in the Florida limestone FPL-1 concretes. The

concrete series with normal alkali content (0.5 percent) showed a very slight expansion (0.0020 percent at one year and 0.0008 percent at two years).

Petrographic examination of the FPL-3 concrete prisms after the one and two year exposure revealed no evidence of cracking distress or of any ASR activity. Photographs of prisms 46d and 48d following one year exposure are shown in Figure VIII-28. The molded surfaces of the prisms were free of any exudate. Prism 46d had the highest alkali content (1.2 percent) and no lithium admixture; and, as such, should have the highest potential for ASR activity. In fact, the average one and two year expansions of this concrete (series 46) was lower than all of the other FPL-3 concretes with the exception of series 44, which had the lowest alkali level (0.5 percent).

Summary: The FPL-3 Florida limestone aggregate is relatively pure with a CaO content of around 94 percent and a SiO_2 content (both crystalline quartz and chert) at or below two percent. The SiO_2 phase is primarily present as crystalline quartz with a grain size in excess of 0.05 mm, and this showed normal extinction behavior. This form of quartz is not expected to be vulnerable to ASR, and no petrographic evidence of such activity was found in the FPL-3 concretes.

The chert phase is present as trace numbers of discrete aggregate particles composed principally or wholly of this phase. As such, chert is not widely distributed in this aggregate. Although local ASR activity can be expected when the alkali content of the concrete is high, the worse case scenario in service is popouts when the chert particles are located near a free concrete surface. This assumes that the low level and type of chert seen in the sample that was examined is typical for the FPL-3 aggregate.

The significant observations relating to the performance of the six FPL-3 aggregate concretes in the ASTM C1293 test are summarized below:

- At the normal alkali content of 0.5 percent, prisms showed no significant change in length over the two year exposure period.

- All five of the elevated alkali content (1.0 and 1.2 percent) FPL-3 concretes showed a slight expansion during the first year of exposure. Despite differences in alkali and lithium admixture contents, the magnitude of expansion was similar for the five concretes (range of 0.0089 to 0.0108 percent with an average of 0.0098 percent).

Figure VIII-28: Prisms 46d and 48d following one year of ASTM C1293 exposure. At the highest alkali content of 1.2 percent, prism 46d (no lithium admixture) had a one year expansion of 0.0089 percent. Prism 48d, with

- No significant change in expansion occurred in any of the five elevated alkali content FPL-3 concretes between years one and two of exposure. The average expansion at the end of the second year was 0.0111 percent compared with 0.0098 percent at the end of year one.

- Expansion of the FPL-3 concrete prisms at the end of both the one and two year exposure periods was well below the ASTM C1293 threshold value (0.04 percent at one year).

- None of the six FPL-3 Florida limestone aggregate concretes showed any cracking distress or any ASR activity over the two years of ASTM C1293 exposure.

On the basis of the above results, it is judged that the Florida FPL-3 limestone is a suitable coarse aggregate phase in FDOT Class V concretes intended for use in further study and field trials to evaluate the utility of high-alkali concretes to increase time-to-corrosion in reinforced concrete Florida bridge structures. This recommendation is contingent upon confirmation that the chert identified in the present study of this aggregate occurs in the same form and amount on a global basis for this aggregate source.

Petrographic Analyses - Concrete Series with Coarse Aggregate GG (Georgia Granite)

Physical Features: Figures VIII-29 and VIII-30 show lapped section views of Prism 15a which was prepared with the concrete containing the GG coarse aggregate. Maximum particle size is 25 mm.

Color: The mineral species present in this rock include the light colored minerals 1) albite, the sodium-rich plagioclase feldspar, 2) orthoclase, an alkali feldspar, and 3) quartz. Dark colored minerals include 1) biotite, an iron-rich mica mineral, 2) hornblende, an amphibole mineral, and 3) clinochlore, a chlorite mineral. Albite is the dominant feldspar mineral in this rock. Individual aggregate particles are mixtures of the light and dark minerals. As can be seen in Figures VIII-29 and VIII-30, when viewed with the unaided eye, the particles are light in color for those particles where the light colored minerals dominate. Where the dark colored minerals dominate, the rock particles appear black. Occasional particles exhibit a pink color due to the presence of orthoclase.

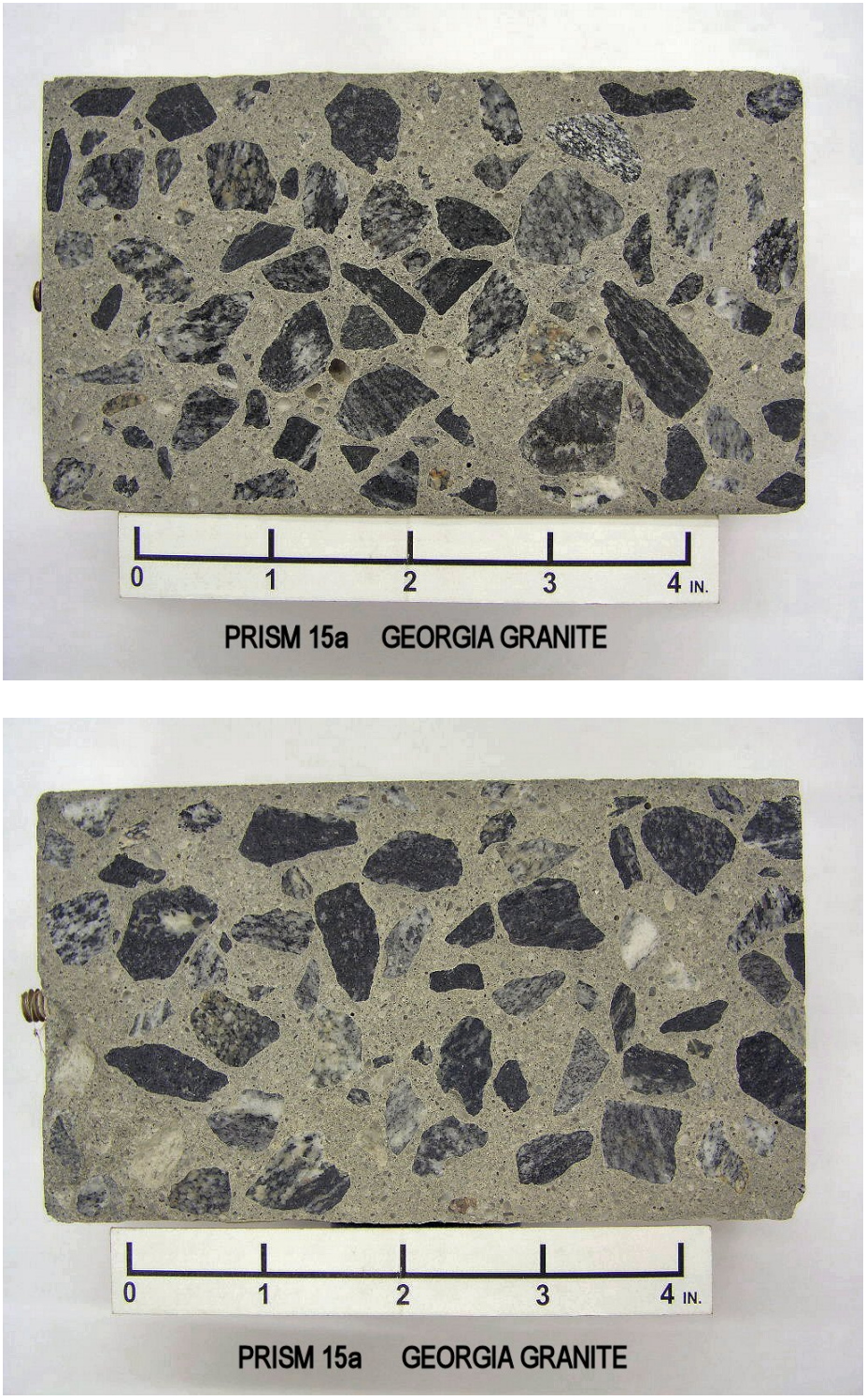

Figure VIII-29: Lapped section views of Prism 15a which contains the Georgia granite coarse aggregate. This concrete contains an alkali content of 1.2 percent and no lithium admixture.

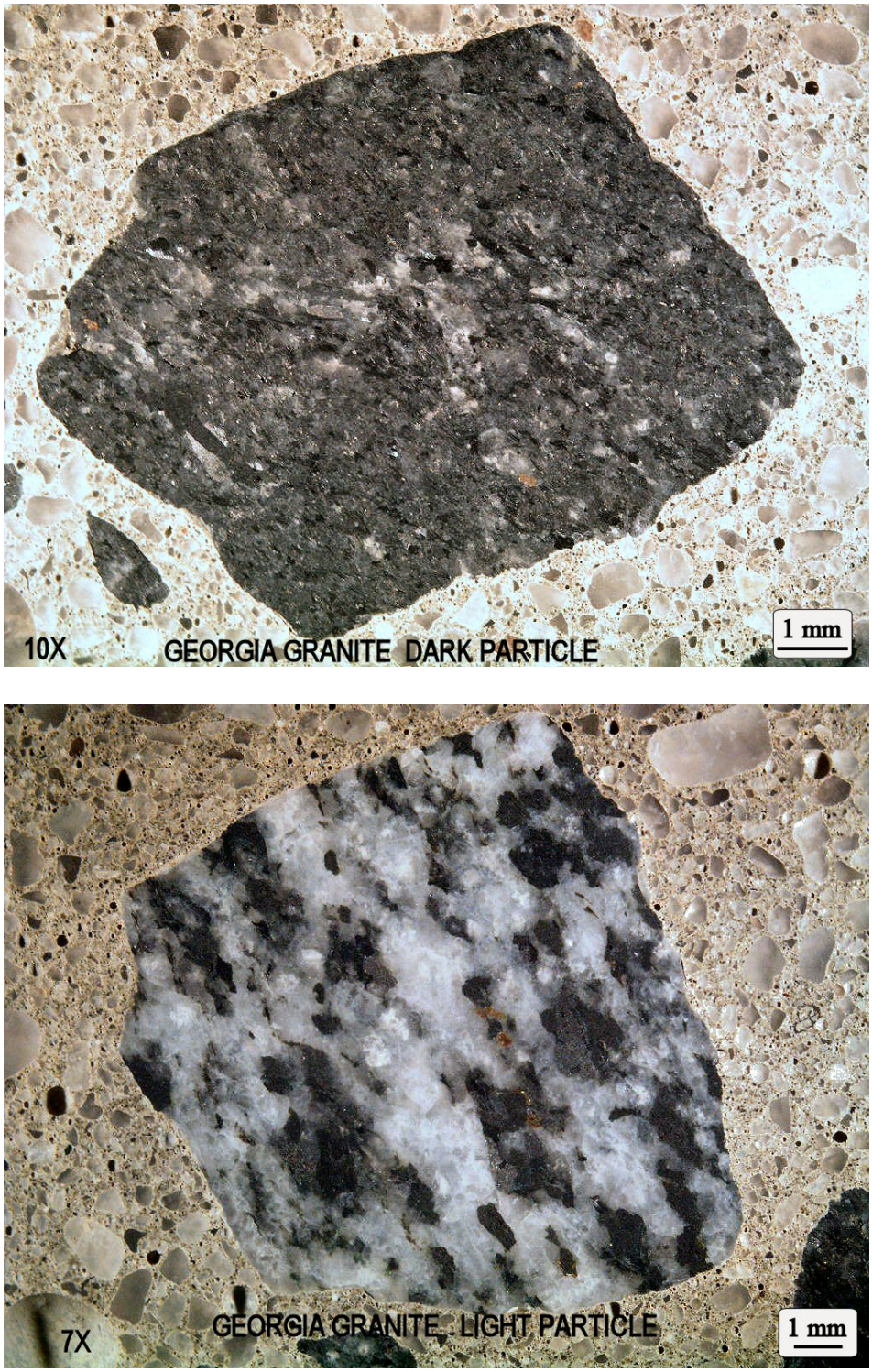

Figure VIII-30: Lapped section views of Prism 15a showing enlarged views (7X and 10X) of a typical dark and light GG coarse aggregate particle.

Shape and Angularity: The aggregate particles are sub-angular to angular with a shape that tends from compact to platy or bladed.

Hardness: Most of the mineral species in this rock are hard, dense, and resist penetration with a steel probe. An exception is the chlorite mineral phase, which is relatively soft and can be easily scratched with a steel probe.

Chemistry and Mineralogy: Chemical analyses (EDX) were made on five GG aggregate particles that were selected to represent the extremes of light and dark mineral content. These analyses showed a range of SiO_2 content of 45 to 70 weight percent with an average of 55 percent. At this intermediate average SiO_2 content and with the plagioclase feldspar dominant over the alkali feldspar, the rock can be classified as a granodiorite or quartz diorite. However, the individual aggregate particles range in composition from dioritic to granitic. This is a medium grained rock with many of the individual particles showing a well developed foliation (various degrees of gneissic banding). This feature indicates that the rock has experienced metamorphic alteration.

The SiO_2 phases in this rock include both crystalline quartz and the silicate phases of the other dominant mineral species. From the point of view of potential ASR activity, the type and distribution of the crystalline quartz phase is of greatest interest.

Individual particles of the GG coarse aggregate show widely varied degrees of metamorphic alteration. In those aggregate particles in which the feldspar phases have undergone extensive alteration, the quartz is present as polycrystalline grains, typically ranging in size from 0.1 to 1 mm. These polycrystalline quartz grains typically have a planar orientation and commonly are present interstitially to the altered feldspar grains. Individual quartz crystallites making up the polycrystalline quartz grains range from as small as 5 μm to as large as 0.4 mm. Quartz crystallites in the 5 to 25 μm size range are common in the heavily altered GG aggregate particles.

Relative to the dark GG aggregate particles, the quartz content is highest in the light-colored particles. In the light-colored ones that do not show extensive alteration, the quartz is typically present as polycrystalline grains up to 3 mm in size. Individual crystallites within the polycrystalline quartz grains range in size from 10 μm to 1 mm. Quartz crystallites in the 10 to 20 μm size range are common. Although most of the quartz grains show uniform extinction in

microscopic examination, some degree of undulatory extinction is present in some of the grains, indicating that the rock has experienced some strain.

The quartz mineral content is lowest in the dark GG aggregate particles and is typically present as single crystal grains ranging in size from 0.2 to 0.5 mm. Most, but not all, of these grains show uniform extinction behavior. Other potentially ASR forms of SiO_2, including classic chert, chalcedony, and opal, were not found in the GG rock particles that were examined.

Behavior of the GG Concretes in the ASTM C1293 Test: Eight concrete series were prepared using the GG coarse aggregate. Expansions for these concretes were summarized in Table VIII-6, which shows the length change of prisms following one and two years exposure. Significant observations regarding the data in Table XIV include the following:

- The concrete containing the normal alkali content of 0.5 percent (Series 05) showed a slight shrinkage at the end of the one and two year exposure period.

- The three high-alkali GG concretes (Na_2O_e = 1.0 or 1.2 percent) with no lithium admixture (Series 04, 14, and 15) showed a one year expansion ranging from 0.0091 to 0.0158 percent with an average of 0.0130 percent, but expansion continued during the second year. The expansion measured at two years for these concretes ranged from 0.0250 to 0.0289 percent with an average of 0.0263 percent.

- Presence of the lithium admixture had a mitigating effect on expansion of the high alkali GG concretes in the ASTM C1293 test. The one year expansion of series 16, 17, 18, and 19 concretes averaged 0.0052 percent compared with 0.0130 percent for the companion concretes with no lithium admixture.

- The series 16, 17, 18, and 19 concretes also showed continuing expansion during the second year of exposure. However, the average expansion measured after two years (0.0111 percent) is less than half that of the companion concretes (series 04, 14, and 15) without the lithium admixture (0.0263 percent).

- The highest rate of expansion of the GG concretes occurred for concrete series 15 which contained the highest alkali level (1.2 percent) and no lithium admixture (0.0158 percent at one year and 0.0289 percent at two).

- Although no expansions of the Georgia granite aggregate concretes exceeded the ASTM C1293 threshold of 0.04 percent at one year, expansion for the high alkali GG concretes with no lithium admixture approached 0.03 percent after two years.

Alkali-Silica Reaction Activity in the GG Concretes: Petrographic examinations of the GG concrete prisms were conducted after one year of ASTM C1293 exposure. At that time none of the eight concretes showed any cracking; however, ASR products were confirmed for the concrete with the highest alkali level (1.2 percent), both with the lithium admixture (series 19) and without (series 15). Each of these concretes is described below.

No Lithium Admixture (concrete series 15): Photographs of Prisms 15a and 19d following one year of ASTM C1293 exposure are shown in Figure VIII-31. This concrete would be expected to have the greatest potential for ASR activity and did show the highest one and two year expansion of the eight GG concretes. When examined after one year, Prism 15a showed no cracking, although as can be seen in the top photograph of Figure VIII-31, the molded sides of the prism exhibited light exudate streaks. White, opaque secondary deposits were also present on air void surfaces in Prism 15a. EDX analyses of the exudate and secondary deposits confirmed that these materials were alkali-silica gel. An EDX analysis of the deposit collected from an air void surface in Prism 15a after the one year exposure period is shown in Figure C-2 (Appendix C). An EDX analysis also confirmed presence of ASR gel on the surface of a granite aggregate particle at this time.

Lithium Admixed (Concrete Series 19): Prism 19d had the same alkali content as Prism 15a but contained the highest level of the lithium admixture. Its one year expansion (0.0059 percent) was less than half that of Prism 15a (0.0158 percent).

Exudate was present on the molded surfaces of Prism 19d after one year of ASTM C 1293 exposure (Figure VIII-31) but to a lesser degree than for Prism 15a. EDX analysis of the exudate material confirmed that it is ASR gel. Figure C-3 (Appendix C) shows the EDX analysis results of secondary deposit material taken from the surface of an air void in Prism 19d following the one year test exposure. This also confirmed that the material is ASR gel.

Evidence of ASR activity was confirmed in the high alkali GG concretes by the presence of ASR gel as exudate on molded prism surfaces, as secondary deposits on air void surfaces, and in

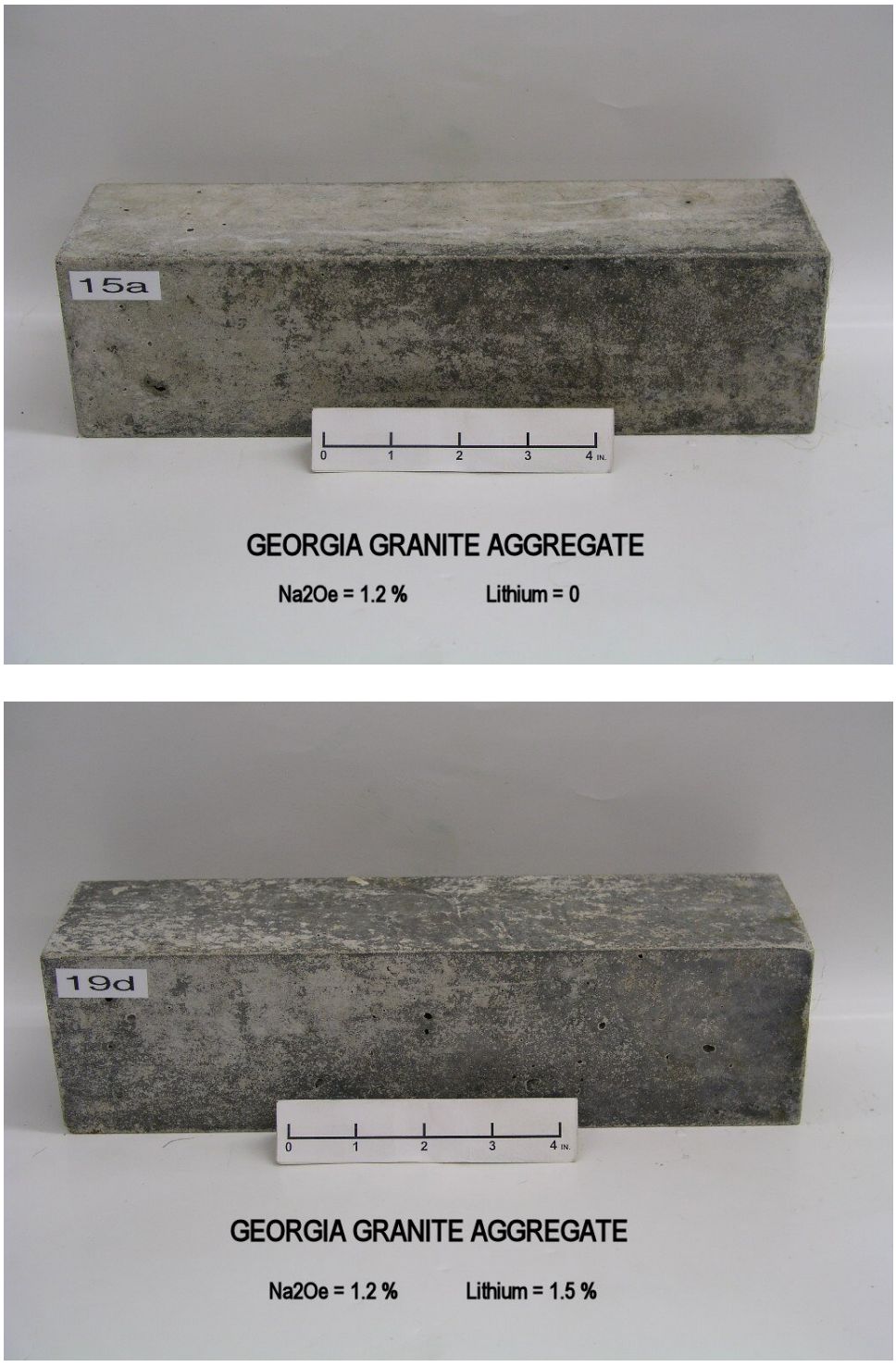

Figure VIII-31: Prisms 15a and 19d following one year exposure in the ASTM C 1293 test.

one case as exudate material on the surface of a granite aggregate particle. No cracking or reaction rims were observed in any of the GG coarse aggregate particles following the one year exposure period.

Summary: On the basis of the above results, it is judged that the Georgia granite coarse aggregate is not a suitable candidate in Class V concretes intended for further study and field trials to evaluate the utility of high-alkali concretes to increase time to corrosion in reinforced concrete Florida bridge structures. This is based on the finding that at the highest level of alkali content (1.2 percent) and even with the benefit of the lithium admixture, GG concretes experienced ASR activity.

Petrographic Analyses - Concrete Series with Coarse Aggregate NG (Nova Scotia Granite)

Physical Features: Figure VIII-32 shows a photograph of a lapped section of Prism 21b prepared with concrete containing the NG coarse aggregate. This is a crushed stone with a nominal maximum particle size of 25 mm.

Color: Enlarged views that reveal extremes in the color of individual NG particles are shown in Figure VIII-33. The aggregate particles are identified as "light-colored" and "dark-colored" in Figure VIII-32. Many of the particles are intermediate to these extremes. This aggregate is a medium-grained rock with very little macroporosity. The light-colored NG particles are primarily the classic pink granite that is shown in the top photograph of Figure VIII-33. The phases here include the light colored minerals 1) albite, the sodium-rich plagioclase feldspar, 2) orthoclase and microcline, which are alkali feldspars, and 3) quartz. The major dark colored mineral in the pink granite is clinochlore, a chlorite mineral. The dark colored NG aggregate particles are dominated by the dark green chlorite mineral clinochlore. The light-colored minerals in the dark particles include the plagioclase feldspar albite, the alkali feldspar microcline, and quartz.

Shape and Angularity: The aggregate particles are angular with a shape that tends from compact to platy or bladed.

Hardenss: Overall the NG aggregate particles are hard and dense although clinochlore, one of the chlorite phases in the rock, is relatively soft and can be scratched with a steel probe.

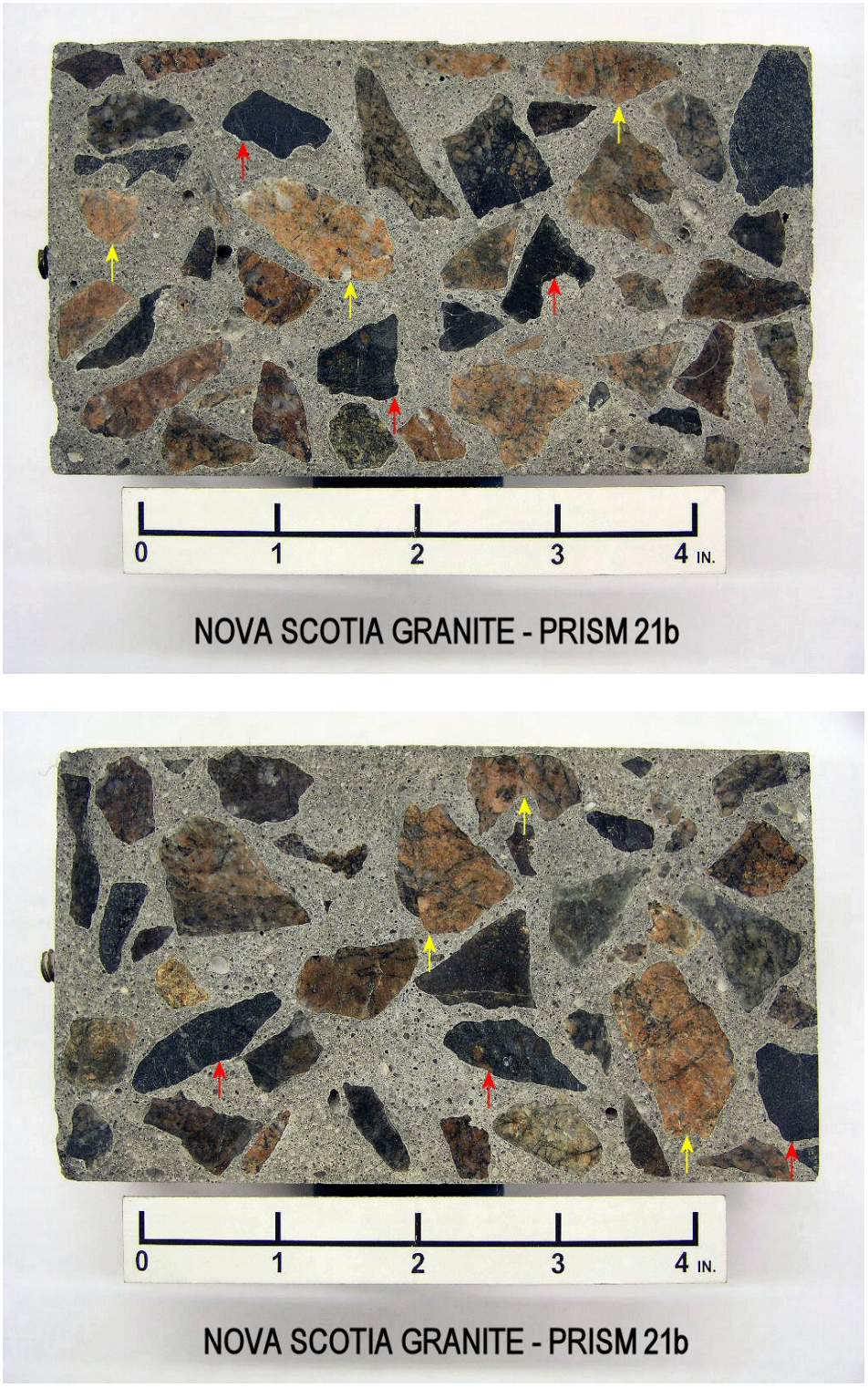

Figure VIII-32: Lapped section views of Prism 21b which contains the NG coarse aggregate. The yellow arrows point to particles referred to as light-colored particles. The red arrows point to particles referred to as dark particles.

Figure VIII-33: Lapped section views of Prism 21b showing enlarged views of the light and dark NG coarse aggregate particles.

Chemistry and Mineralogy: Chemical analyses (EDX) were made on NG rock particles that were selected to span the extremes of light and dark mineral content. The light colored particles show a SiO_2 content as quartz and silicates near 73 percent, placing it firmly in the granite category. The dark particles show high levels of Mg and Fe (ca. 30 percent) with a much lower SiO_2 content (ca 40 percent), reflecting domination of the chlorite phase.

The SiO_2 phases in this rock include both crystalline quartz and the silicate phases of the other dominant mineral species. From the point of view of potential ASR activity, the type and distribution of the crystalline quartz phase is of greatest interest.

Many of the NG particles examined here show extensive fracturing at the microscopic level with the fractures being filled with chlorite minerals or quartz (or both). The fractures are varied in width, ranging from a low of around 10 μm up to 500 μm or more. Figure VIII-34 shows crossed polars thin section views at 100X of one of the granite particles that is intermediate in color to the extremes of light and dark described above. The top photograph in Figure VIII-34 shows microfractures in a feldspar grain, which are filled with microcrystalline quartz. The microfractures in this example are around 10 to 20 μm wide. Many of the microcrystalline quartz particles are in the 5 to 20 μm size range.

The bottom photograph in Figure VIII-34 shows a field of microcrystalline quartz that fills a much wider fracture in the same granite aggregate particle. Many of the quartz crystals are in the size range ≤20 μm which makes them relatively vulnerable to ASR. The microcrystalline quartz is present mainly in the light and intermediate colored particles. Presence of the microcrystalline quartz has led to an onset of ASR in some of the high-alkali NG concretes in this study. In one of the concretes, this has led to cracking distress.

Behavior of the NG Concretes in the ASTM C1293 Test: Eight concrete series were prepared using the Nova Scotia granite coarse aggregate, and expansions for these were summarized in Table VIII-7. Significant observations regarding expansion include the following:

- The concrete series containing the lowest alkali content (series 01 with 0.5 percent alkali) showed a slight shrinkage (ca. 0.0005 percent) at the end of both the one and two year exposures.

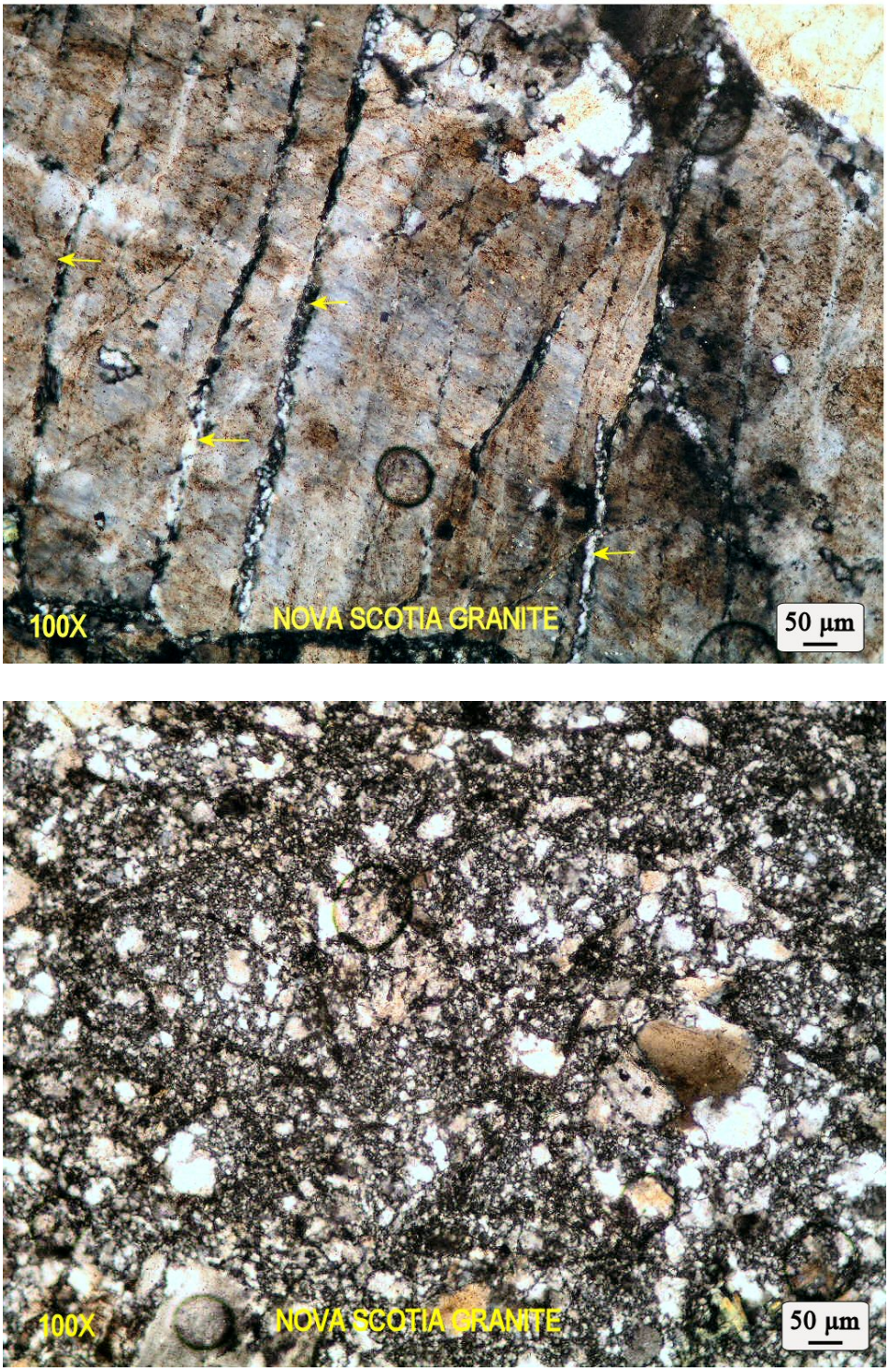

Figure VIII-34: Thin section views (crossed polars) of a NG aggregate particle. The particle is extensively fractured. Top photograph shows fractures in a feldspar grain that have been filled with microcrystalline quartz (arrows). The fractures are 10 to 20 µm wide in this example. The bottom photograph shows a field of microcrystalline quartz filling a larger fracture in the particle. Many of the quartz grains are 5 to 20 µm in size.

- The seven concretes containing the elevated levels of alkali (1.0 and 1.2 percent) all showed an expansion after one and two years. The one year values ranged from 0.0051 to 0.0100 percent, all of which fall below the ASTM C1293 threshold value of 0.04 percent expansion at one year.

- For the three elevated alkali concretes without the lithium admixture (Series 02, 20, and 21) the one year expansions ranged from 0.0051 to 0.0075 percent with an average of 0.0066 percent. The four elevated alkali concretes with the lithium admixture (Series 22, 23, 24, and 25) actually had slightly higher one year expansions which ranged from 0.0073 to 0.0100 percent with an average of 0.0087 percent.

- All of the NG elevated alkali concretes exhibited a continuing increase in expansion during the second year of exposure.

- For the three elevated alkali concretes with no lithium admixture (Series 02, 20, and 21), the two year expansion values ranged from 0.0097 to 0.0160 percent with an average of 0.0139 percent. The four elevated alkali concretes with the lithium admixture (Series 22, 23, 24, and 25) again showed slightly higher two year expansions (0.0137 to 0.0192 percent with an average of 0.0157 percent) relative to the no-lithium concretes.

Alkali-Silica Reaction Activity in the NG Concretes: Petrographic examinations of the NG concrete prisms were conducted after the one year ASTM C1293 exposure. At this time none of the eight concretes showed any cracking; however, all of the high-alkali concretes showed a small amount of exudate material as streaks and patches on the molded prism surfaces.

Photographs of Prisms 21b and 25d are shown in Figure VIII-35 following the one year exposure. Prism 21b was the NG concrete having the highest alkali content (1.2 percent) and no lithium admixture. This concrete would be expected to have the greatest potential for ASR activity. Prism 25d had the same alkali content as Prism 21b but with a high level of the lithium admixture. Surprisingly, the average one year expansion of the series 21 concrete (0.0071 percent) was less than that of the Series 25 concrete (0.0100 percent).

As seen in Figure VIII-35, the cast and molded surfaces of the Series 21 and 25 test prisms show streaks and small patches of white exudate material, the amount of which is greater in the

Figure VIII-35: Prisms 21b and 25d following one year. Neither prism showed any cracking at one year.

concrete without the lithium admixture (Prism 21b). Exudate material was collected from both of these prism specimens for subsequent SEM/EDX examination. Material suspected of being ASR reaction product was also collected from coarse aggregate particles and air void surfaces in these prism specimens and subsequently analyzed by EDX.

Figure C-4 (Appendix C) shows results of this analysis for Prism 21b and confirms that the material is ASR gel. The same is true for material collected as exudate on molded surfaces and as secondary deposits in air voids of this prism. However, only one of three samples from Prism 25d was confirmed as being ASR product with the other two being principally $Ca(OH)_2$, although each spectrum did identify 2 to 3 percent SiO_2. As observed for the GG concretes, the amount of ASR gel that is exudate material and secondary deposits on air void surfaces in the NG concretes was not large, but its presence and the analysis results provide incontrovertible evidence that there was ASR activity in the high-alkali NG concretes after one year

A thorough reflected light microscopy examination of the molded and cast surfaces of the NG concrete prisms at the end of the one year exposure did not reveal any cracking in the prisms. Following this, the prisms that were examined petrographically at one year were sealed in a plastic wrapping and stored at normal ambient temperature prior to a second examination at the end of year two. Cracking associated with the NG particles was observed in Prism 21b, which is the concrete containing the highest alkali level (1.2 percent) and no lithium admixture. Examples of this cracking are shown in Figure VIII-36. The cracks, which originate within the NG particles, pass into the adjacent cementitious matrix phase of the concrete and in some cases traverse the entire aggregate particle. In others, the crack originates in the interior of the aggregate particle before passing into the cementitious matrix. In the example shown in the bottom photograph of Figure VIII-35, a number of air voids near the cement paste/aggregate boundary in the vicinity of the crack are partially filled with a white secondary deposit. In the portions of Prism 21b that were examined, approximately ten percent of the NG particles showed this cracking phenomenon. In all cases, the aggregate particles exhibit coloring intermediate to the light and dark extremes.

Despite the presence of microcrystalline quartz in many of the aggregate particles, expansion of the three high-alkali (no lithium) NG prism specimens was very slight at the end of year one (average of 0.0066 percent). Expansions did continue after the first year, but at the end of the second year the average expansion was still only 0.0139 percent. This relatively modest

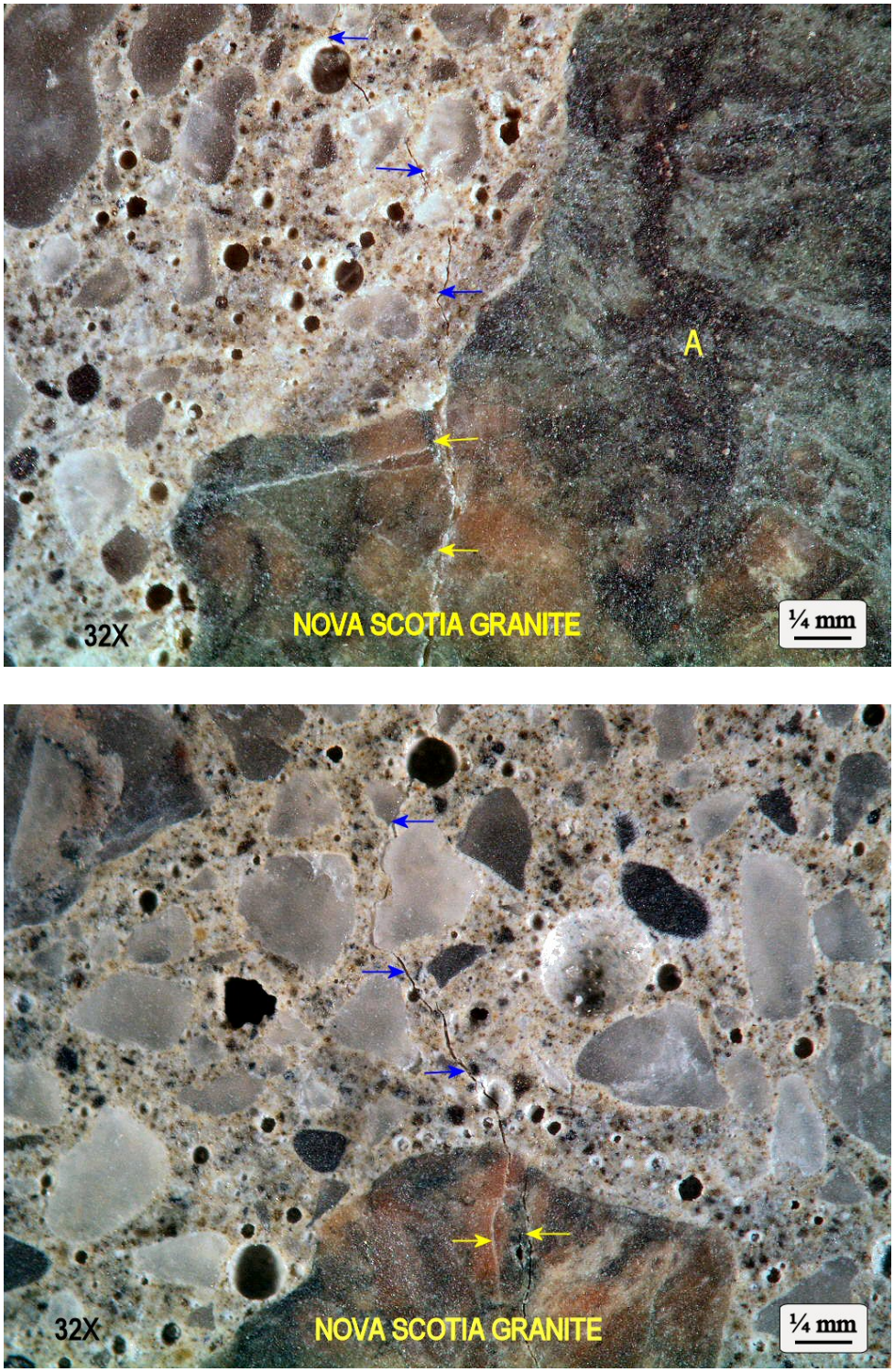

Figure VIII-36: Lapped section views (32X) of NG concrete prism 21b after two years. Cracks (arrows) originating in two of the granite aggregate particles have propagated into the cementitious matrix. Note the white secondary deposits in air voids adjacent to the aggregate particle in the bottom photograph.

expansion can be attributed in part to the presence of FA in the concretes. As will be shown for the Spratt limestone and Sudbury gravel concretes, FA contributed significantly toward mitigating ASR activity in these concretes. However, the low level of expansion in the high-alkali NG aggregate may also be due to the unique microstructure of this rock. Thus, much of the microcrystalline quartz is "entombed" within tight, narrow fractures and, therefore, is not readily accessible to contact by pore water.

Summary: On the basis of the above results, it is judged that the NG aggregate is not a suitable candidate as coarse aggregate for FDOT Class V concretes intended for use in further studies and field trials to evaluate the utility of high alkali concretes to increase time-to-corrosion in reinforced concrete Florida bridge structures. At the highest level of alkali content (1.2 percent), and even with the benefit of the lithium admixture, concretes with this aggregate experienced ASR.

Petrographic Analyses - Concrete Series with Coarse Aggregate H1 (Sprat Limestone)

Physical Features: Figure VIII-37 shows lapped section views of Prism 36d with H1 aggregate particles. As noted above, this is one of two aggregates obtained from the Ontario (Canada) Ministry of Transportation (OMT) from quaries that are known to have a history of ASR activity. The OMT provides these aggregates to researchers who are investigating ASR in concretes. This aggregate, characterized historically as being "highly reactive," comes from the Spratt quarry near Ottawa, Ontario.

Color: The color of the aggregate particles ranges from medium gray to dark gray. Although this is predominantly a finely crystalline limestone, occasional particles (commonly those lighter in color) contain grains in the 0.25 to 1 mm size range. An example of a coarser grained particle is shown in the bottom photograph of Figure VIII-38.

Shape and Angularity: The H1 aggregate provided for this study has angular particles that are commonly platy or bladed.

Hardness: This limestone aggregate is considerably harder and denser and has a lower absorption than the Florida limestone aggregates used in the study.

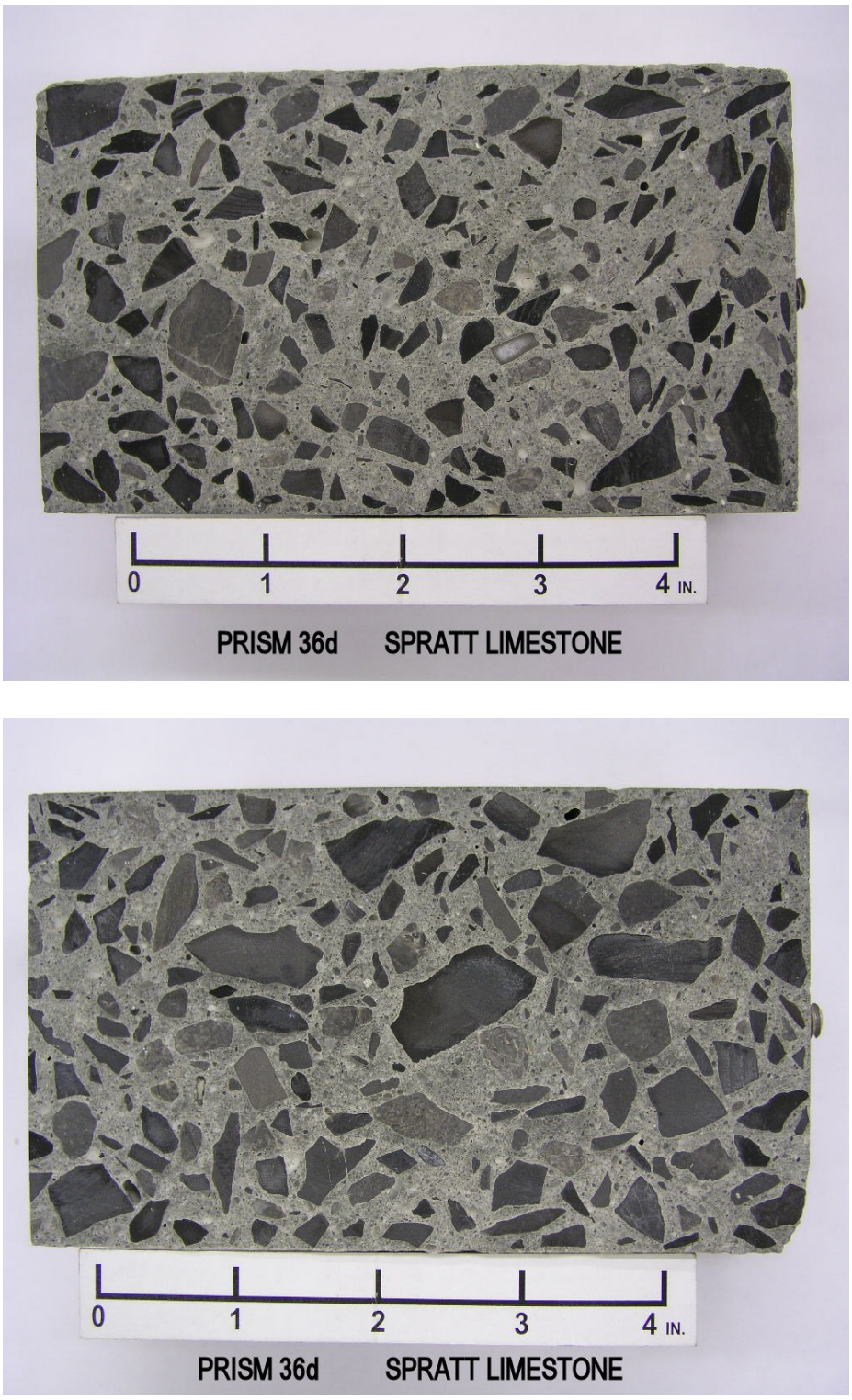

Figure VIII-37: Lapped section views of Prism 36d following one year exposure in the ASTM C 1293 test. This concrete series (36) had an alkali content of 1.2 percent and the higher lithium admixture dosage.

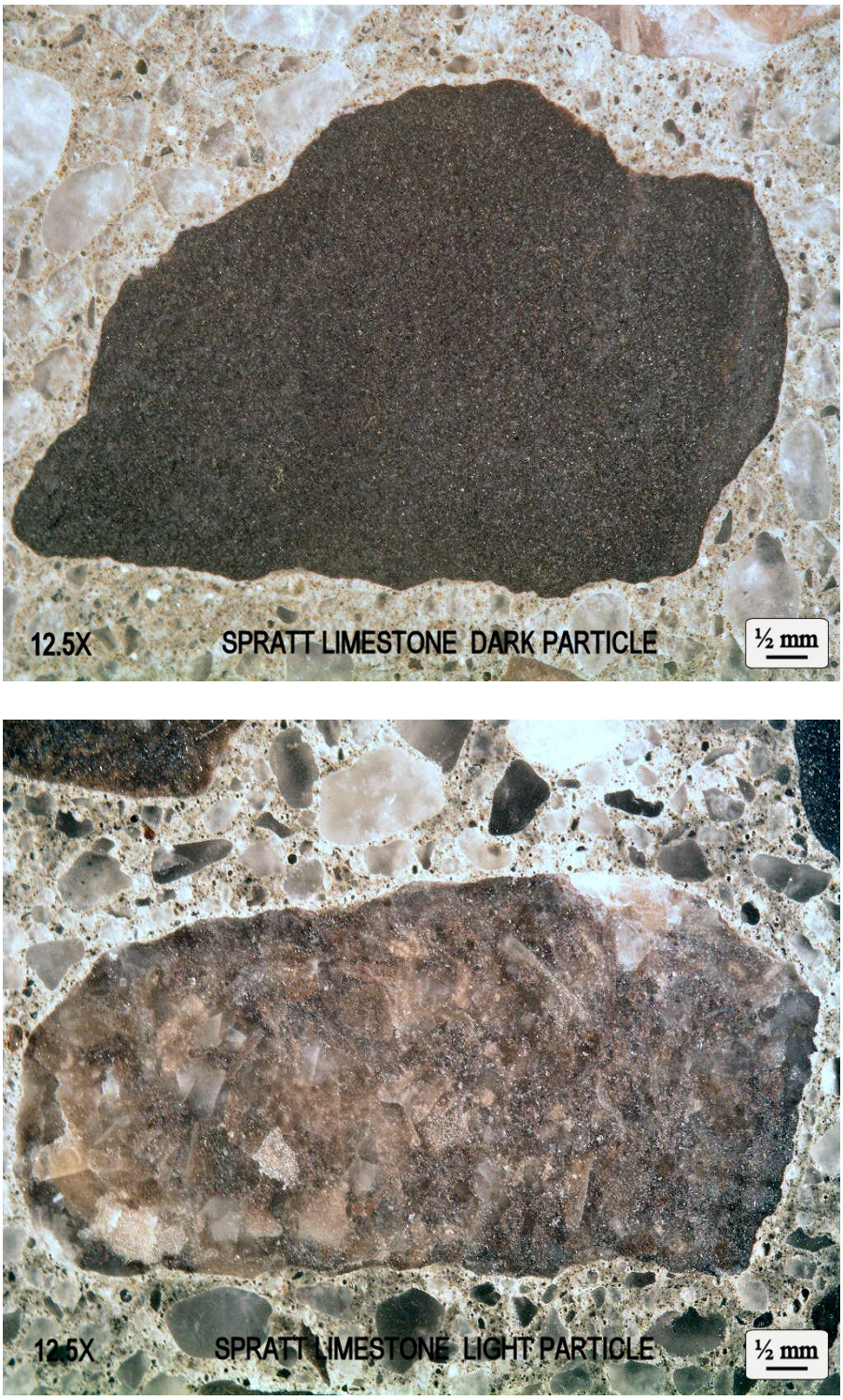

Figure VIII-38: Lapped section photographs of Prism 36d showing enlarged views (12.5X) of a typical dark and light H1 coarse aggregate particle.

Chemistry and Mineralogy: The Spratt limestone is described by the individual who provided the sample for this study as, "A horizontally bedded limestone containing 3 to 4 percent microscopic chalcedony and black chert. The rock consists of calcite and small amounts of dolomite with an insoluble residue of 10 percent, consisting of silica, illite, and pyrite. The principle reactive component is finely disseminated silica not visible with normal optical methods.[77]

A typical fine-grained Spratt Limestone particle was used for EDX chemical analysis. This was performed on minus 50 mesh samples of the entire aggregate and showed a CaO content of 88.1 percent, a SiO_2 content of 11.0 percent, a MgO content of 0.67 percent, and an Al_2O_3 content of 0.27 percent. The XRD analysis of the crystalline mineral phases made on -200 mesh material obtained from a light and a dark particle showed calcite ($CaCO_3$) as the major phase, quartz (SiO_2) as a minor phase, and a small but detectable amount of dolomite (Ca Mg $[CO_3]_2$).

Behavior of the H1 Concretes in the ASTM C1293 Test: Nine concrete series were prepared using the H1 coarse aggregate, and expansion data in the ASTM C1293 test following one and two years exposure are summarized in Table VIII-8. Eight of the nine H1 concretes were prepared with the project concrete (FDOT Class V) which contains 19 percent FA. The presence of the FA had a large moderating effect on the rate and magnitude of the expansions due to ASR relative to the historic performance of the Spratt aggregate in the ASTM C1293 test. The lithium admixture had a further beneficial effect.

Results for the H1 Concrete with No Fly Ash (Series 54): Concrete in this series contained only portland cement as the cementitious phase and an elevated alkali content of 1.0 percent without lithium admixture. These concretes had an average one year expansion of 0.363 percent. In the 1996 multi-laboratory Canadian study,[25] the one year expansion of the Spratt limestone concretes was lower (ca. 0.17 percent). However, for these the cement content was 418 kg/m^3 and the w/cm 0.42 to 0.45. The 2001 study of the Spratt limestone used a lower cement content concrete (348 kg/m^3) and a higher w/cm (0.5);[29] and the one year expansion in this case was ca. 0.30 percent which is close to the value from the present experiments.

The Series 54 concrete specimens reached the ASTM C1293 threshold expansion of 0.04 percent after approximately 56 days, which is in good agreement with the 60 days time reported by the inter-laboratory Canadian study.[25] For the companion project concrete with FA (Series 31), the time-to-threshold expansion was approximately 305 days. In the case of prisms with FA

and lithium (Series 33 through 36) the average two year expansion was 0.0165 percent, and so the threshold expansion was not reached.

Effect of Fly Ash on Expansion of High-Alkali Concretes (Series 30, 31, 32, and 37): The following conclusions were reached regarding the effect of the present FA on expansion of concretes with the H1 coarse aggregate:

- The H1 concrete series of normal alkali content (0.5 percent, Series 30) showed a slight expansion after both one and two years (0.0018 and 0.0034 percent, respectively). This concrete did not show any cracking after two years.

- The three concretes containing elevated levels of alkali (1.0 and 1.2 percent) all showed an expansion after one and two years. The magnitude of this expansion varied depending upon the cement source and alkali content.

- For the three elevated alkali content concretes without the lithium admixture (Series 31, 32, and 37), the one year expansions varied widely (0.0322 to 0.0796 percent). The lowest expansion (0.0322 percent) occurred in the concrete containing the HAC cement (Series 37). The ASTM C1293 threshold expansion of 0.04 percent was reached in the Series 31 concrete (alkali content of 1.0 percent) at around 305 days and in the Series 32 concrete (alkali content of 1.2 percent) at around 230 days. In the multi-laboratory study of the Canadian equivalent of the ASTM C 1293 test,[25] the Spratt limestone concretes reached the threshold expansion of 0.04 percent in about 60 days. The reduced expansion rate of the present concretes containing the H1 coarse aggregate is attributed to the FA.

- Concrete Series 31, 32 and 37 prisms continued to expand during the second year of exposure, although only in the case of the Series 31 did the two year expansion significantly exceed that for the first year.

Effect of Lithium on Expansion of High-Alkali Concretes (Series 33, 34, 35 36): The following observations and conclusions were reached regarding the effect of lithium on expansion of concretes with the H1 coarse aggregate:

- For the four elevated alkali content concretes with the lithium admixture (concrete Series 33, 34, 35, and 36), the one year expansion values ranged from 0.0093 to 0.0142 percent

with an average of 0.0121 percent. Without the lithium admixture the average one year expansion was over four times higher (0.0530 percent).

- The four lithium-containing H1 concretes continued to expand during the second year of exposure and at the end of year two ranged from 0.0149 to 0.0176 percent. The average two year expansion for these series (0.0162 percent) is only twenty five percent of that for companion high-alkali concretes without the lithium admixture (0.0626 percent).

- The lithium admixture at both dosage levels had a significant positive effect on suppressing expansion of concretes with the H1 coarse aggregate. Even after two years exposure, none of the high-alkali lithium concretes had an expansion greater than 0.0176 percent. In this regard, the lithium admixture combined with FA had a much greater effect in reducing the rate and magnitude of ASR-related expansion in the high-alkali H1 concretes than did the FA alone.

Alkali-Silica Reaction Activity in the H1 Concretes: Alkali silica reaction activity was revealed as 1) large expansions (≥ 0.04 percent) of prisms in the ASTM C1293 test, 2) presence of ASR product as exudate on molded and lapped surfaces and as secondary deposits on air void surfaces, and 3) ubiquitous cracking on and within the test prisms. Although the fly ash and lithium admixture significantly reduced the rate and magnitude of expansion, these additives did not completely eliminate ASR in that some of these concretes did show cracking distress. Significant observations relating to suppression of ASR activity by the FA and lithium admixture are summarized below:

- Following the one year exposure, high alkali H1 concrete prisms (Series 31 and 32) had extensive exudate material on the surfaces as shown in the top photograph of Figure VIII-39. These concretes contained the same cement and no lithium admixture. EDX analyses of exudate material and secondary material collected from air void surfaces confirmed that these were ASR reaction product in all cases. An example EDX spectrum of material collected from a secondary deposit on the surface of an air void in Prism 32d at one year is shown in Figure C-5 (Appendix C). The average expansion of the Series 32 concrete at this time was 0.0796 percent. Prisms from the Series 31 and 32 concretes showed cracking distress at one year, as shown in the top photograph of Figure VIII-39 for Prism 32d.

Figure VIII-39: Prisms 32d and 36d following one year exposure in the ASTM C 1293 test. At the highest alkali content (1.2 percent) Prism 32d with no lithium admixture had an expansion of 0.0796 percent. Prism 36d, with the same alkali content and the higher lithium admixture dosage had an expansion of 0.0142 percent. Only Prism 32d shows cracking (arrows).

- As discussed previously, the presence of the lithium admixture in combination with FA had a significant effect in reducing the rate and magnitude of ASR-related expansion in the H1 concretes. This is consistent with the observation that these concretes (Series 33, 34, 35, and 36) showed very little exudate on prism surfaces after one year. The bottom photograph in Figure VIII-39 shows the relatively clean surfaces of Prism 36d (1.2 percent alkali and the higher lithium dosage); however, the EDX analyses from a small amount of exudate material taken from this prism did confirm that this was ASR gel. Average expansion of the Series 36 concretes was 0.0142 percent at one year, and the prisms showed no cracking.

- The portland cement source had a significant effect on ASR activity in the H1 concretes. Concrete Series 37 is a companion concrete to Series 31 with the only intended difference being the source of portland cement. Concrete Series 37, which contains the HA cement, had a one year expansion of 0.0322 percent with very little exudate on the prism surfaces at that time. Concrete Series 31 with the F1 cement had a one year expansion of 0.0473 percent and a large coverage of exudate material that was confirmed as ASR gel on prism surfaces. In this instance, the portland cement source definitely influenced intensity of ASR reactivity for the H1 concretes.

- At the normal alkali content of 0.5 percent (Series 30), the H1 concrete had a very low average one year expansion (0.0018 percent); and the prisms showed virtually no exudate material on molded or cast surfaces. Also, after one year expansion of this concrete was higher than three of the five FDOT relevant coarse aggregates (FPL-1, FPL-2, and NG) but lower for two (FPL-3 and GG) attests to a very low level of ASR activity, if any, in the FA-containing H1 concrete.

Summary: The H1 aggregate was chosen to represent a concrete material with known history of large, destructive ASR. The offending SiO_2 in this aggregate is a very fine-grained quartz phase that is dispersed throughout the particles and has crystallites so small (less than 1 μm) they are difficult to see with ordinary optical microscopy. Both the FA and lithium admixture had the desired effect of suppressing, first, ASR activity and, second, resultant expansion and cracking distress in the seven high alkali H1 concretes that were examined.

The H1 aggregate functioned as a benchmark to provide a well documented service record

as a "highly reactive" aggregate relative to the ASR phenomenon. Performance of the H1 concretes in the present study validated utility of the ASTM C1293 test procedure to provide guideline criteria for identifying Florida coarse aggregates that can be safely used in high alkalinity concretes.

Petrographic Analyses - Concrete Series with Coarse Aggregate H2 (Sudbury Gravel)

Physical Features: The Sudbury aggregate, which is a siliceous gravel, is a complex mix of sedimentary, igneous, and metamorphic rock types that is deposited and mined as a natural gravel. As an example, Figure VIII-40 shows photographs of lapped surfaces from Prism 40d. The material furnished for the current project had a nominal maximum particle size of 19 mm.

Shape and Angularity: This aggregate is comprised mostly of sub-angular to well-rounded particles but with a few of the platy particles having a maximum dimension over 25 mm.

Hardness: Most of the H2 aggregate particles are hard, dense, and resist penetration with a steel probe.

Chemistry and Mineralogy: Sudbury gravel has been characterized by researchers in previous ASR investigations[78] as being composed of the following:

- Abundant volcaniclastic rocks having significant amounts of feldspar and quartz phenocrystals of variable size embedded in a very fine-grained quartz and chlorite matrix (rhyolitic tuffs).

- Common quartzites, sandstones, and feldspar arenites consisting of reworked feldspars and quartz grains and of a cementing matrix ranging from a pure siliceous composition (microquartz) to a mixture of mica and quartz and chlorite.

- Less common gneissic granites with abundant sericite, and

- Rare amphibolite-like rock fragments.

From the above description, it is apparent that the primary contributor to the ASR activity in this aggregate is "microcrystalline quartz" that is present as a constituent of a number of the rock

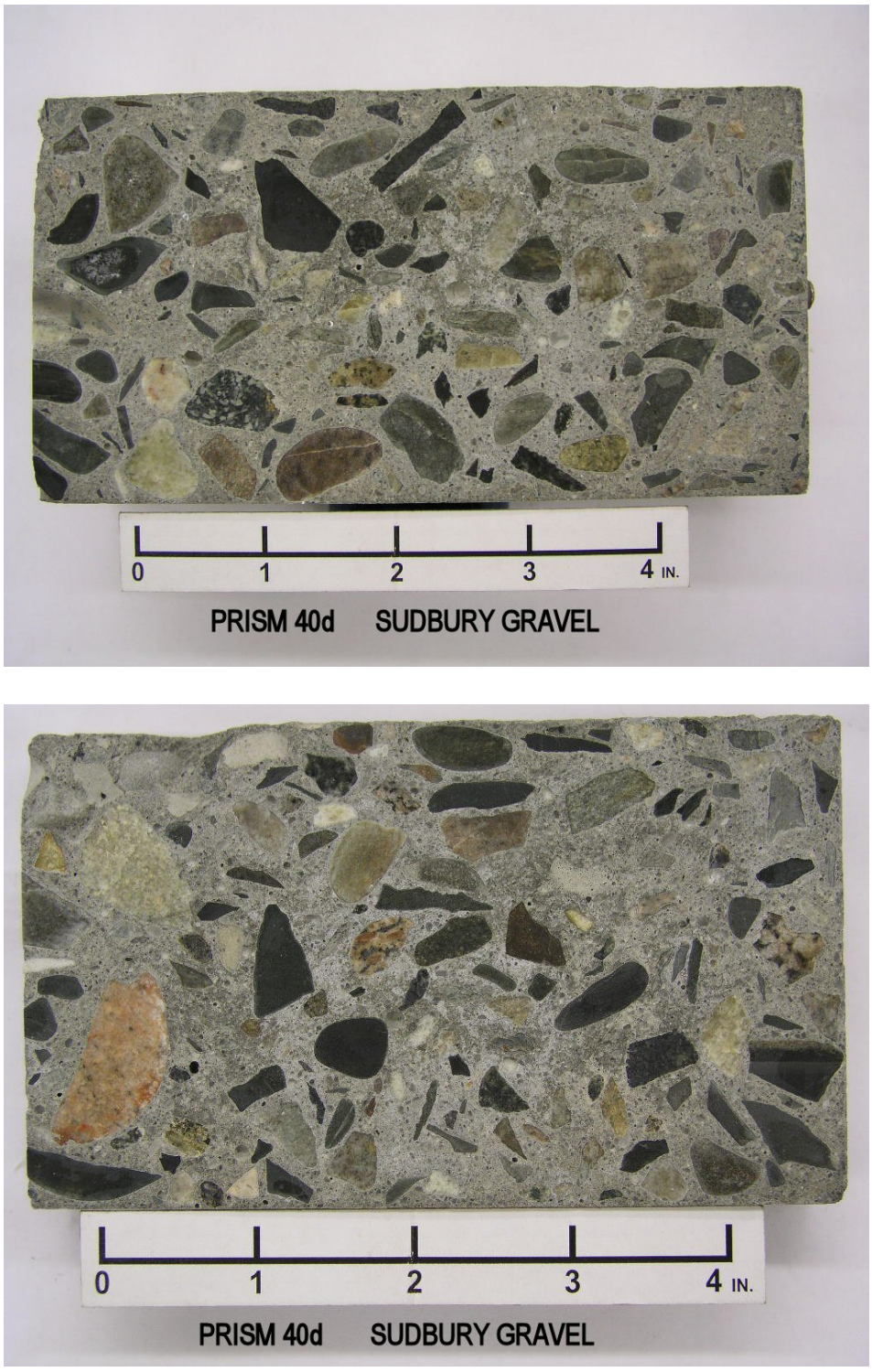

Figure VIII-40: Lapped section views of Prism 36d following one year exposure in the ASTM C 1293 test. This concrete series (40) had an alkali content of 1.2 percent and no lithium admixture.

types making up the gravel. Other authors[79] have identified the reactive component in this gravel as "unstable meta-argillite particles". Alternatively, the Sudbury gravel has been classified as an "argillaceous greywacke."[80]

Behavior of the H2 Concretes in the ASTM C1293 Test: Seven concrete series were prepared using the H2 coarse aggregate with length change behavior during the ASTM C1293 exposure being summarized in Table VIII-9. All of these concretes showed an expansion over the two year exposure; however, with the exception of the concrete prepared without FA (Series 55), the one and two year expansions were below the ASTM C 1293 threshold of 0.04 percent.

Results for the Sudbury Gravel Concretes Containing Fly Ash: Six of the H2 concretes were prepared with the FDOT Class V concrete, for which fly ash is 19 percent of the total cementitious material by weight (concrete Series 38-43). Length change behavior in the ASTM C1293 test is as summarized below:

- The concrete containing the normal alkali of 0.5 percent (Series 38) showed modest expansion (ca. 0.005 percent) at the end of the one and two year exposures. There was no increase in expansion during the second year.

- The three high-alkali H2 concretes (1.0 and 1.2 percent alkali) that contained FA but no lithium admixture (Series 39, 40, and 43) showed a one year expansion ranging from 0.0090 to 0.0144 percent with an average of 0.0124 percent. These concretes continued to expansion during the second year, and expansions after two years ranged from 0.0147 to 0.0323 percent (twice those for year one) with an average of 0.0236 percent.

- Presence of the lithium admixture at the lower dosage had a mitigating effect on expansion of the high alkali H2 concretes, where the one year expansion (Series 41 and 42) averaged 0.0057 percent compared with an average 0.0124 percent for the companion concretes with no lithium admixture. These concretes also showed continuing expansion during the second year; however, the average expansion at two years (0.0078 percent) was only one-third that of the companion high-alkali concretes (Series 39, 40, and 43) which did not have the lithium admixture (0.0236 percent).

- The highest rate and magnitude of expansion of the H2 concretes occurred for Series 39

and 40 which contained high alkali levels (1.0 and 1.2 percent) and no lithium admixture. The expansion for these averaged 0.0142 percent at one year, and this had doubled by the end of the second (0.0280 percent).

- Although none of the fly ash-containing H2 concrete expansions exceeded the ASTM C1293 threshold of 0.04 percent at one year, expansion of the high alkali concretes with no lithium admixture was approaching 0.03 percent after two years.

Results for the Sudbury Gravel Concrete with No Fly Ash: Sudbury gravel aggregate concrete Series 55 contained only portland cement as the cementitious phase (no FA) with an elevated alkali content of 1.0 percent and no lithium admixture. These prisms exhibited an expansion of 0.04 percent (the ASTM C1293 threshold) at approximately 200 days and of 0.1038 percent after one year. In contrast, expansion for companion specimens (same Na_2O_e) with FA (Series 39 and 43) was 0.0139 and 0.0090 percent, respectively. Thus, the Boral Class F FA used in this study provided an order of magnitude reduction in expansions of the high-alkali H2 concretes.

Alkali-Silica Reaction Activity in the H2 Concretes: Petrographic examinations of the six H2 concrete prisms with FA were conducted after the one year of ASTM C1293 exposure. As described for the other concretes, ASR activity was indicated by the presence of, first, exudate material on the molded and cast surface of test prisms and, second, secondary deposit material on the surface of air voids in the concretes. Chemical analyses (EDX) of these materials confirmed that this material was ASR reaction product.

During the one year petrographic examination of the H2 concrete, exudate material was observed on all of the high-alkali concretes (1.0 and 1.2 percent alkali) that did not contain the lithium admixture (Series 39, 40, and 43). Exudate material was also observed on the concrete containing the highest alkali content (1.2 percent) and the lithium admixture (Series 42). At this time, none of these concretes showed any cracking distress; and the amount of exudate on the prism surfaces was not large. Figure VIII-41 shows photographs of Prisms 40d and 42d following the one year test period. A few thin streaks and patches of exudate can be seen on Prism 40d, but only one small patch was present on Prism 42d. EDX analyses confirmed that the exudate material on both prisms was ASR reaction product. The Series 40 concrete has the highest alkali content (1.2 percent) and no lithium admixture. Expansion of the Series 40 concrete at this time was 0.0144 percent. Presence of the lithium admixture in this concrete

Figure VIII-41: Prisms 40d and 42d following one year exposure in the ASTM C 1293 test. At the highest alkali content of 1.2 percent, Prism 40d with no lithium admixture had an expansion of 0.0144 percent. Prism 42d, with the same alkali content and the higher lithium admixture dosage, had an expansion of 0.0069 percent. Neither prism showed any cracking at one year.

reduced both expansion and the amount of exudate produced during the first year of the test. In this case, the one year expansion of the Series 42 concrete was less than 50 percent of that for the concrete without the admixture (Series 40).

An example EDX spectrum from secondary deposit material taken from the surface of an air void in Prism 40d that confirms the material collected from the molded surfaces (exudate) and air voids (secondary deposits) in prism specimens 40d and 42d is alkali-silica gel is shown in Figure C-6 (Appendix C). As noted previously, no cracking was observed in the FA containing H2 concretes through the first year of exposure; and expansions in these concretes at one year were under 0.0144 percent. However, cracking was observed in the high-alkali H2 concretes without the lithium admixture at 400 to 450 days; and the two year expansions ranged from 0.024 to 0.032 percent (Series 40 and 39).

Summary: ASR activity was confirmed in the high alkali H2 concretes by the presence of ASR gel as exudate on molded prism surfaces and as secondary deposits on air void surfaces. Cracking occurred in the highest-alkali concretes with no lithium admixture after 400 to 450 days exposure in the ASTM C 1293 test. The H2 coarse aggregate functioned as a benchmark material with a well established service record as a "moderately reactive" aggregate relative to the ASR phenomenon. In this context, it provided valuable insight into the effectiveness of the Boral FA and lithium admixture in suppressing expansion and subsequent cracking distress that accompanies ASR activity in concretes.

Alkali Silica Reaction Summary Based on Prism Length Change and Petrography

Table XXII summarizes the prism length change and petrographic results for prisms with Na_2O_e = 1.2 and no lithium admixture, which should be the most ASR susceptible for each of the respective concrete series. While all of the concretes with Florida relevant coarse aggregates (FPL-1, FPL-2, FPL-3, GG, and NG) had one year expansions below the ASTM C1293 threshold criterion of 0.04 percent, only two (FPL-1 and FPL-3) qualified petrographically as not exhibiting indications of ASR.

Compressive Strength

Figures VIII-42 and VIII-43 show the average compressive strength of three identical

Table VIII-14: Summary of length change and petrographic observations for Na_2O_e concretes without lithium admixture.

Prism No.	Coarse Aggr. Type	Average Expansion of Na_2O_e = 1.0 and 1.2 Percent Prisms, percent		ASR Confirmed by SEM	Cracking On Molded or Cast Surfaces After One Year
		One Year	Two Years		
9b	FPL-1	0.0065	0.006	NO	NO
27d	FPL-2	0.0152	0.0236	YES	YES
46d	FPL-3	0.0089	0.0097	NO	NO
15a	GG	0.0158	0.0289	YES	NO[a]
21b	NG	0.0071	0.016	YES	NO[b]
32d	H1	0.0796	0.0801	YES	YES
40d	H2	0.0144	0.0281	YES	NO[a]

a. Cracks observed on molded/cast surfaces after 400-450 days exposure.
b. Cracks that extended into the adjacent cement paste phase observed in several aggregate particles.

cylinders of each mix at 28 and 365 days, respectively. Results for individual tests are listed in Appendix D. Although all concrete batches were based on the same FDOT Class V concrete mix design, compressive strengths varied from 20 to 55 MPa (2,899 to 7,971 psi) depending principally on the aggregate type. Mixes containing aggregate FPL-1 exhibited the highest strengths, followed by FPL-2, H1, H2, NG, GG, and FPL-3. In general, the crushed aggregates (FPL-1, FPL-2, FPL-3, and H1) with rougher surfaces and irregular shape provided a stronger mechanical bond than the more rounded gravel stone types (H2, NG, and GG). An exception to this trend was FPL-3; however, as noted above, material from this source was judged be unclean and of generally poor quality.

It is recognized that, subsequent to adequate curing, FA enhances concrete strength as a consequence of its pozzolanic nature which yields a less porous paste microstructure than that of plain cement. Figure VIII-44 shows compressive strength at 365 days for specimens with and without admixed FA and NaOH and three different coarse aggregates. While the beneficial effect of FA upon compressive strength is clear, also apparent is that admixing with NaOH caused some strength reduction. The latter finding was probably a result of ASR in conjunction with the elevated Na_2O_e, although a more porous paste at the elevated alkalinity level may also have contributed.[55]

Figure VIII-45 shows the average compressive strength for each mix and coarse aggregate type at 365 days. This indicates that for mixes with coarse aggregates FPL-1, FPL-2, GG, and H1

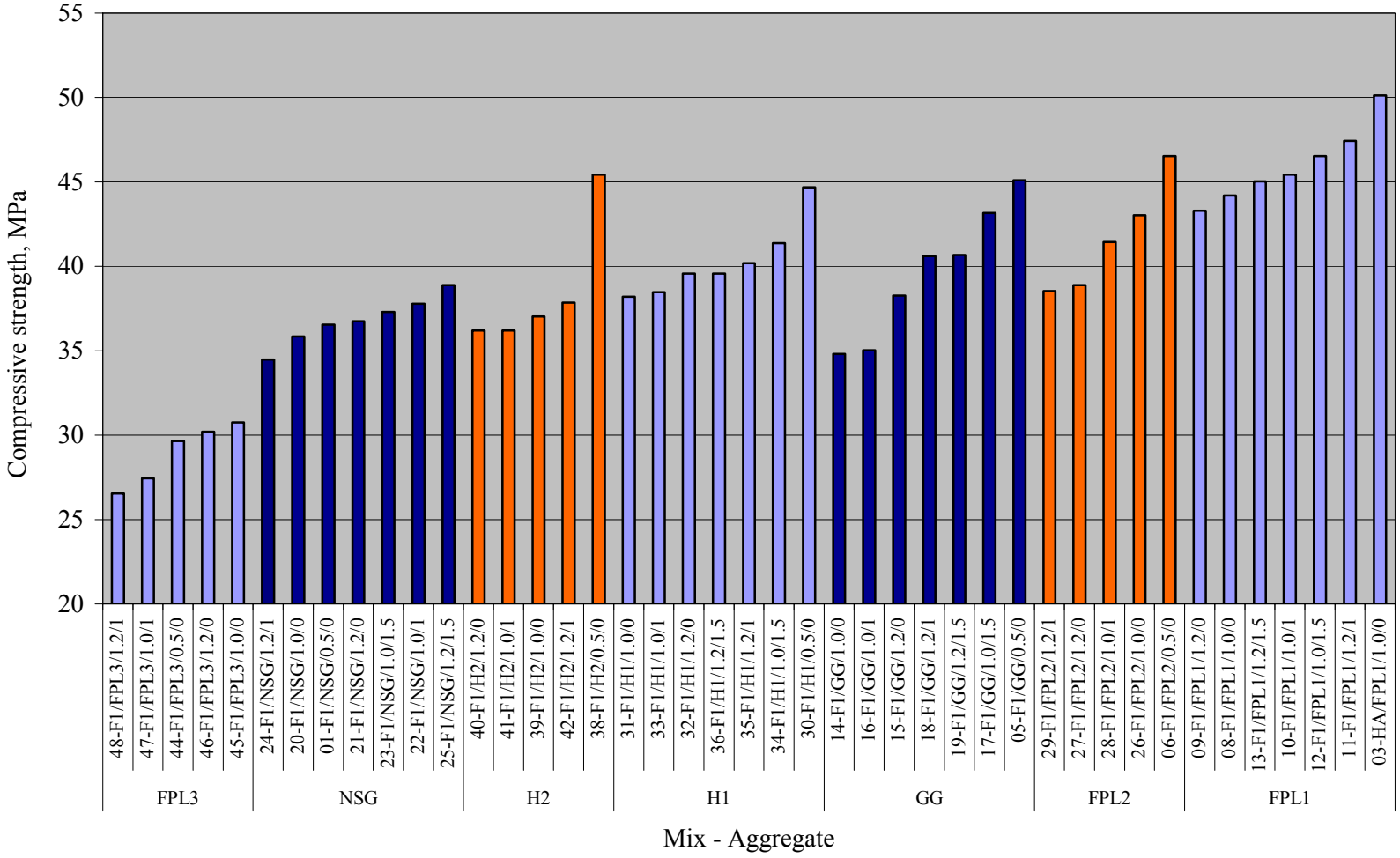

Figure VIII-42: Average concrete compressive strength at 28 days.

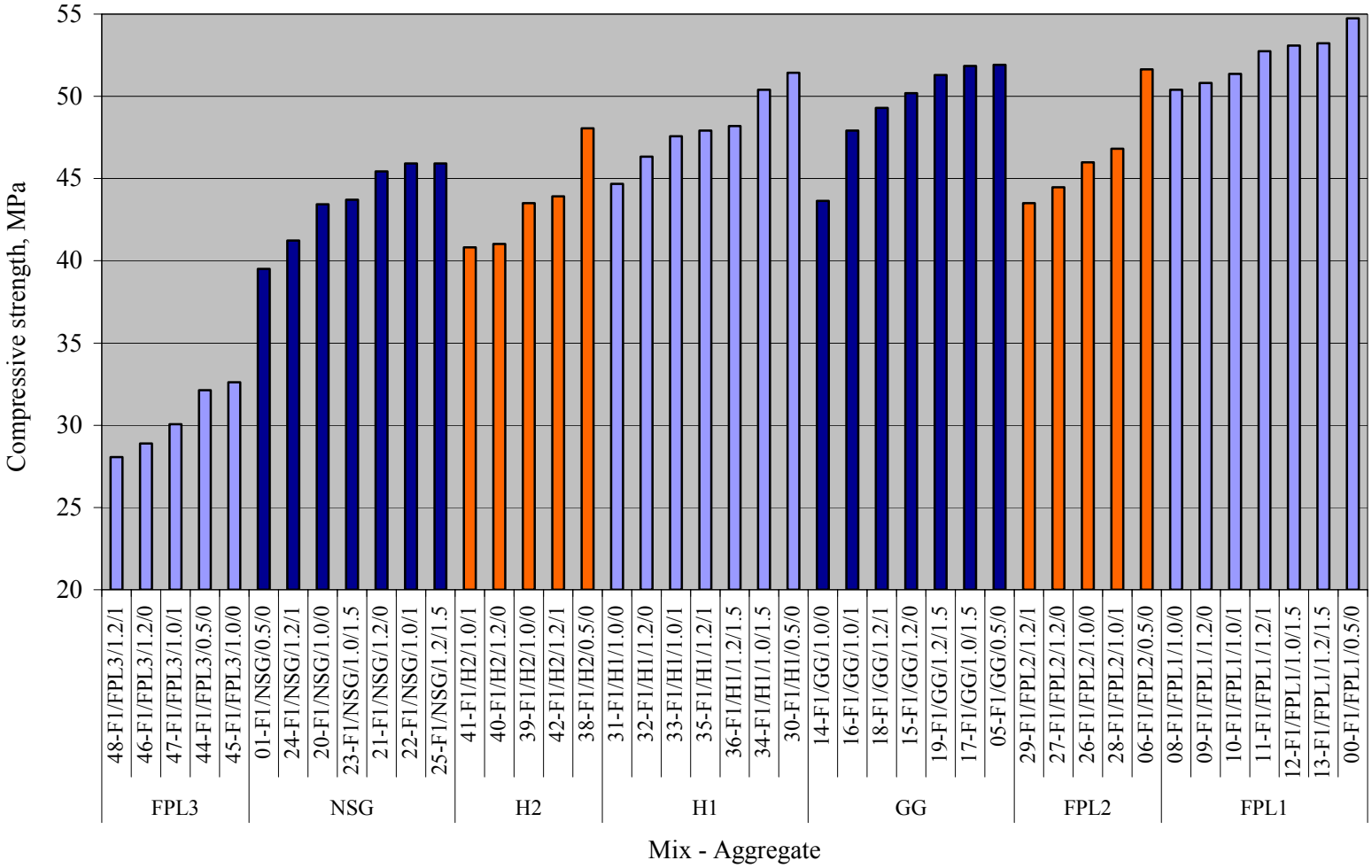

Figure VIII-43: Average concrete strength at 365 days.

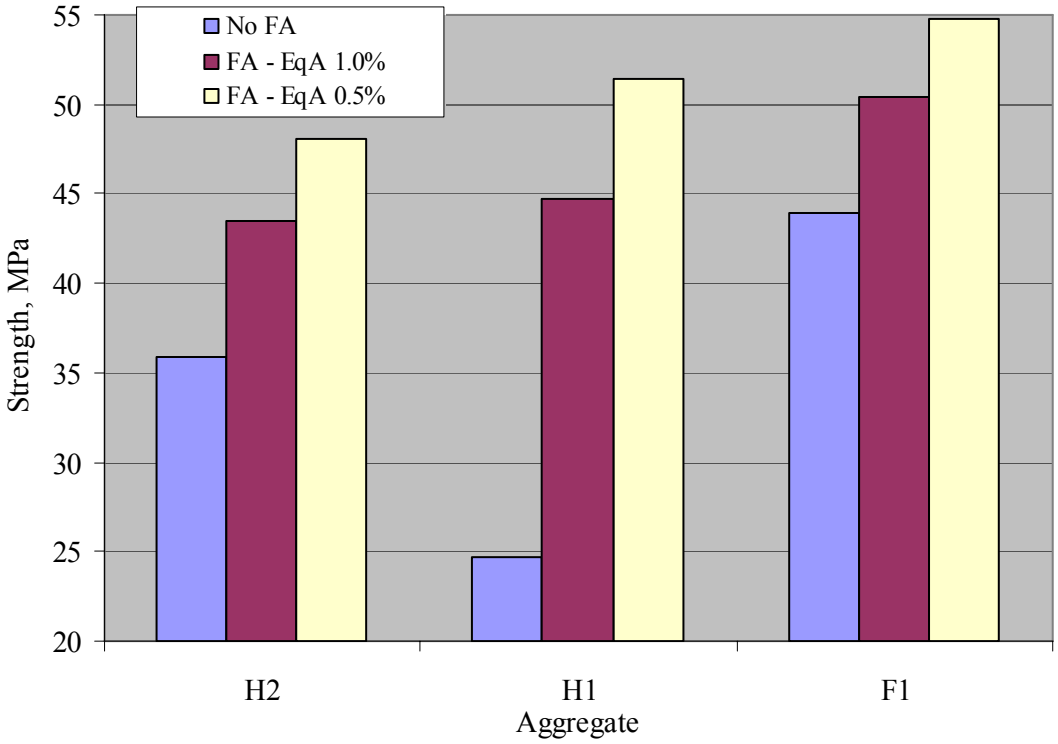

Figure VIII-44: Effects of FA and NaOH on concrete compressive strength.

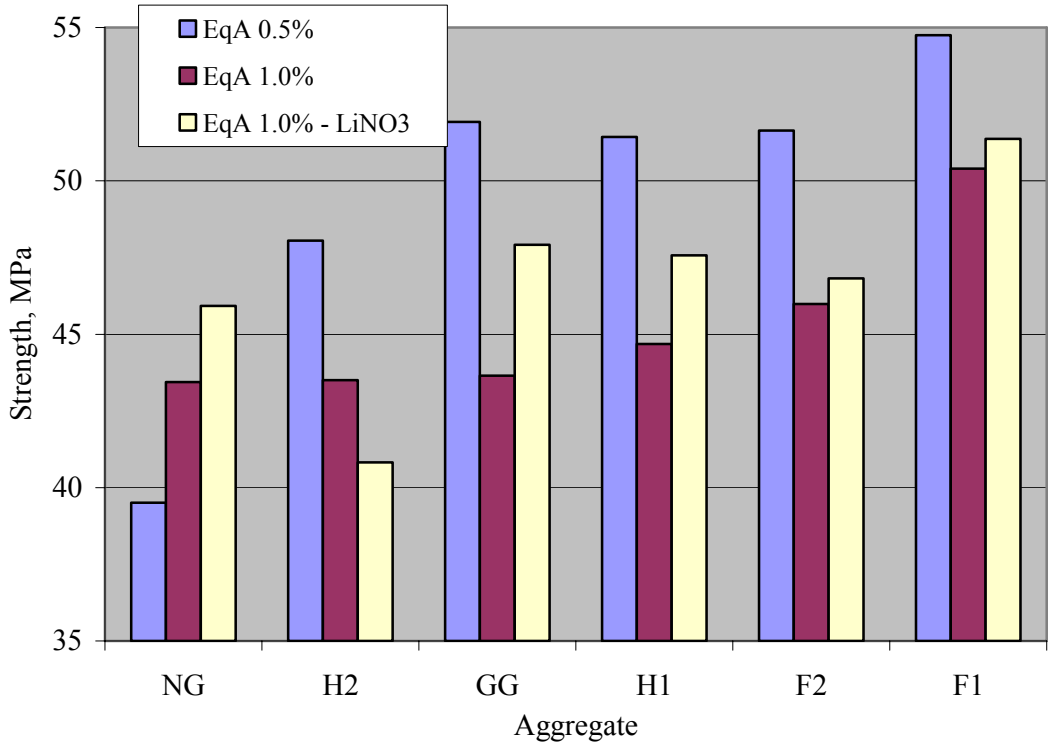

Figure VIII-45: Effects of NaOH and $LiNO_3$ on the concrete compressive strength of the different mixes at 365 days.

strength was highest for the Na_2O_e = 0.5 mixes, followed by those with Na_2O_e = 1.0 and admixed $LiNO_3$, and lastly Na_2O_e = 1.0 without $LiNO_3$. This ordering is consistent with mixes that promoted ASR having lowered strength. For mixes with the H2 coarse aggregate, the Na_2O_e ones with admixed $LiNO_3$ had the lowest strength, whereas for NG ones the Na_2O_e = 0.5 mixes were of lowest strength. The reason for this is unclear but may relate to these aggregates being rounded stone rather than crushed gravel and reduced aggregate-paste bond, as discussed above.

Figure VIII-46 plots the percentage difference of the 365 day strength to that at 28 days. The results suggest that any affects of the NaOH and $LiNO_3$ admixtures and of ASR, where this occurred, did not significantly alter the normal trend where strength increases with time. This is consistent with the understanding that any ASR induced microcracking would not be expected to significantly affect compressive strength.

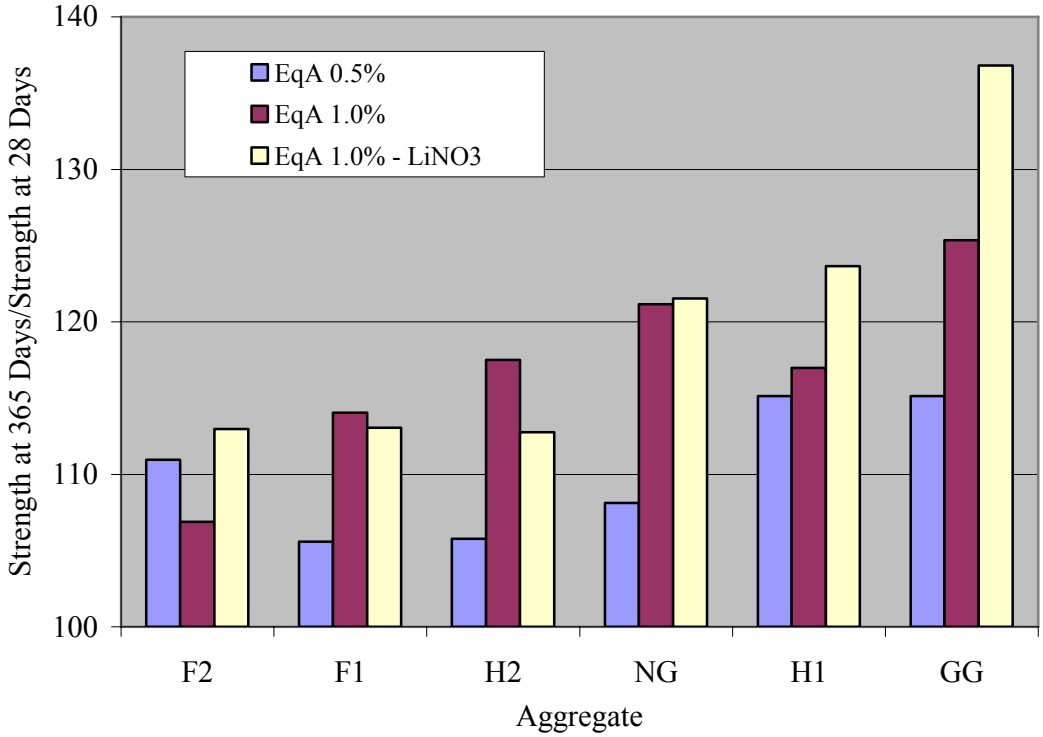

Figure VIII-46: Effect of NaOH and $LiNO_3$ on the compressive strength at 365 compared to 28 days.

Flexural Strength

While concrete per se is normally designed with compressive loadings in mind, there are situations where tensile stresses occur, particularly for members such as pilings. Consequently,

flexural strength tests were also performed on specimens that represented the range of ASR damage.

Figure VIII-47 shows a photograph of the test setup with a specimen still in place after testing to failure. Table VIII-15 lists the modulus of rupture that was measured for individual specimens that were tested according to ASTM C78.[81] The results are generally consistent with FA and $LiNO_3$ having a beneficial effect on flexural strength and high Na_2O_e (without $LiNO_3$) having a negative effect, although only limited data are involved. Figure VIII-48 shows a magnified view subsequent to flexural testing of the tensile (bottom) face of specimen 54b

Figure VIII-47: Specimen 54b after flexural stress testing.

Table VIII-15: Modulus of rupture of selected concrete prisms.

Mix	Modulus of Rupture, MPa
10/F1/F1/1.0/1	7.2
27/F1/F2/1.2/0	3.1
28/F1/F2/1.0/1	4.8
33/F1/H1/1.0/1	7.8
54/F1/H1/1.0/0/NF	2.7

Figure VIII-48: Photograph of the bottom (tensile) face of the specimen of mix 54 showing the primary fracture (top to bottom) and highlighted ASR microcracks.

(54/F1/H1/1.0/0) which had no FA. Here, the major fracture is from top to bottom in the figure; and ASR micro-cracks, which are mostly horizontal, have been highlighted.

Figure VIII-49 provides a plot of compressive versus flexural strength for specimens that were tested according to the latter method. Disregarding the specimen without FA (54/F1/H1/1.0/0/NFA), flexural strength was lowest for the specimen without $LiNO_3$ and highest for the two specimens with Na_2O_e = 1.0 and admixed $LiNO_3$. This ordering is generally consistent with expected occurrence of ASR (greater strength, less ASR). Because the difference in flexural strength for these four specimens is by a factor of 2.5, flexural strength may be a more sensitive and revealing indicator of ASR than is tensile strength.

Electrical Resistivity

Figures VIII-50 to VIII-56 show electrical resistivity versus time data for each set of specimens with the same coarse aggregate. Maximum and minimum readings for individual cylinders of each series are indicated by the range bar upon each data column. All concretes

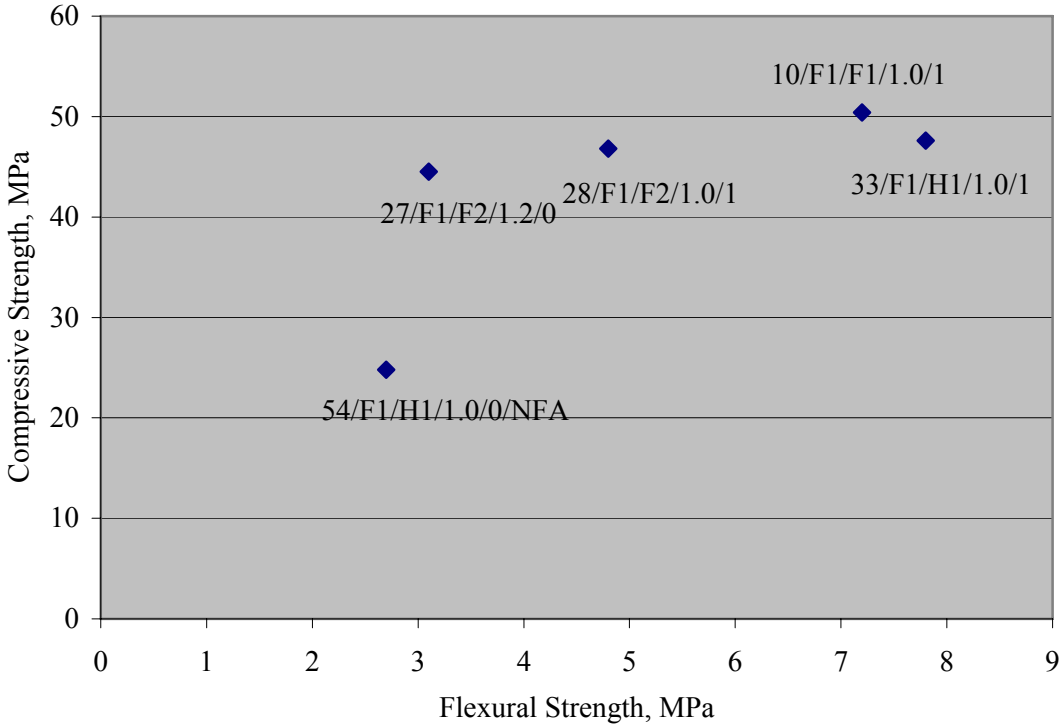

Figure VIII-49: Plot of compressive versus flexural strength for prism specimens.

exhibited a resistivity greater than 21 kOhm·cm and, therefore, are classified as low permeability in accordance to Table II. With a few exceptions, resistivity increased with time, as is normally expected because of continued cement hydration. For instances where mixes exhibited ASR, the resistivity decrease with time can be explained by development of the conductive gel. No explanation is apparent, however, for the resistivity decrease in cases where ASR was minimal or not detected.

Although electrical resistivity and its inverse, electrical conductivity, are thought to depend primarily on properties of the cementitious paste, the results reflect an influence of the coarse aggregate as well. This is illustrated by the representation in Figure VIII-57, where average resistivity of all concrete series at 365 days is presented in the same plot.

Qualitatively, concrete permeability depends on two characteristics of the paste: first, the concrete pore structure as this reflects tortuosity and path length for diffusing ions and, second, composition of the pore water. Consequently, most aggregates are viewed as obstacles to diffusion that increase tortuosity, although some, such as those classified as ASR-reactive, can effect chemistry of the pore solution as well. In contrast, chemical admixtures modify the pore

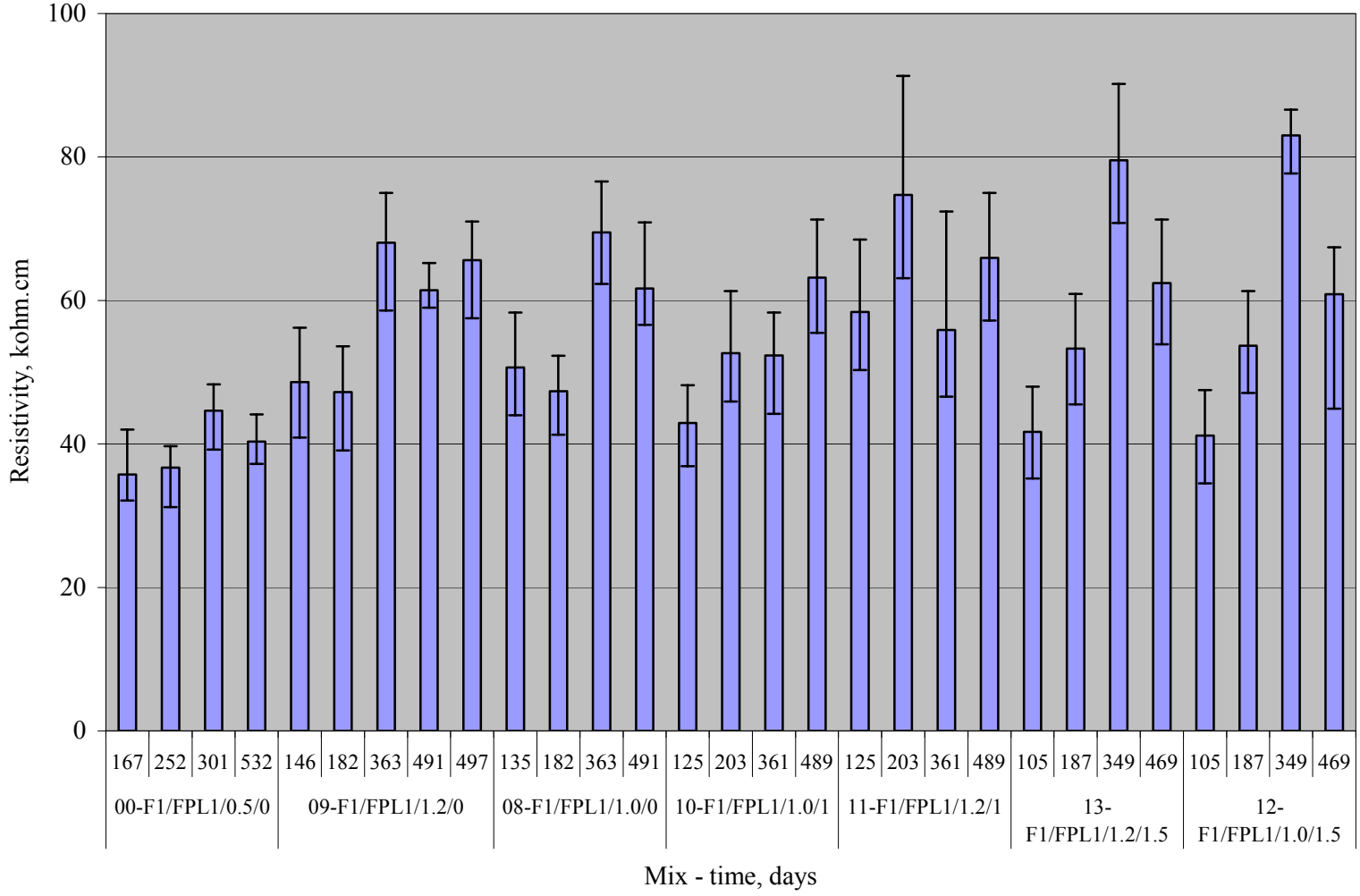

Figure VIII-50: Concrete resistivity on mixes containing Florida porous limestone FPL-1.

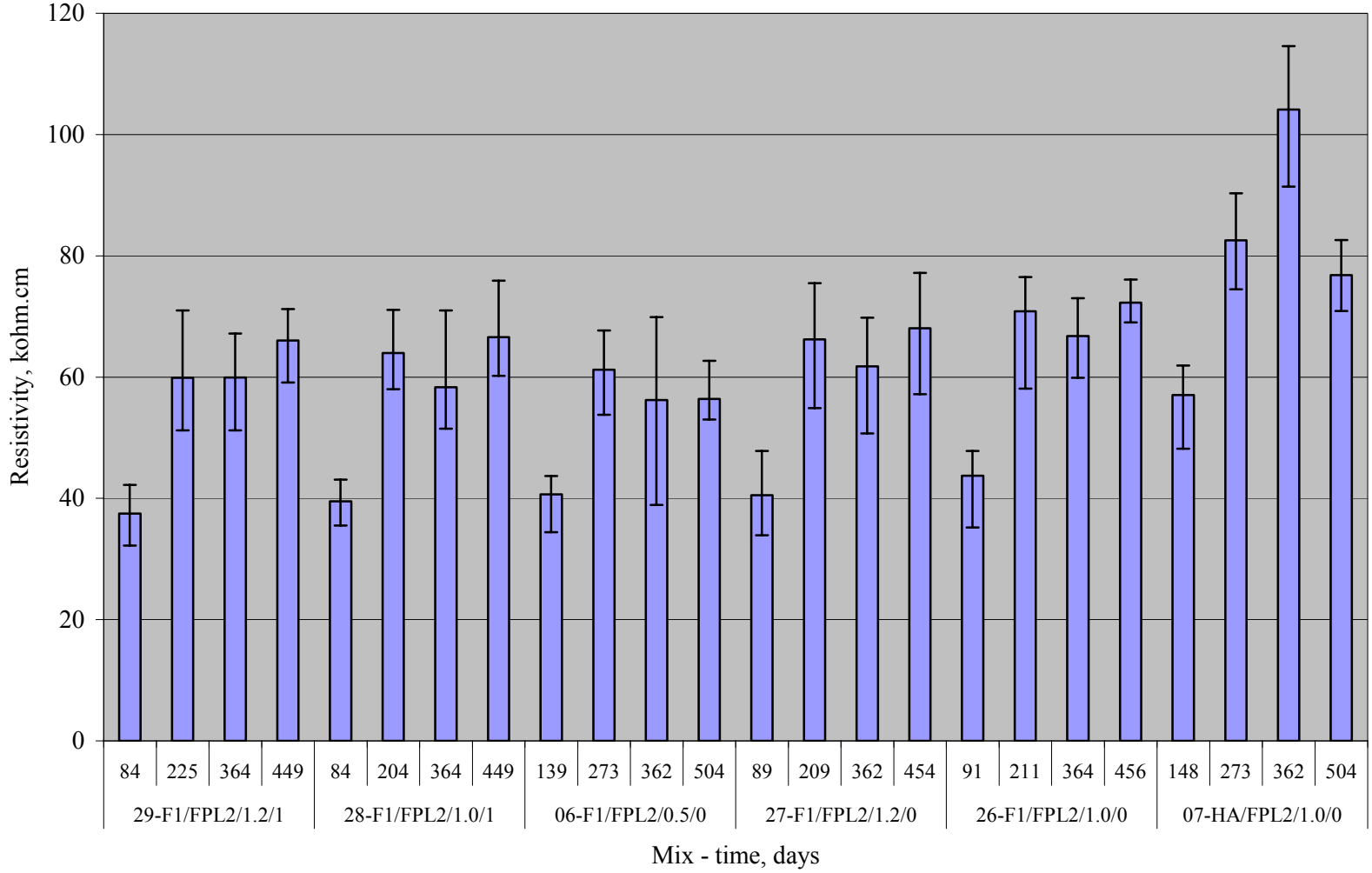

Figure VIII-51: Concrete resistivity on mixes containing Florida porous limestone FPL-2.

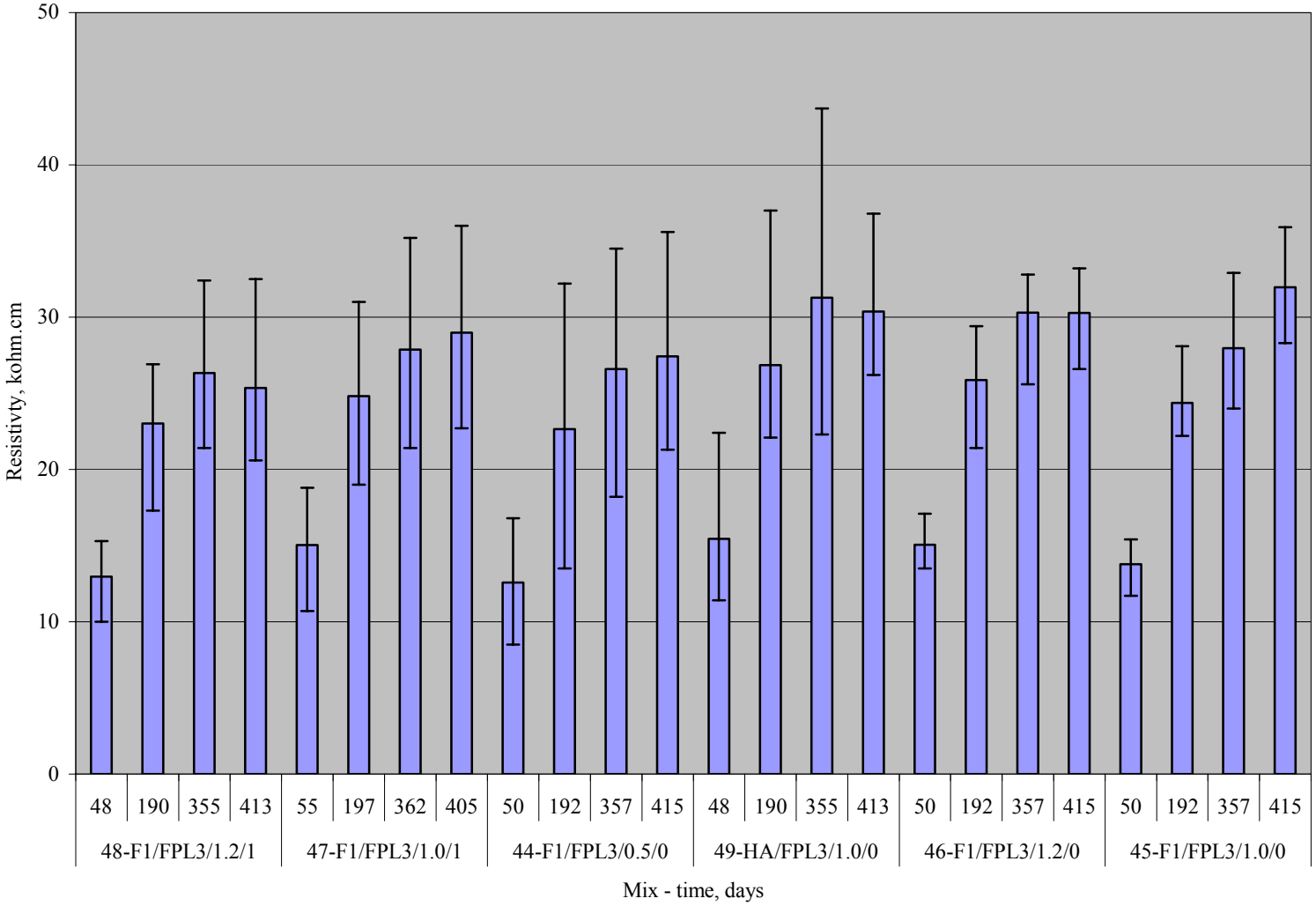

Figure VIII-52: Concrete resistivity in mixes containing Florida porous limestone FPL-3.

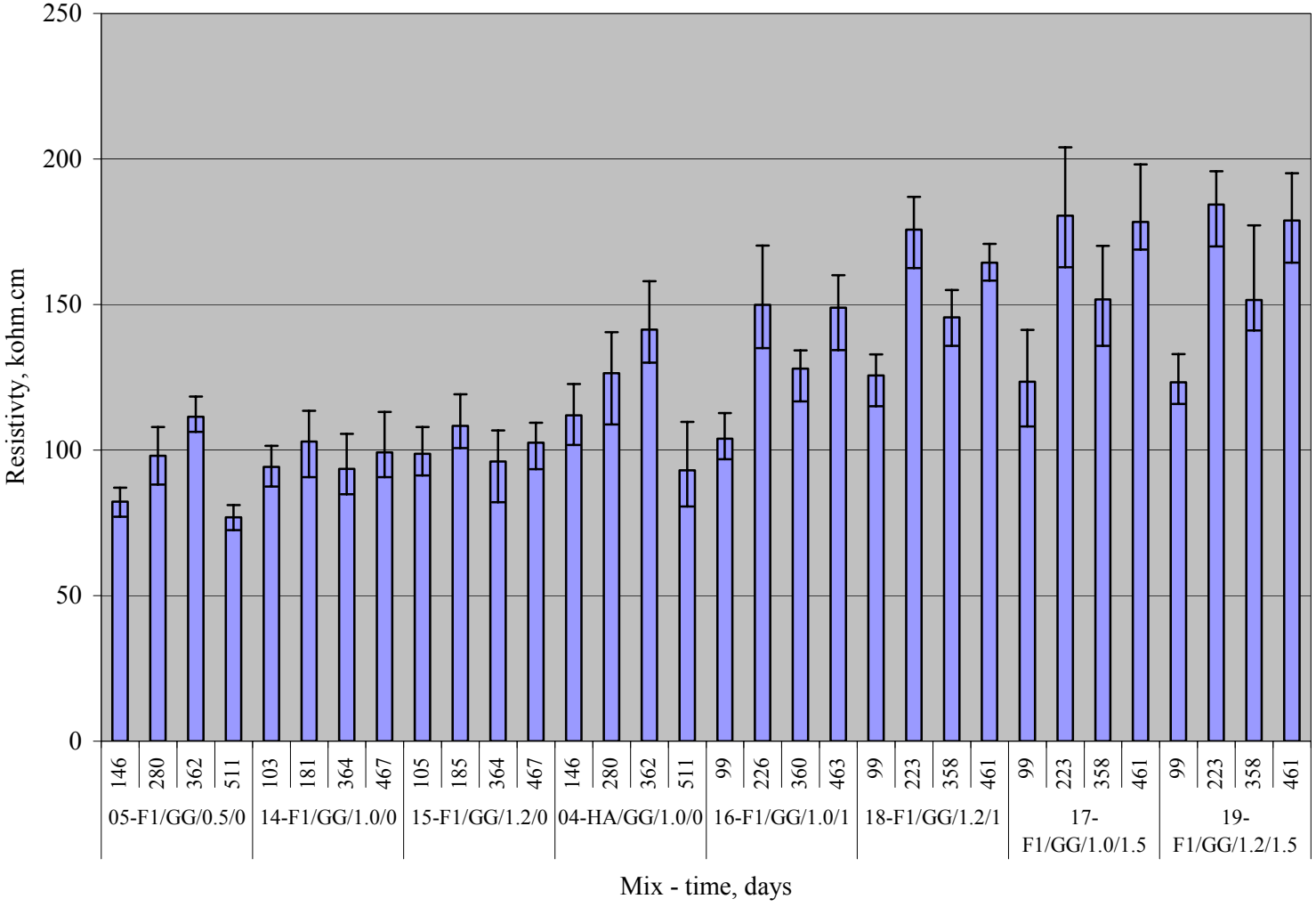

Figure VIII-53: Concrete resistivity in mixes containing Georgia granite (GG).

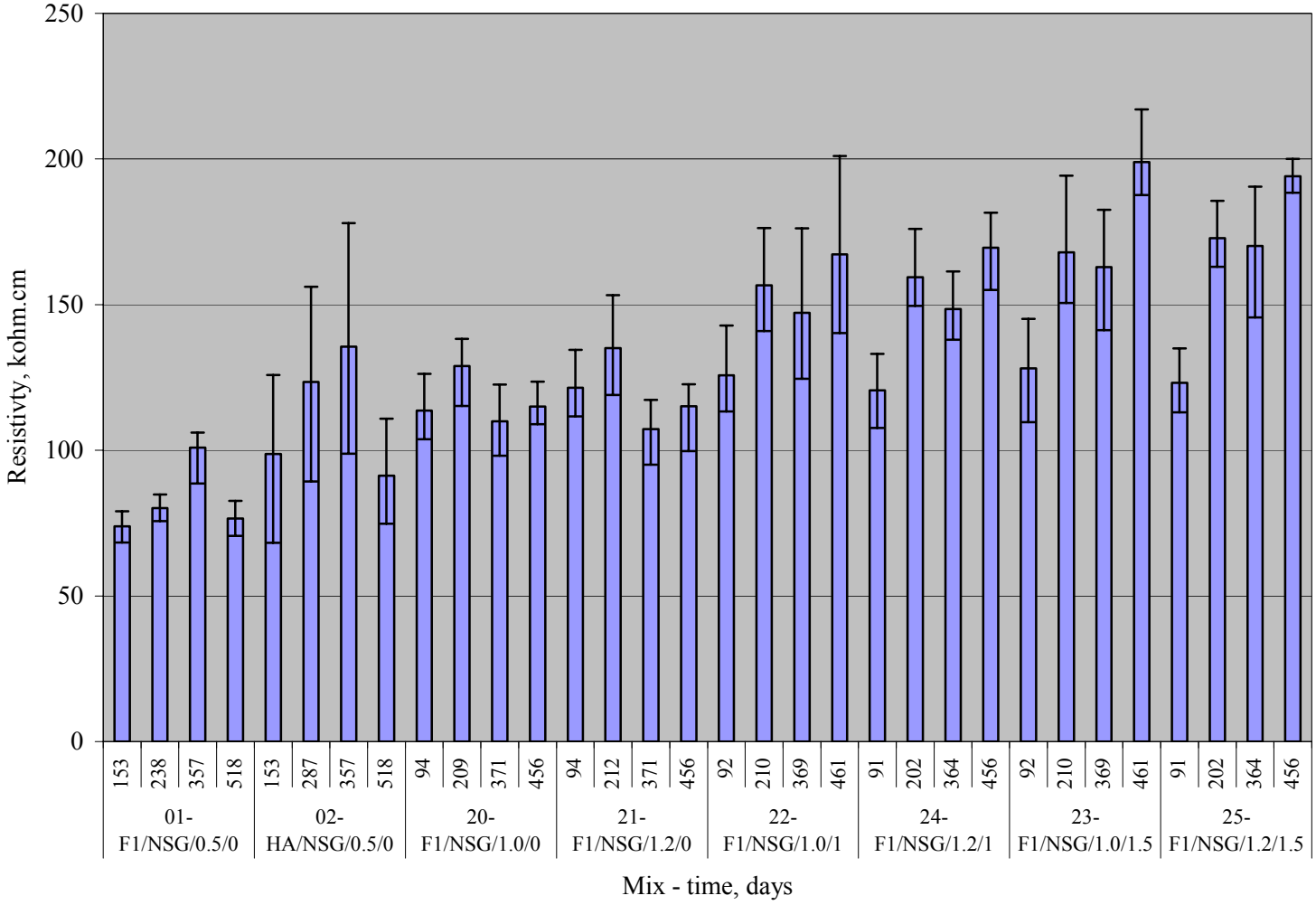

Figure VIII-54: Concrete resistivity in mixes containing Nova Scotia granite (NG).

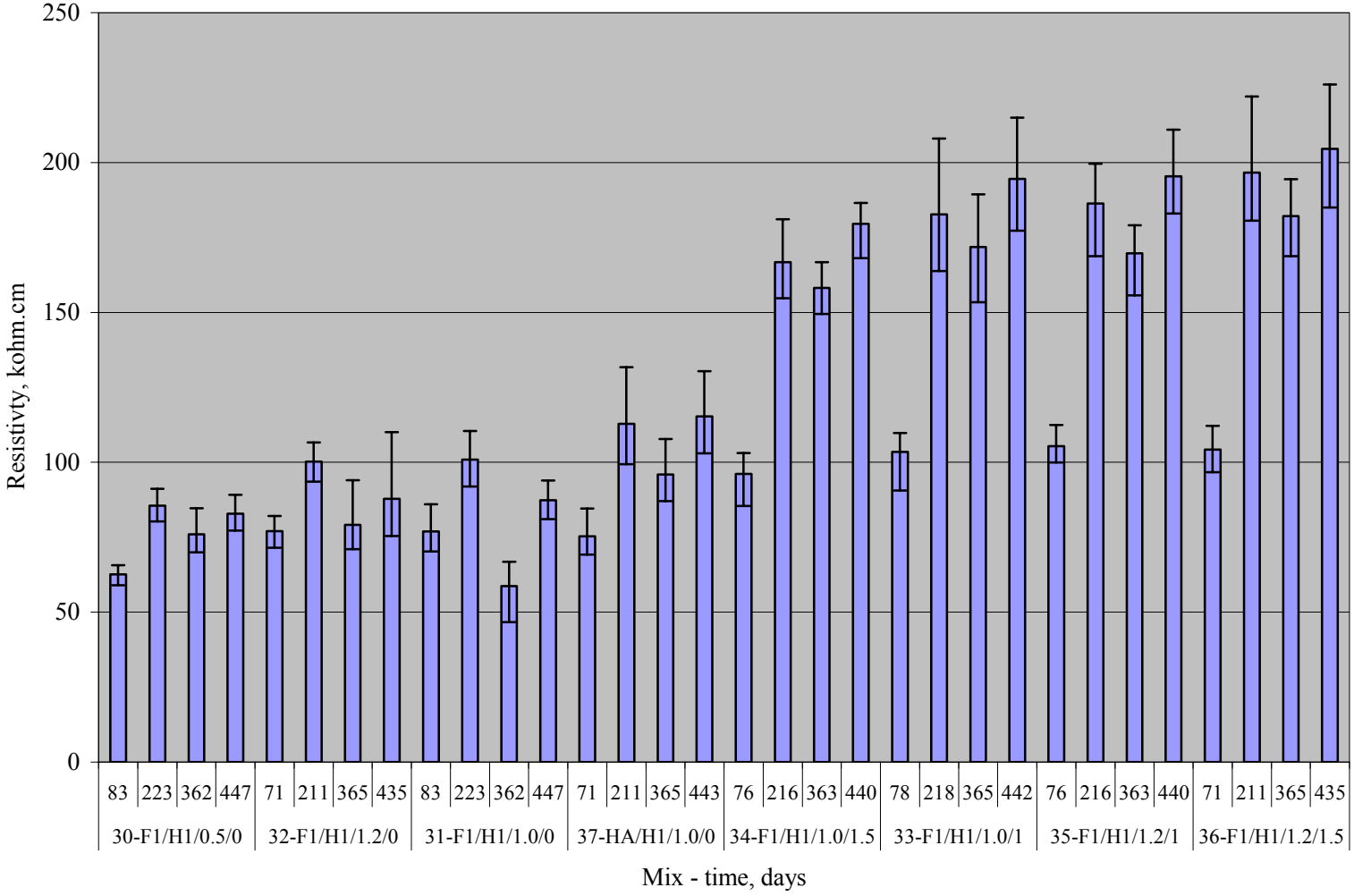

Figure VIII-55: Concrete resistivity in mixes containing alkali reactive Spratt limestone (H1).

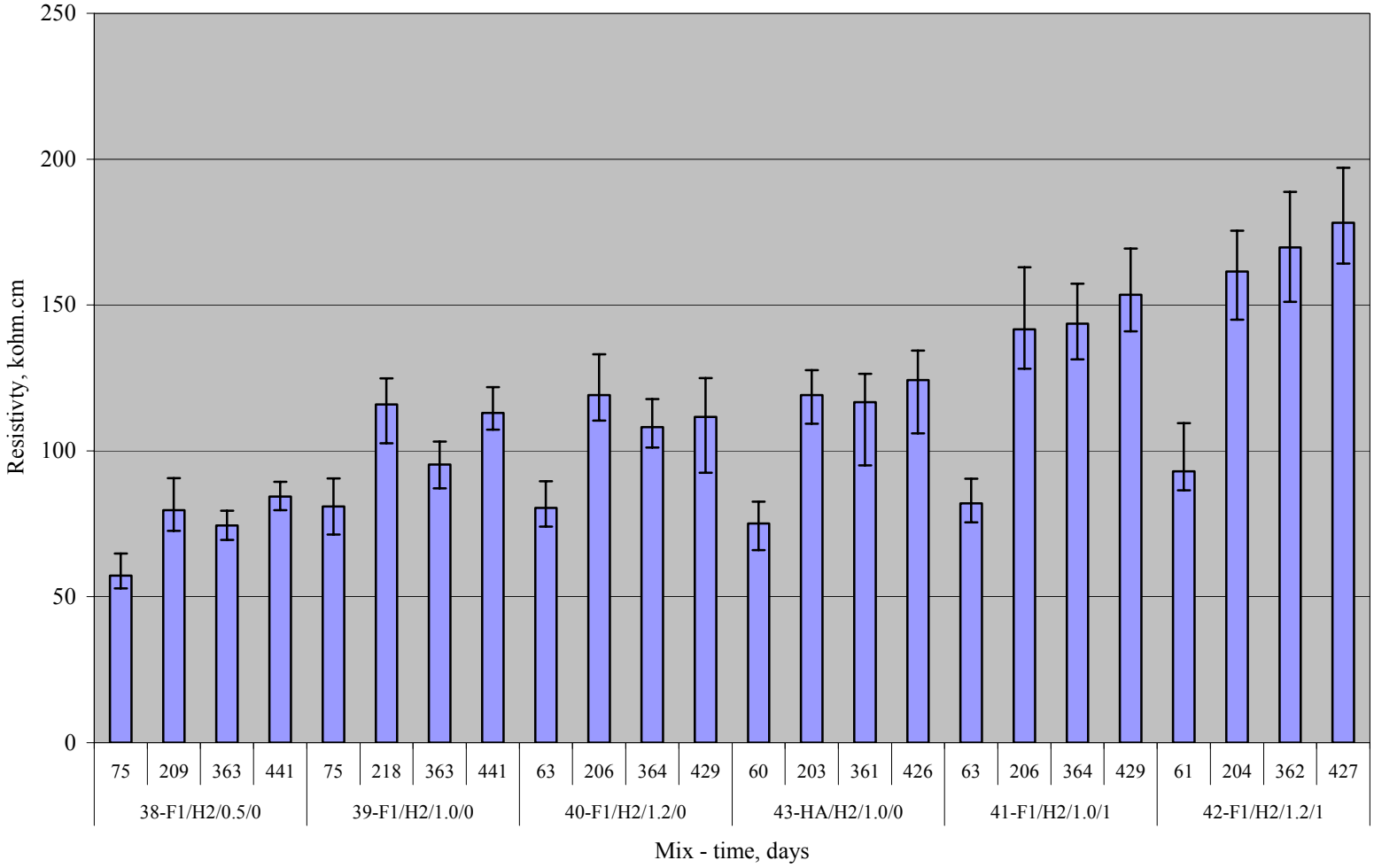

Figure VIII-56: Concrete resistivity in mixes containing moderately alkali reactive Sudbury gravel (H2).

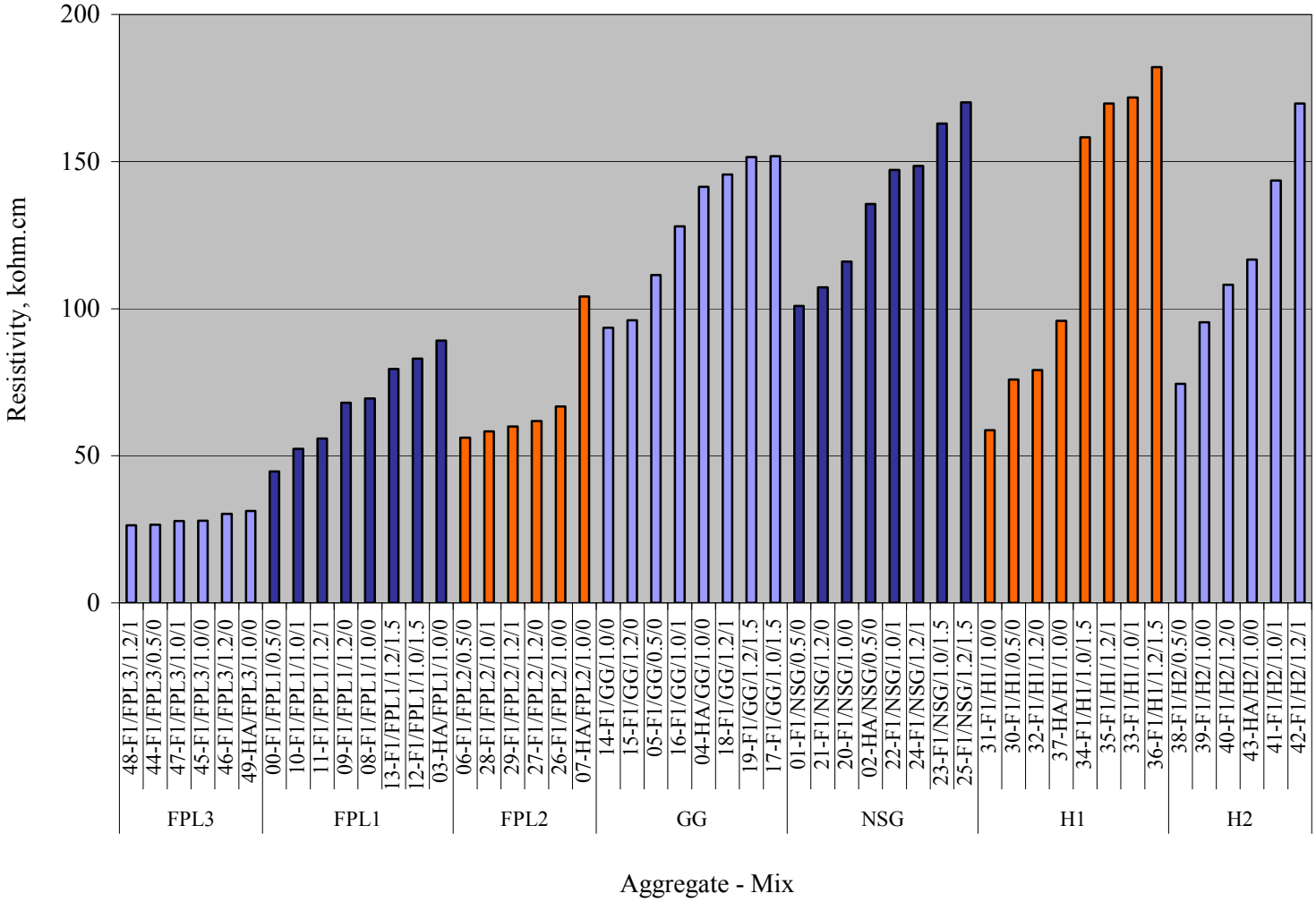

Figure VIII-57: Concrete resistivity measured at 365 days.

solution chemistry without significantly altering path tortuosity.[53] Fly ash modifies both tortuosity and pore water composition and, therefore, is expected to have a relatively large effect on concrete permeability as discussed below.

Resistivity measurements were also made on cementitious paste and mortar specimens, and Figure VIII-58 summarized these along with measurements for comparable concretes. It is apparent from these that fly ash, silica sand, and coarse aggregate each increased resistivity compared to paste alone. Magnitude of the increase varied with mix design and coarse aggregate type.

To project the effect of NaOH and $LiNO_3$ on resistivity, the difference for mixes containing these admixtures was calculated at 90 and 365 days relative to that for comparable mixes without these additions. Figure VIII-59 presents the results, from which the following conclusions were made:

- Addition of NaOH increased resistivity for all mixes. However, its impact depended on the concrete constituents. Except for specimens with NG coarse aggregate, for which resistivity was greater for Na_2O_e = 1.2 than for 1.0, the effect of enhanced alkalinity was modest and probably within expected scatter. The resistivity increase for Florida coarse aggregate FPL-1 was greater than for FPL-2 and FPL-3.

- The effect of admixed $LiNO_3$ on resistivity was similar to that of NaOH for the three Florida coarse aggregates (relatively large increase for FPL-1 compared to FPL-2 and FPL-3). For the other coarse aggregates, a relatively large resistivity increase resulted from admixed $LiNO_3$ with this being greater for the normal compared to elevated dosage.

At least a portion of the observed resistivity changes may have been related to characteristics of the electrical double layer at the cement paste-pore water interface. Here, negatively charged particles of hydrated cement cause a non-homogeneous distribution of pore solution ions, where positive ions group within approximately 20Å from the charged particles in two layers: the Stern layer which adheres to the negatively charged surface and the more loosely bound Gouy Chapman layer. Negative ions remain in the bulk electrolyte solution. As a consequence of this partitioning, diffusing anions are thought to move through the bulk solution, whereas cations are present in the double layer. Consistent with this, diffusivity of anions has been reported to be one

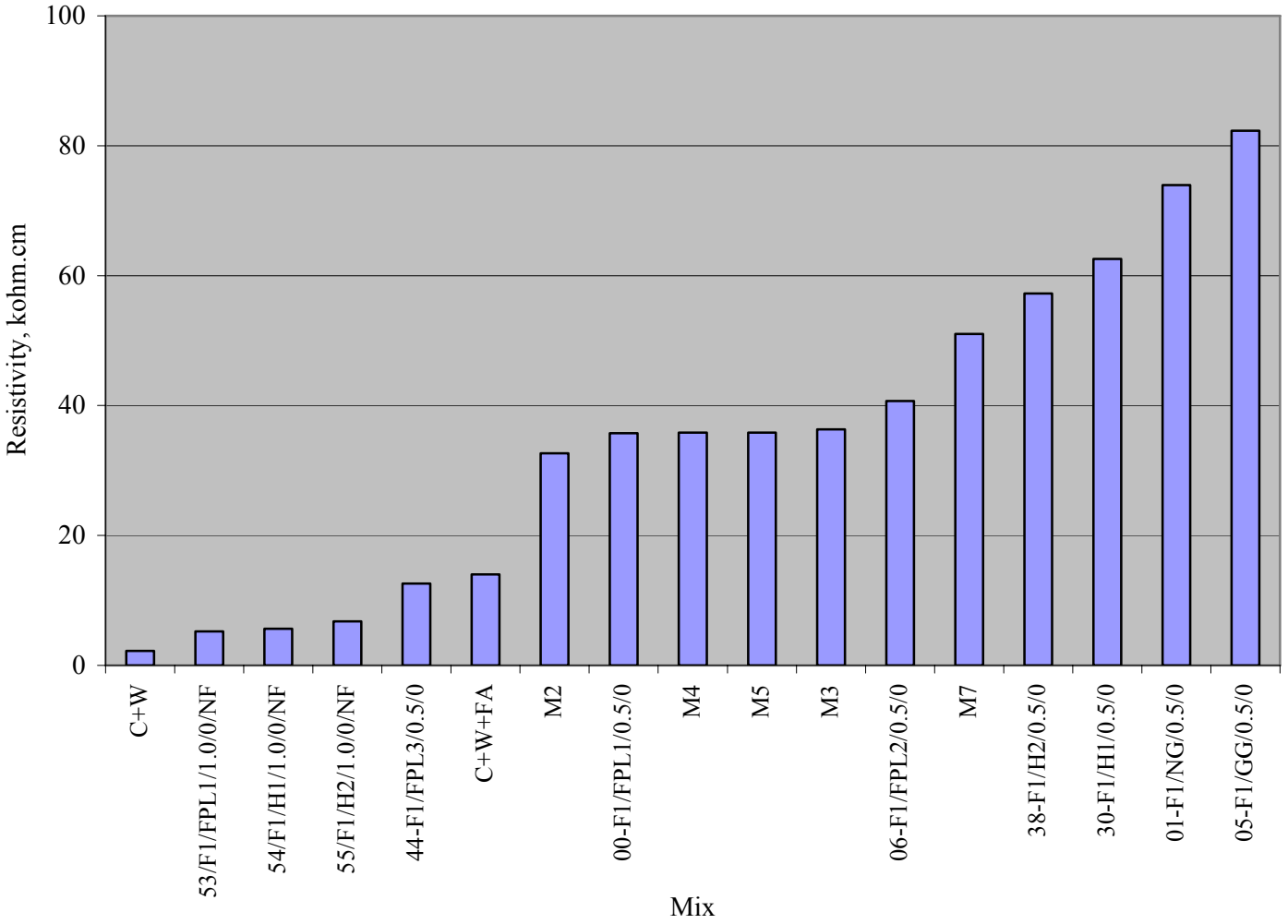

Figure VIII-58: Resistivity of cementitious paste, mortar and comparable concrete mixes.

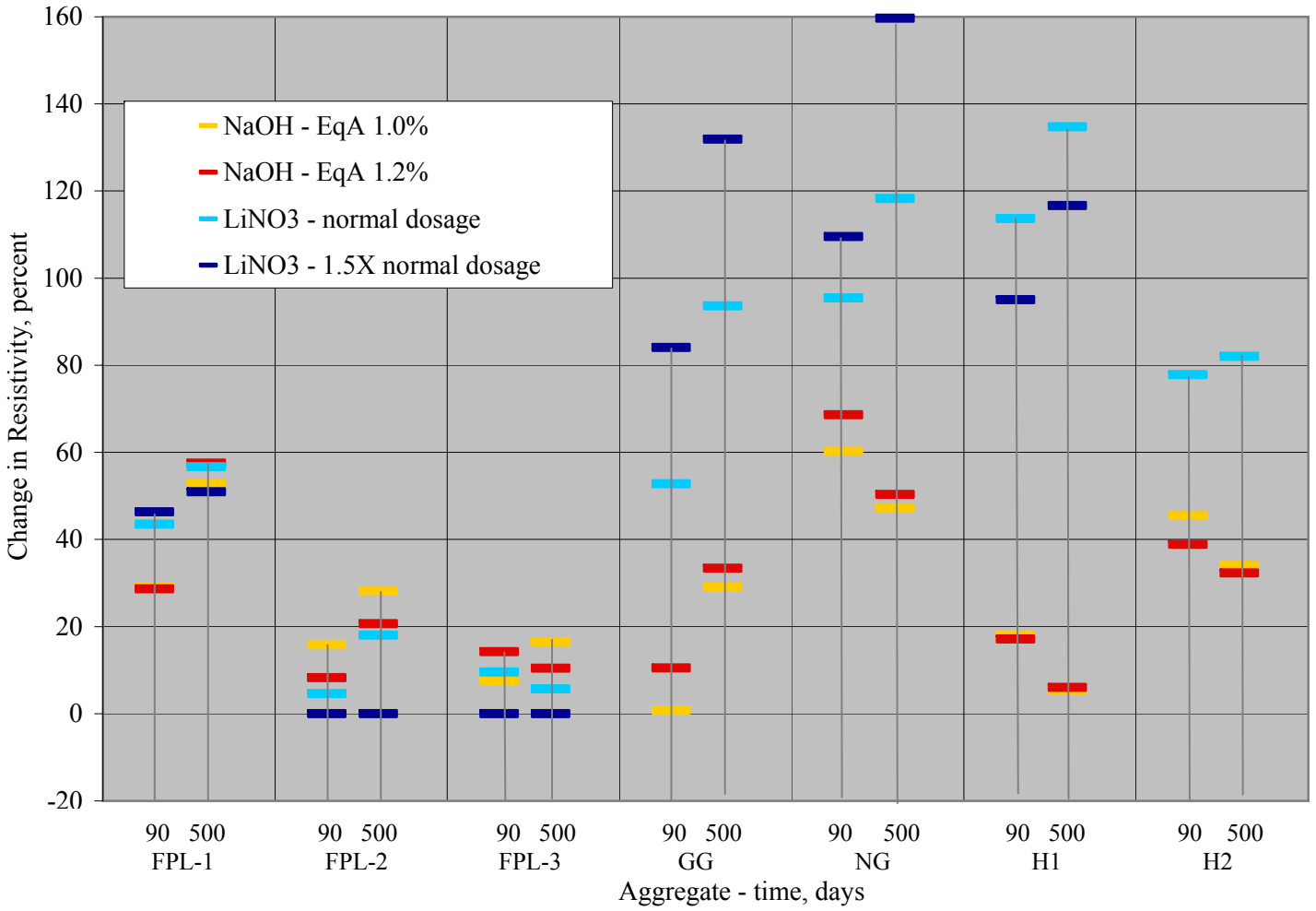

Figure VIII-59: Effects of the NaOH and lithium-based ASR-preventing admixture in concrete resistivity.

order of magnitude greater than that of the cations.[82] Thus, in order to conform to the principle of electroneutrality, other species must contribute in the conduction process.[83,84] Calcium ions, which exist in the hardened cement paste as $Ca(OH)_2$ and in the pore water at low concentrations (0.003 M) are probably involved. Thus, despite its low concentration, Ca^{2+} and other divalent ions are preferentially bound in the double layer and, therefore, contribute to cation diffusion.[85]

When class F fly ash is added to concrete, $Ca(OH)_2$ is consumed; and its cations in the double layer are replaced by alkali ions. As a consequence, alkali concentration in the double layer increases, while it decreases in the bulk pore water, as observed in the pore water alkalinity results from PWE (Table VIII-2 and Figure VIII-3). Thus, for an equivalent charge transfer, each Ca^{2+} must be replaced by two alkali ions; and so mobility of positive charges decreases in an alkali-rich environment. If NaOH in addition to FA is admixed, the alkali concentration in both the pore water and double layer increases, which for a strong electrolyte can result in a decrease in conductivity.[86] Since resistivity and conductivity are inversely related, an increase in resistivity is then expected.

However, a contribution to resistivity change from ASR may also have resulted. Thus, generation of both gel and cracking from ASR should contribute to lower resistivity. Figure VIII-59 indicates that for most aggregate types, the resistivity increase for NaOH admixed specimens was modest compared to that for the $LiNO_3$ admixed ones.

IX. SUMMARY AND CONCLUSIONS

Previous research has indicated that time-to-corrosion of reinforcing steel in concrete can be increased by as much as a factor of ten by use of high alkali cement. The present study was undertaken to determine the effect of high alkali in concrete on other properties that are relevant to performance in Florida bridge structures. These properties include 1) susceptibility to cement-aggregate reactions, particularly alkali-silica reactions (ASR), 2) compressive strength, 3) flexural strength, and 4) electrical resistivity as an indicator of chloride permeability. This study focused upon identifying one or more high-alkali concretes that employ materials available to FDOT but that do not compromise durability from a cause(s) other than reinforcing steel corrosion, namely ASR. To accomplish this, coarse aggregates from five sources that have been used in the past for bridge construction in Florida were acquired. These included Florida limestone from three different quarries about the State and granites from Georgia and Nova Scotia. As far as could be

determined, there have been no reported incidences of ASR activity with these aggregates in past FDOT concrete applications. Two other coarse aggregates, Sprat limestone and Sudbury gravel, both of which are known to be ASR reactive and which have been studied extensively in the past, were included for baseline purposes. The fine aggregate was a local quartz sand with no history of ASR susceptibility. Two additional mix design variables included the use of fly ash and of an ASR inhibiting lithium admixture ($LiNO_3$).

The test procedure included measurement of concrete specimen 1) length change according to ASTM C1293, "Standard Test Method for Determination of Length Change of Concrete Due to Alkali-Silica Reaction," 2) alkalinity by both ex-situ leaching and pore water expression, 3) compression and flexural strength, and 4) electrical resistivity.

Criteria for qualifying a coarse aggregate for use in FDOT Class V concrete with high alkali based on results from specimens that contained 1.2 percent alkali and no lithium admixture are proposed as listed below:

- Concrete prism expansion should not exceed 0.010 percent after one year and two years of ASTM C1293 exposure.

- There should be no significant length change of prisms between the first and second years of ASTM C1293 exposure.

- There should be a complete absence of cracking after two years of ASTM C1293 exposure, as determined by microscopic examination of molded and cast surfaces of prisms.

- There should be confirmation by petrographic examination (ASTM C295) that the fine and coarse aggregates contain no known silica phases that are potentially alkali-silica reactive (strained quartz, microcrystalline quartz, chalcedony, chert, tridymite, cristobalite, opal, and others).

- There should be confirmation by petrographic examination (ASTM C856) of absence of any microstructual features indicative of ASR activity. (alkali-silica gel, diagnostic cracking within aggregate particles and within cement paste adjacent to cracked

aggregate particles, reaction rims on aggregate particles, and gel-stained cement paste adjacent to cracked aggregate particles) after two year of ASTM C1293 exposure.

- There should be confirmation of a normal, expected increase in flexural and compressive strengths as measured at one year compared to that at 28 days.

Based upon the above criteria, two of the five experimental concretes were qualified for further study. In order of preference, these are concrete containing 1) Florida limestone aggregate FPL-1 (Rinker materials, Miami Oolitic Limerock, Pit 87-089), and 2) Florida limestone aggregate FPL-3 (Aggrisource, Naples Florida). Features of the FPL-l limestone aggregate concrete that support its ranking include the following:

- Petrographic examination confirmed that 1) no potentially ASR reactive forms of silica are present and 2) no microstructural features indicative of ASR activity and no cracking of any type were observed in prisms after two years exposure.

- After experiencing a very slight average prism expansion of 0.0060 percent after two months of ASTM C1293 exposure, no significant length change occurred during two subsequent years of testing.

- Concrete with the highest alkali content had greater compressive strength after 365 days of ASTM C1293 exposure than at 28 days (51 MPa (7400 psi) compared to 43 MPa (6200 psi)). Flexural strength of the FPL-1 concrete containing 1.0 percent alkali and the lithium admixture was 7.2 MPa (1050 psi) following two years exposure.

On the basis of this performance, it is recommended that the FPL-1 Florida limestone aggregate concrete be considered for further trials leading to the possible eventual use of high-alkali concretes in FDOT reinforced concrete bridge structures. These concretes should also contain 1) fly ash of an equivalent alkalinity comparable to the one studied here and 2) admixed Li at the manufacturer's recommended dosage.

Appendix A

Concretes mix design

Mix 00/F1/F1/0.5/0

Material	kg/m^3
Cement	363
Fly Ash	83
Water	178
Fine aggregate SSD	607
Coarse aggregate SSD	1005
Air Admixture [ml]	110
$LiNO_3$ Admixture [l]	0
NaOH addition	0

Date	3/25/04
Na_2Oe [%]	0.5
Specific gravity	2.26
Air content [%]	3.2
Slump [mm]	162

Mix 01/F1/NG/0.5/0

Material	kg/m^3
Cement	363
Fly Ash	83
Water	178
Fine aggregate SSD	607
Coarse aggregate SSD	1085
Air Admixture [ml]	218
$LiNO_3$ Admixture [l]	0
NaOH addition	0

Date	4/8/04
Na_2Oe [%]	0.5
Specific gravity	2.34
Air content	3.5
Slump	158

Mix 02/HA/NG/1.0/0

Material	kg/m^3
Cement	363
Fly Ash	83
Water	178
Fine aggregate SSD	607
Coarse aggregate SSD	1085
Air Admixture [ml]	436
$LiNO_3$ Admixture [l]	0
NaOH addition	0

Date	4/8/04
Na_2Oe [%]	1.0
Specific gravity	2.34
Air content	3.4
Slump	146

Mix 03/HA/F1/1.0/0

Material	kg/m^3
Cement	363
Fly Ash	83
Water	178
Fine aggregate SSD	607
Coarse aggregate SSD	1005
Air Admixture [ml]	436
$LiNO_3$ Admixture [l]	0
NaOH addition	0

Date	4/12/04
Na_2Oe [%]	1.0
Specific gravity	2.26
Air content	3.5
Slump	140

Mix 04/HA/GG/1.0/0

Material	kg/m^3
Cement	363
Fly Ash	83
Water	178
Fine aggregate SSD	607
Coarse aggregate SSD	1085
Air Admixture [ml]	436
$LiNO_3$ Admixture [l]	0
NaOH addition	0

Date	4/15/04
Na_2Oe [%]	1.0
Specific gravity	2.37
Air content	3.6
Slump	184

Mix 05/F1/GG/.5/0

Material	kg/m^3
Cement	363
Fly Ash	83
Water	178
Fine aggregate SSD	607
Coarse aggregate SSD	1085
Air Admixture [ml]	436
$LiNO_3$ Admixture [l]	0
NaOH addition	0

Date	4/15/04
Na_2Oe [%]	0.5
Specific gravity	2.37
Air content	3.2
Slump	190

Mix 06/F1/F2/0.5/0

Material	kg/m^3
Cement	363
Fly Ash	83
Water	178
Fine aggregate SSD	607
Coarse aggregate SSD	994
Air Admixture [ml]	218
$LiNO_3$ Admixture [l]	0
NaOH addition	0

Date	4/22/04
Na_2Oe [%]	0.5
Specific gravity	2.27
Air content	3.6
Slump	120

Mix 07/HA/F2/1.0/0

Material	kg/m^3
Cement	363
Fly Ash	83
Water	178
Fine aggregate SSD	607
Coarse aggregate SSD	994
Air Admixture [ml]	218
$LiNO_3$ Admixture [l]	0
NaOH addition	0

Date	4/22/04
Na_2Oe [%]	1.0
Specific gravity	2.27
Air content	3.6
Slump	146

Mix 08/F1/F1/1.0/0

Material	kg/m^3
Cement	363
Fly Ash	83
Water	178
Fine aggregate SSD	607
Coarse aggregate SSD	1005
Air Admixture [ml]	218
$LiNO_3$ Admixture [l]	0
NaOH addition	3.42

Date	5/5/04
Na_2Oe [%]	1.0
Specific gravity	2.27
Air content	3.6
Slump	165

Mix 09/F1/F1/1.2/0

Material	kg/m^3
Cement	363
Fly Ash	83
Water	178
Fine aggregate SSD	607
Coarse aggregate SSD	1005
Air Admixture [ml]	218
$LiNO_3$ Admixture [l]	0
NaOH addition	4.57

Date	5/5/04
Na_2Oe [%]	1.2
Specific gravity	2.26
Air content	3.9
Slump	165

Mix 10/F1/F1/1.0/1

Material	kg/m^3
Cement	363
Fly Ash	83
Water	178
Fine aggregate SSD	607
Coarse aggregate SSD	1005
Air Admixture [ml]	218
$LiNO_3$ Admixture [l]	20.48
NaOH addition	3.42

Date	5/13/04
Na_2Oe [%]	1.0
Specific gravity	2.23
Air content [%]	3.9
Slump [mm]	171

Mix 11/F1/F1/1.2/1

Material	kg/m^3
Cement	363
Fly Ash	83
Water	178
Fine aggregate SSD	607
Coarse aggregate SSD	1005
Air Admixture [ml]	218
$LiNO_3$ Admixture [l]	24.59
NaOH addition	3.42

Date	5/13/04
Na_2Oe [%]	1.2
Specific gravity	2.26
Air content [%]	3.8
Slump [mm]	133

Mix 12/F1/F1/1.0/2

Material	kg/m^3
Cement	363
Fly Ash	83
Water	178
Fine aggregate SSD	607
Coarse aggregate SSD	1005
Air Admixture [ml]	218
$LiNO_3$ Admixture [l]	25.61
NaOH addition	3.42

Date	6/02/04
Na_2Oe [%]	1.0
Specific gravity	2.26
Air content [%]	3.5
Slump [mm]	158

Mix 13/F1/F1/1.2/2

Material	kg/m^3
Cement	363
Fly Ash	83
Water	178
Fine aggregate SSD	607
Coarse aggregate SSD	1005
Air Admixture [ml]	218
$LiNO_3$ Admixture [l]	30.73
NaOH addition	4.57

Date	6/02/04
Na_2Oe [%]	1.2
Specific gravity	2.26
Air content [%]	3.7
Slump [mm]	140

Mix 14/F1/GG/1.0/0

Material	kg/m^3
Cement	363
Fly Ash	83
Water	178
Fine aggregate SSD	607
Coarse aggregate SSD	1085
Air Admixture [ml]	436
$LiNO_3$ Admixture [l]	0
NaOH addition	3.42

Date	6/04/04
Na_2Oe [%]	1.0
Specific gravity	2.36
Air content [%]	4.0
Slump [mm]	178

Mix 15/F1/GG/1.2/0

Material	kg/m^3
Cement	363
Fly Ash	83
Water	178
Fine aggregate SSD	607
Coarse aggregate SSD	1085
Air Admixture [ml]	436
$LiNO_3$ Admixture [l]	0
NaOH addition	4.57

Date	6/04/04
Na_2Oe [%]	1.2
Specific gravity	2.38
Air content [%]	3.7
Slump [mm]	146

Mix 16/F1/GG/1.0/1

Material	kg/m^3
Cement	363
Fly Ash	83
Water	178
Fine aggregate SSD	607
Coarse aggregate SSD	1085
Air Admixture [ml]	436
$LiNO_3$ Admixture [l]	20.49
NaOH addition	3.42

Date	6/08/04
Na_2Oe [%]	1.0
Specific gravity	2.37
Air content [%]	4.0
Slump [mm]	165

Mix 17/F1/GG/1.0/2

Material	kg/m^3
Cement	363
Fly Ash	83
Water	178
Fine aggregate SSD	607
Coarse aggregate SSD	1085
Air Admixture [ml]	436
$LiNO_3$ Admixture [l]	25.61
NaOH addition	3.42

Date	6/08/04
Na_2Oe [%]	1.0
Specific gravity	2.42
Air content [%]	3.0
Slump [mm]	140

Mix 18/F1/GG/1.2/1

Material	kg/m^3
Cement	363
Fly Ash	83
Water	178
Fine aggregate SSD	607
Coarse aggregate SSD	1085
Air Admixture [ml]	436
$LiNO_3$ Admixture [l]	24.59
NaOH addition	4.57

Date	6/10/04
Na_2Oe [%]	1.2
Specific gravity	2.42
Air content [%]	3.0
Slump [mm]	114

Mix 19/F1/GG/1.2/2

Material	kg/m^3
Cement	363
Fly Ash	83
Water	178
Fine aggregate SSD	607
Coarse aggregate SSD	1085
Air Admixture [ml]	436
$LiNO_3$ Admixture [l]	30.73
NaOH addition	4.57

Date	6/10/04
Na_2Oe [%]	1.2
Specific gravity	2.40
Air content [%]	3.3
Slump [mm]	146

Mix 20/F1/NG/1.0/0

Material	kg/m^3
Cement	363
Fly Ash	83
Water	178
Fine aggregate SSD	607
Coarse aggregate SSD	1085
Air Admixture [ml]	436
$LiNO_3$ Admixture [l]	0
NaOH addition	3.42

Date	6/15/04
Na_2Oe [%]	1.0
Specific gravity	2.34
Air content [%]	3.4
Slump [mm]	146

Mix 21/F1/NG/1.2/0

Material	kg/m^3
Cement	363
Fly Ash	83
Water	178
Fine aggregate SSD	607
Coarse aggregate SSD	1085
Air Admixture [ml]	436
$LiNO_3$ Admixture [l]	0
NaOH addition	4.57

Date	6/15/04
Na_2Oe [%]	1.2
Specific gravity	2.36
Air content [%]	3.0
Slump [mm]	120

Mix 22/F1/NG/1.0/1

Material	kg/m^3
Cement	363
Fly Ash	83
Water	178
Fine aggregate SSD	607
Coarse aggregate SSD	1085
Air Admixture [ml]	436
$LiNO_3$ Admixture [l]	20.49
NaOH addition	3.42

Date	6/17/04
Na_2Oe [%]	1.0
Specific gravity	2.34
Air content [%]	3.7
Slump [mm]	152

Mix 23/F1/NG/1.0/2

Material	kg/m^3
Cement	363
Fly Ash	83
Water	178
Fine aggregate SSD	607
Coarse aggregate SSD	1085
Air Admixture [ml]	436
$LiNO_3$ Admixture [l]	25.61
NaOH addition	3.42

Date	6/15/04
Na_2Oe [%]	1.0
Specific gravity	2.34
Air content [%]	3.5
Slump [mm]	171

Mix 24/F1/NG/1.2/1

Material	kg/m^3
Cement	363
Fly Ash	83
Water	178
Fine aggregate SSD	607
Coarse aggregate SSD	1085
Air Admixture [ml]	436
$LiNO_3$ Admixture [l]	24.59
NaOH addition	4.57

Date	6/21/04
Na_2Oe [%]	1.2
Specific gravity	2.34
Air content [%]	3.6
Slump [mm]	171

Mix 25/F1/NG/1.2/2

Material	kg/m^3
Cement	363
Fly Ash	83
Water	178
Fine aggregate SSD	607
Coarse aggregate SSD	1085
Air Admixture [ml]	436
$LiNO_3$ Admixture [l]	30.73
NaOH addition	4.57

Date	6/22/04
Na_2Oe [%]	1.2
Specific gravity	2.36
Air content [%]	3.0
Slump [mm]	120

Mix 26/F1/F2/1.0/0

Material	kg/m^3
Cement	363
Fly Ash	83
Water	178
Fine aggregate SSD	607
Coarse aggregate SSD	978
Air Admixture [ml]	218
$LiNO_3$ Admixture [l]	0
NaOH addition	3.42

Date	6/22/04
Na_2Oe [%]	1.0
Specific gravity	2.27
Air content [%]	3.4
Slump [mm]	120

Mix 27/F1/F2/1.2/0

Material	kg/m^3
Cement	363
Fly Ash	83
Water	178
Fine aggregate SSD	607
Coarse aggregate SSD	978
Air Admixture [ml]	218
$LiNO_3$ Admixture [l]	0
NaOH addition	4.57

Date	6/24/04
Na_2Oe [%]	1.2
Specific gravity	2.26
Air content [%]	3.7
Slump [mm]	133

Mix 28/F1/F2/1.0/1

Material	kg/m^3
Cement	363
Fly Ash	83
Water	178
Fine aggregate SSD	607
Coarse aggregate SSD	978
Air Admixture [ml]	218
$LiNO_3$ Admixture [l]	20.49
NaOH addition	3.42

Date	6/29/04
Na_2Oe [%]	1.0
Specific gravity	2.27
Air content [%]	3.9
Slump [mm]	165

Mix 29/F1/F2/1.2/1

Material	kg/m^3
Cement	363
Fly Ash	83
Water	178
Fine aggregate SSD	607
Coarse aggregate SSD	978
Air Admixture [ml]	218
$LiNO_3$ Admixture [l]	24.59
NaOH addition	4.57

Date	6/29/04
Na_2Oe [%]	1.2
Specific gravity	2.27
Air content [%]	3.5
Slump [mm]	146

Mix 30/F1/H1/0.5/0

Material	kg/m^3
Cement	363
Fly Ash	83
Water	178
Fine aggregate SSD	607
Coarse aggregate SSD	1105
Air Admixture [ml]	218
$LiNO_3$ Admixture [l]	0
NaOH addition	0

Date	7/01/04
Na_2Oe [%]	0.5
Specific gravity	2.35
Air content [%]	3.5
Slump [mm]	133

Mix 31/F1/H1/1.0/0

Material	kg/m^3
Cement	363
Fly Ash	83
Water	178
Fine aggregate SSD	607
Coarse aggregate SSD	1105
Air Admixture [ml]	218
$LiNO_3$ Admixture [l]	0
NaOH addition	3.42

Date	7/01/04
Na_2Oe [%]	1.0
Specific gravity	2.34
Air content [%]	4.0
Slump [mm]	152

Mix 32/F1/H1/1.2/0

Material	kg/m^3
Cement	363
Fly Ash	83
Water	178
Fine aggregate SSD	607
Coarse aggregate SSD	1105
Air Admixture [ml]	218
$LiNO_3$ Admixture [l]	0
NaOH addition	4.57

Date	7/13/04
Na_2Oe [%]	1.2
Specific gravity	2.38
Air content [%]	3.4
Slump [mm]	146

Mix 33/F1/H1/1.0/1

Material	kg/m^3
Cement	363
Fly Ash	83
Water	178
Fine aggregate SSD	607
Coarse aggregate SSD	1105
Air Admixture [ml]	218
$LiNO_3$ Admixture [l]	20.49
NaOH addition	3.42

Date	7/06/04
Na_2Oe [%]	1.0
Specific gravity	2.35
Air content [%]	3.2
Slump [mm]	146

Mix 34/F1/H1/1.0/2

Material	kg/m^3
Cement	363
Fly Ash	83
Water	178
Fine aggregate SSD	607
Coarse aggregate SSD	1105
Air Admixture [ml]	218
$LiNO_3$ Admixture [l]	25.61
NaOH addition	3.42

Date	7/08/04
Na_2Oe [%]	1.0
Specific gravity	2.38
Air content [%]	3.0
Slump [mm]	158

Mix 35/F1/H1/1.2/1

Material	kg/m^3
Cement	363
Fly Ash	83
Water	178
Fine aggregate SSD	607
Coarse aggregate SSD	1105
Air Admixture [ml]	218
$LiNO_3$ Admixture [l]	24.59
NaOH addition	4.57

Date	7/08/04
Na_2Oe [%]	1.2
Specific gravity	2.38
Air content [%]	3.2
Slump [mm]	158

Mix 36/F1/H1/1.2/2

Material	kg/m^3
Cement	363
Fly Ash	83
Water	178
Fine aggregate SSD	607
Coarse aggregate SSD	1105
Air Admixture [ml]	218
$LiNO_3$ Admixture [l]	30.73
NaOH addition	4.57

Date	7/13/04
Na_2Oe [%]	1.2
Specific gravity	2.37
Air content [%]	3.4
Slump [mm]	127

Mix 37/HA/H1/1.0/0

Material	kg/m^3
Cement	363
Fly Ash	83
Water	178
Fine aggregate SSD	607
Coarse aggregate SSD	1105
Air Admixture [ml]	218
$LiNO_3$ Admixture [l]	0
NaOH addition	0

Date	7/13/04
Na_2Oe [%]	1.0
Specific gravity	2.37
Air content [%]	3.0
Slump [mm]	133

Mix 38/F1/H2/0.5/0

Material	kg/m^3
Cement	363
Fly Ash	83
Water	178
Fine aggregate SSD	607
Coarse aggregate SSD	1113
Air Admixture [ml]	218
$LiNO_3$ Admixture [l]	0
NaOH addition	0

Date	7/15/04
Na_2Oe [%]	0.5
Specific gravity	2.37
Air content [%]	3.0
Slump [mm]	96

Mix 39/F1/H2/1.0/0

Material	kg/m^3
Cement	363
Fly Ash	83
Water	178
Fine aggregate SSD	607
Coarse aggregate SSD	1113
Air Admixture [ml]	327
$LiNO_3$ Admixture [l]	0
NaOH addition	3.42

Date	7/15/04
Na_2Oe [%]	1.0
Specific gravity	2.37
Air content [%]	3.7
Slump [mm]	127

Mix 40/F1/H2/1.2/0

Material	kg/m^3
Cement	363
Fly Ash	83
Water	178
Fine aggregate SSD	607
Coarse aggregate SSD	1113
Air Admixture [ml]	327
$LiNO_3$ Admixture [l]	0
NaOH addition	4.57

Date	7/27/04
Na_2Oe [%]	1.2
Specific gravity	2.37
Air content [%]	3.7
Slump [mm]	146

Mix 41/F1/H2/1.0/1

Material	kg/m^3
Cement	363
Fly Ash	83
Water	178
Fine aggregate SSD	607
Coarse aggregate SSD	1113
Air Admixture [ml]	327
$LiNO_3$ Admixture [l]	20.49
NaOH addition	3.42

Date	7/27/04
Na_2Oe [%]	1.0
Specific gravity	2.36
Air content [%]	3.6
Slump [mm]	133

Mix 42/F1/H2/1.2/1

Material	kg/m^3
Cement	363
Fly Ash	83
Water	178
Fine aggregate SSD	607
Coarse aggregate SSD	1113
Air Admixture [ml]	327
$LiNO_3$ Admixture [l]	24.59
NaOH addition	4.57

Date	7/29/04
Na_2Oe [%]	1.2
Specific gravity	2.37
Air content [%]	3.4
Slump [mm]	152

Mix 43/HA/H2/1.0/0

Material	kg/m^3
Cement	363
Fly Ash	83
Water	178
Fine aggregate SSD	607
Coarse aggregate SSD	1113
Air Admixture [ml]	327
$LiNO_3$ Admixture [l]	0
NaOH addition	0

Date	7/29/04
Na_2Oe [%]	1.0
Specific gravity	2.36
Air content [%]	3.3
Slump [mm]	133

Mix 44/F1/F3/0.5/0

Material	kg/m^3
Cement	363
Fly Ash	83
Water	178
Fine aggregate SSD	607
Coarse aggregate SSD	917
Air Admixture [ml]	0
$LiNO_3$ Admixture [l]	0
NaOH addition	0

Date	8/10/04
Na_2Oe [%]	0.5
Specific gravity	2.21
Air content [%]	3.5
Slump [mm]	64

Mix 45/F1/F3/1.0/0

Material	kg/m^3
Cement	363
Fly Ash	83
Water	178
Fine aggregate SSD	607
Coarse aggregate SSD	917
Air Admixture [ml]	0
$LiNO_3$ Admixture [l]	0
NaOH addition	3.42

Date	8/10/04
Na_2Oe [%]	1.0
Specific gravity	2.22
Air content [%]	3.1
Slump [mm]	83

Mix 46/F1/F3/1.2/0

Material	kg/m^3
Cement	363
Fly Ash	83
Water	178
Fine aggregate SSD	607
Coarse aggregate SSD	917
Air Admixture [ml]	0
$LiNO_3$ Admixture [l]	0
NaOH addition	4.57

Date	8/10/04
Na_2Oe [%]	1.2
Specific gravity	2.22
Air content [%]	3.2
Slump [mm]	70

Mix 47/F1/F3/1.0/1

Material	kg/m^3
Cement	363
Fly Ash	83
Water	178
Fine aggregate SSD	607
Coarse aggregate SSD	917
Air Admixture [ml]	218
$LiNO_3$ Admixture [l]	20.49
NaOH addition	3.42

Date	8/5/04
Na_2Oe [%]	1.0
Specific gravity	2.22
Air content [%]	3.4
Slump [mm]	108

Mix 48/F1/F3/1.2/1

Material	kg/m^3
Cement	363
Fly Ash	83
Water	178
Fine aggregate SSD	607
Coarse aggregate SSD	917
Air Admixture [ml]	0
$LiNO_3$ Admixture [l]	24.59
NaOH addition	4.57

Date	8/12/04
Na_2Oe [%]	1.2
Specific gravity	2.21
Air content [%]	3.5
Slump [mm]	102

Mix 49/HA/F3/1.0/0

Material	kg/m^3
Cement	363
Fly Ash	83
Water	178
Fine aggregate SSD	607
Coarse aggregate SSD	917
Air Admixture [ml]	0
$LiNO_3$ Admixture [l]	0
NaOH addition	0

Date	8/12/04
Na_2Oe [%]	1.0
Specific gravity	2.18
Air content [%]	3.5
Slump [mm]	108

Mix 53/F1/F1/1.0/0/NF

Material	kg/m^3
Cement	440
Fly Ash	0
Water	176
Fine aggregate SSD	607
Coarse aggregate SSD	1042
Air Admixture [ml]	218
$LiNO_3$ Admixture [l]	0
NaOH addition	3.1

Date	3/01/05
Na_2Oe [%]	1.0
Specific gravity	2.67
Air content [%]	4.8
Slump [mm]	152

Mix 54/F1/H1/1.0/0/NF

Material	kg/m^3
Cement	440
Fly Ash	0
Water	176
Fine aggregate SSD	607
Coarse aggregate SSD	1146
Air Admixture [ml]	218
$LiNO_3$ Admixture [l]	0
NaOH addition	3.1

Date	3/01/05
Na_2Oe [%]	1.0
Specific gravity	2.80
Air content [%]	4.5
Slump [mm]	177

Mix 55/F1/H2/1.0/0/NF

Material	kg/m^3
Cement	440
Fly Ash	0
Water	176
Fine aggregate SSD	607
Coarse aggregate SSD	1155
Air Admixture [ml]	218
$LiNO_3$ Admixture [l]	0
NaOH addition	3.1

Date	3/01/05
Na_2Oe [%]	1.0
Specific gravity	2.80
Air content [%]	5.5
Slump [mm]	177

Appendix B
Pastes and mortars mixes

Mortar M1/NA/0.4

Material	kg/m^3
Cement	646
Fly Ash	129
Water	307
Fine aggregate SSD	1079
Air Admixture [ml]	390
NaOH addition	0

Date	3/09/04
Na_2Oe [%]	0.4

Mortar M2/F1/0.6

Material	kg/m^3
Cement	646
Fly Ash	129
Water	307
Fine aggregate SSD	1078
Air Admixture [ml]	390
NaOH addition	0.86

Date	3/08/04
Na_2Oe [%]	0.6

Mortar M3/F1/1.2

Material	kg/m^3
Cement	646
Fly Ash	129
Water	307
Fine aggregate SSD	1078
Air Admixture [ml]	390
NaOH addition	4.30

Date	3/08/04
Na_2Oe [%]	1.0

Mortar M4/F1/0.6

Material	kg/m^3
Cement	646
Fly Ash	129
Water	307
Fine aggregate SSD	1078
Air Admixture [ml]	390
NaOH addition	6.02

Date	3/08/04
Na_2Oe [%]	1.2

Mortar M5/F1/1.5

Material	kg/m^3
Cement	646
Fly Ash	129
Water	307
Fine aggregate SSD	1078
Air Admixture [ml]	390
NaOH addition	8.60

Date	3/08/04
Na_2Oe [%]	1.5

Mortar M6/F2/1.0

Material	kg/m^3
Cement	646
Fly Ash	129
Water	307
Fine aggregate SSD	1078
Air Admixture [ml]	390
NaOH addition	3.95

Date	3/04/04
Na_2Oe [%]	1.0

Mortar M7/HA/1.0

Material	kg/m^3
Cement	646
Fly Ash	129
Water	307
Fine aggregate SSD	1078
Air Admixture [ml]	390
NaOH addition	0

Date	3/09/04
Na_2Oe [%]	1.0

Cementitious Pastes

Cement Paste (C+W)

Material	kg/m^3
Cement	1022
Fly Ash	205
Water	583

Date	3/09/04
Na_2Oe [%]	0.5

Cement Paste NF (C+FA)

Material	kg/m^3
Cement	1262
Water	600

Date	3/09/04
Na_2Oe [%]	0.4

Appendix C
EDX Analysis Results

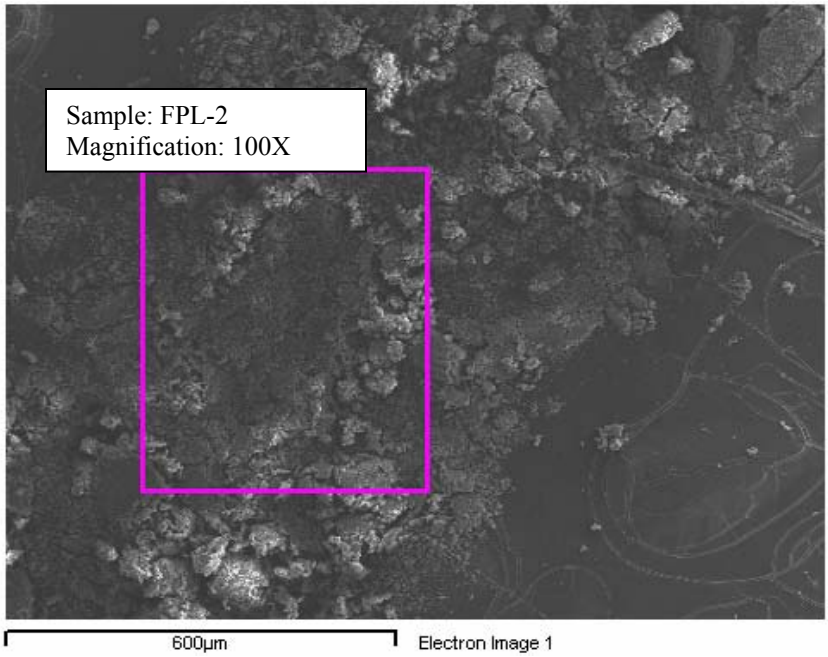

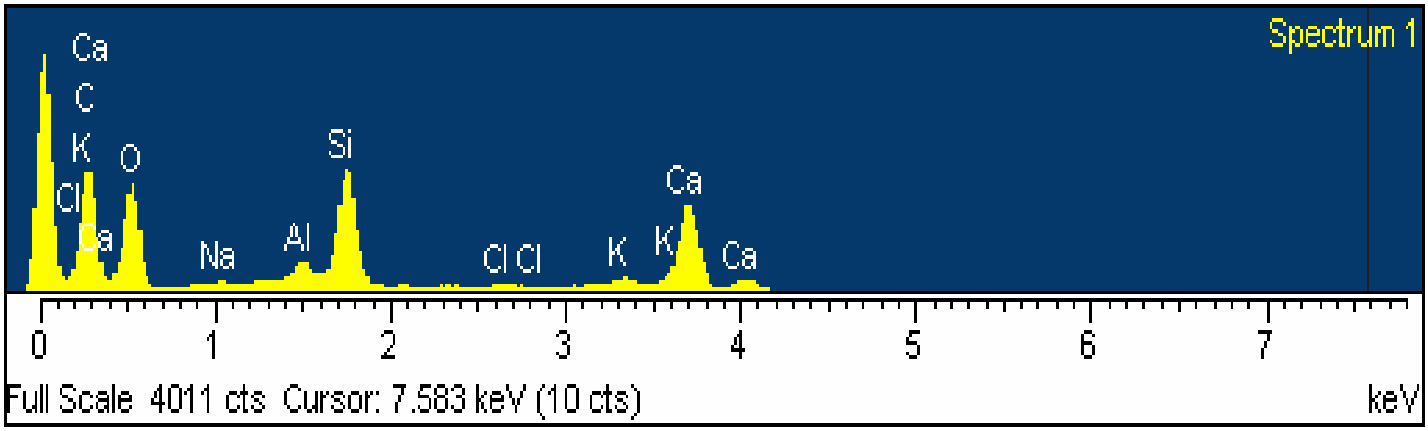

Element	Weight %	Compound	Compound %
Ca	33.74	CaO	47.20
Si	20.20	SiO_2	43.22
Al	2.79	AL_2O_3	5.28
K	2.34	K_2O	2.82
Na	0.64	Na_2O	0.86
O	39.67		

Figure C-1: EDX results for alkali-silica gel present as a white opaque exudate on a molded surface of Prism 27d prepared with Florida Limestone FPL-2 concrete (1.2 % Na_20e = 1.2 % and no lithium).

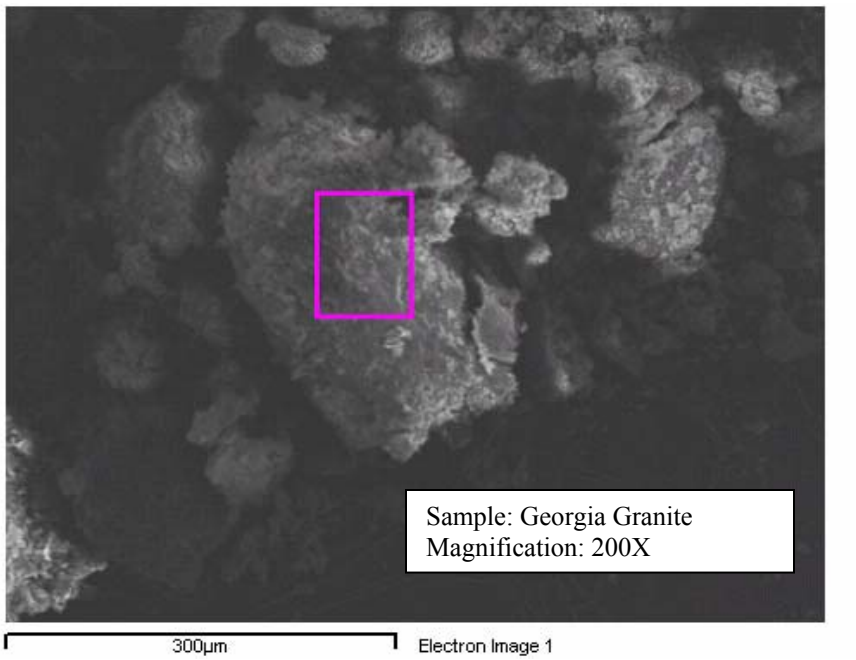

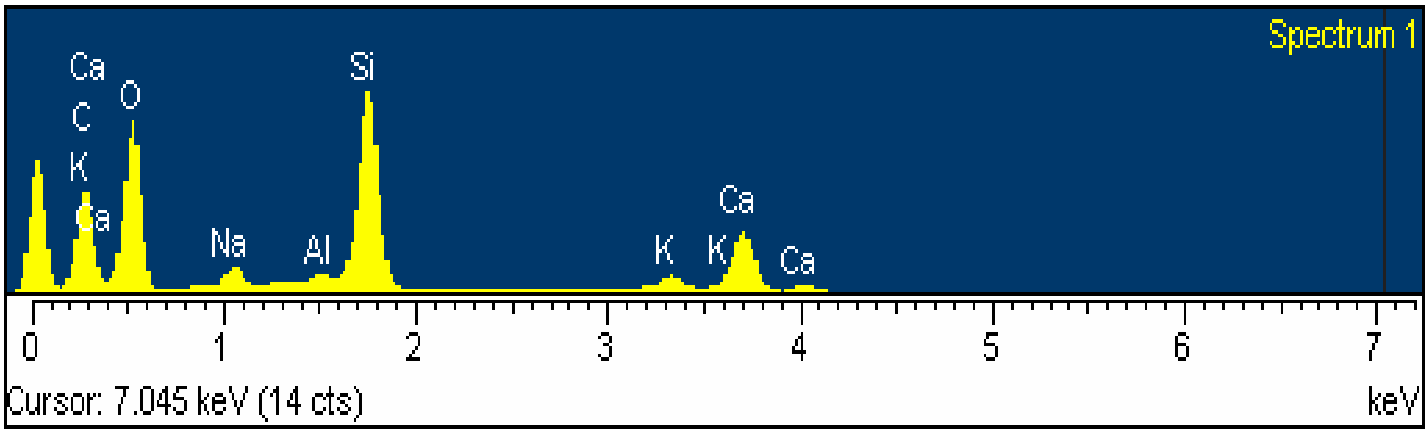

Element	Weight %	Compound	Compound %
Si	27.77	SiO_2	59.42
Ca	20.93	CaO	29.28
Na	4.57	Na_2O	6.16
K	3.37	K_2O	4.06
Al	0.57	AL_2O_3	1.08
O	42.79		

Figure C-2: EXD results for alkali-silica gel present as a secondary deposit on an air void surface in Prism 15a prepared with Georgia granite aggregate concrete (1.2 % Na_2Oe and no lithium admixture).

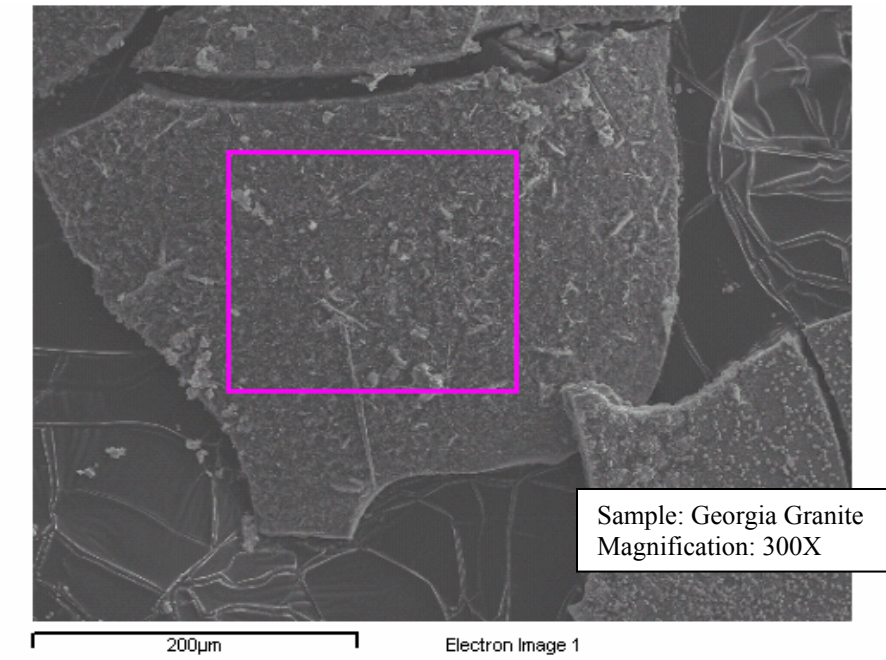

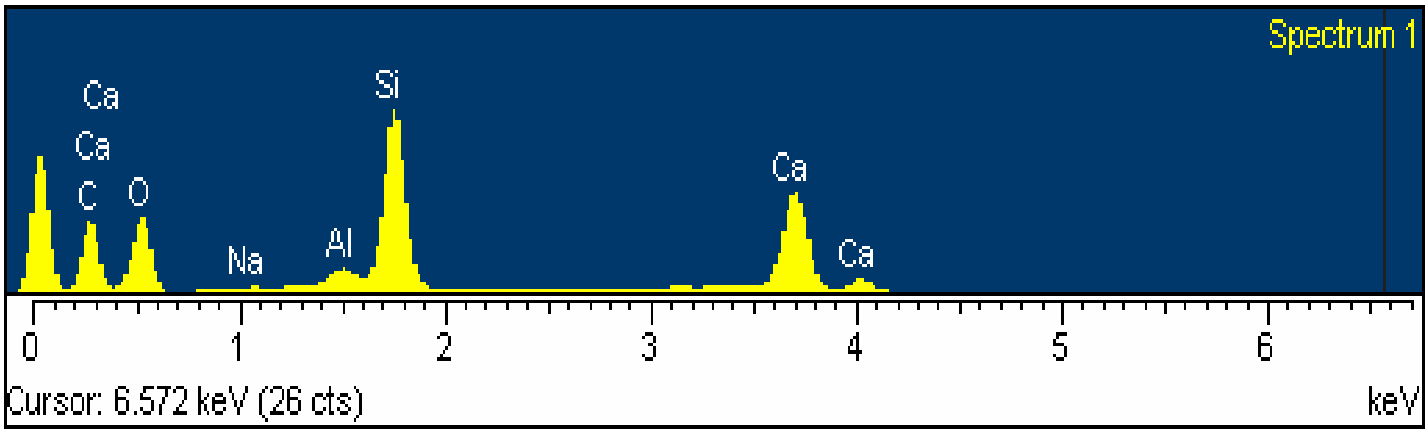

Element	Weight %	Compound	Compound %
Ca	32.43	CaO	45.38
Si	23.69	SiO_2	50.69
Al	1.79	AL_2O_3	3.38
Na	0.41	Na_2O	0.55
O	41.68		

Figure C-3: EDX results for a

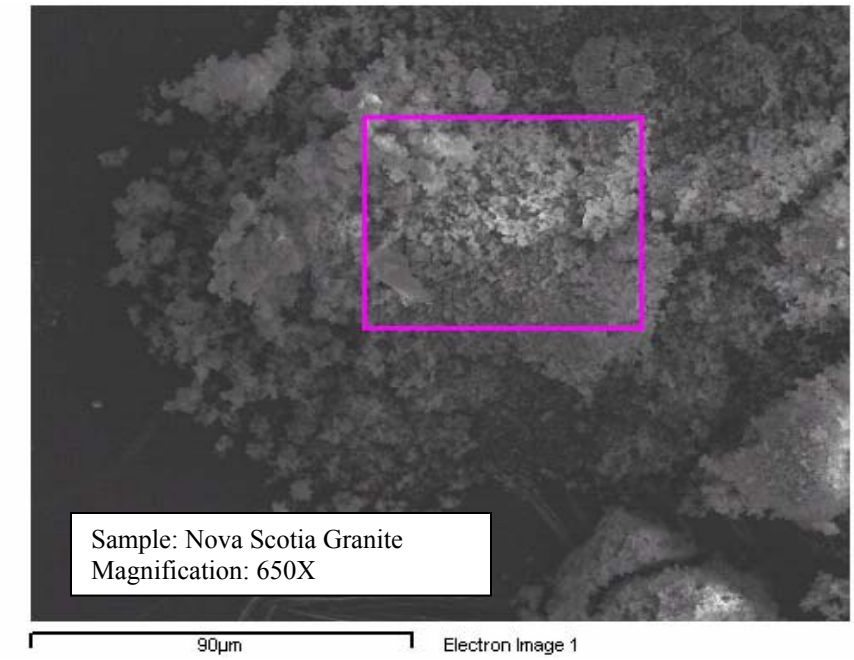

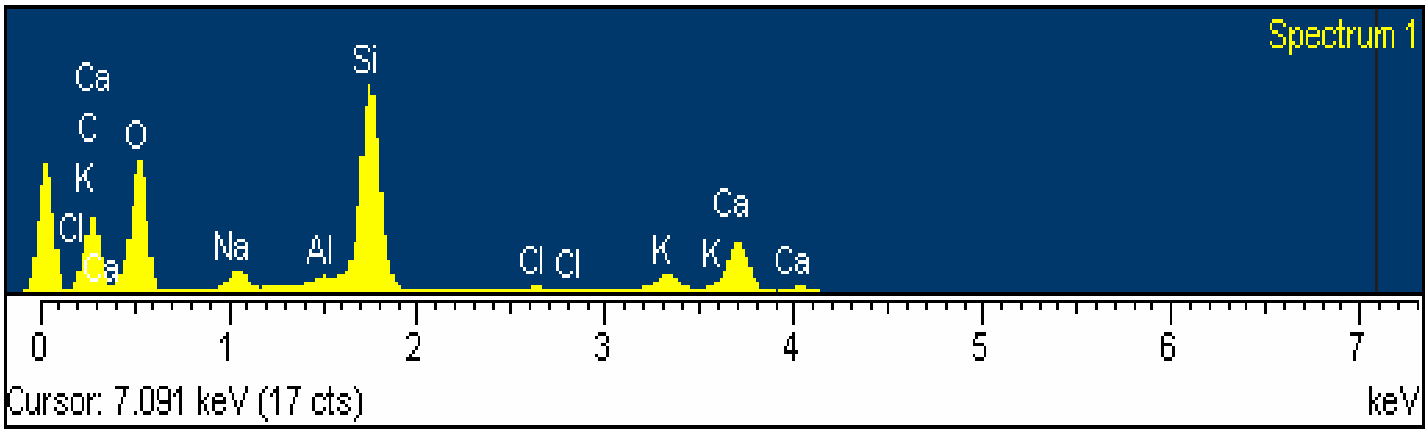

Element	Weight %	Compound	Compound %
Si	29.31	SiO_2	62.69
Ca	17.93	CaO	25.08
Na	3.96	Na_2O	5.33
K	4.12	K_2O	4.97
Al	0.53	AL_2O_3	1.01
O	43.24		

Figure C-4: EDX results for alkali-silica gel present on the surface of a granite aggregate particle in Prism 21b prepared with Nova Scotia granite aggregate concrete (1.2 % Na2O and no lithium admixture).

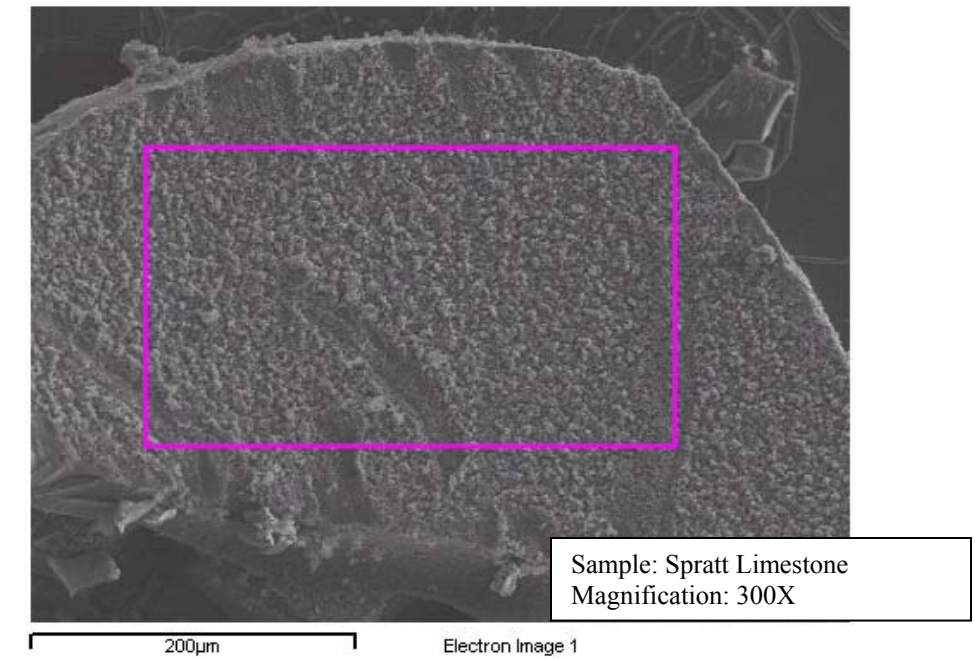

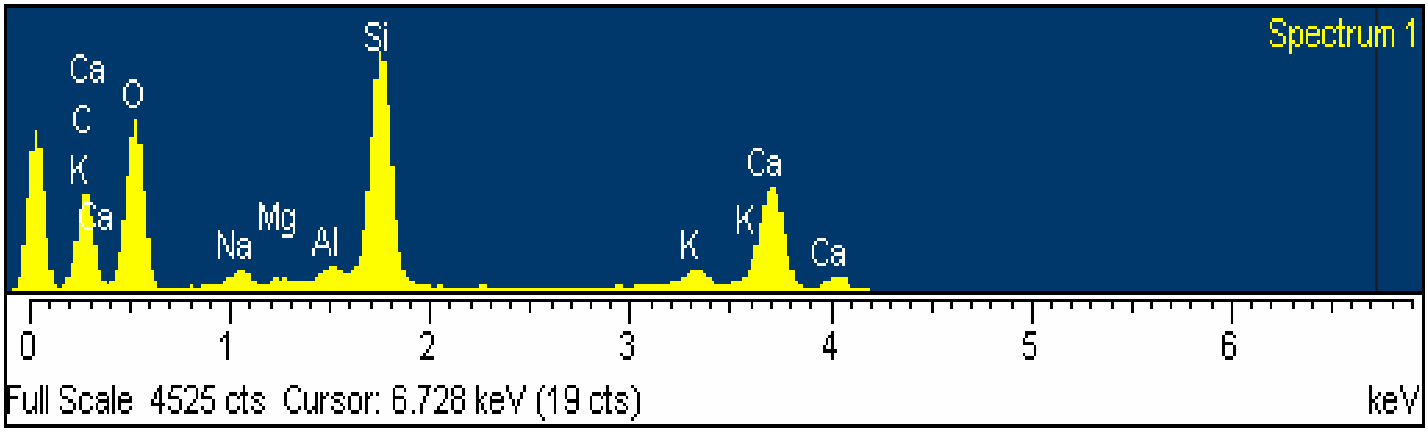

Element	Weight %	Compound	Compound %
Ca	26.80	CaO	37.50
Si	24.55	SiO_2	52.51
K	2.92	K_2O	3.52
Na	2.55	Na_2O	3.44
Al	1.03	AL_2O_3	1.95
Mg	0.66	MgO	1.09
O	41.50		

Figure C-5: EDX results for alkali-silica gel present as a secondary deposit on an air void surface in Prism 32d prepared with Spratt limestone aggregate concrete (1.2 % Na_2O and no lithium admixture)

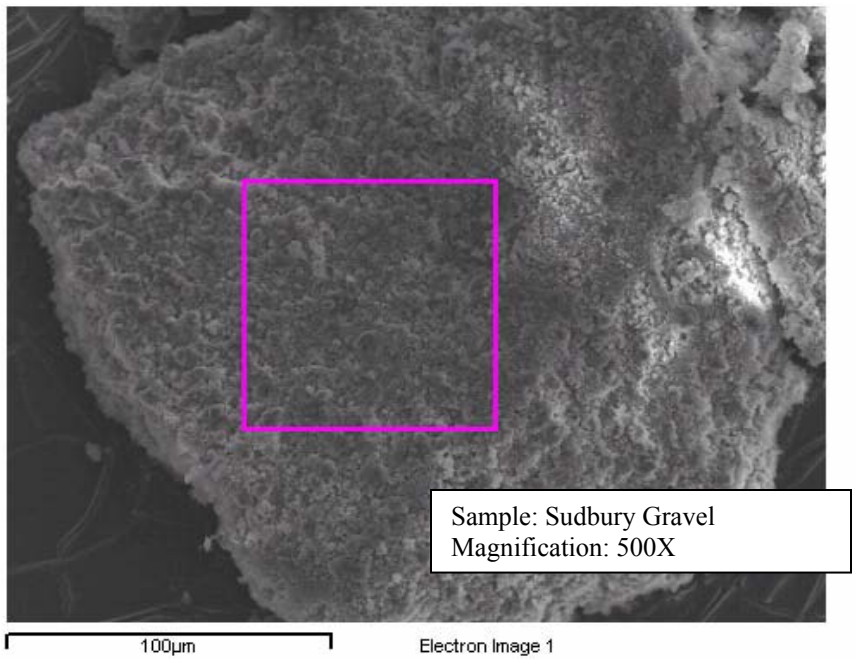

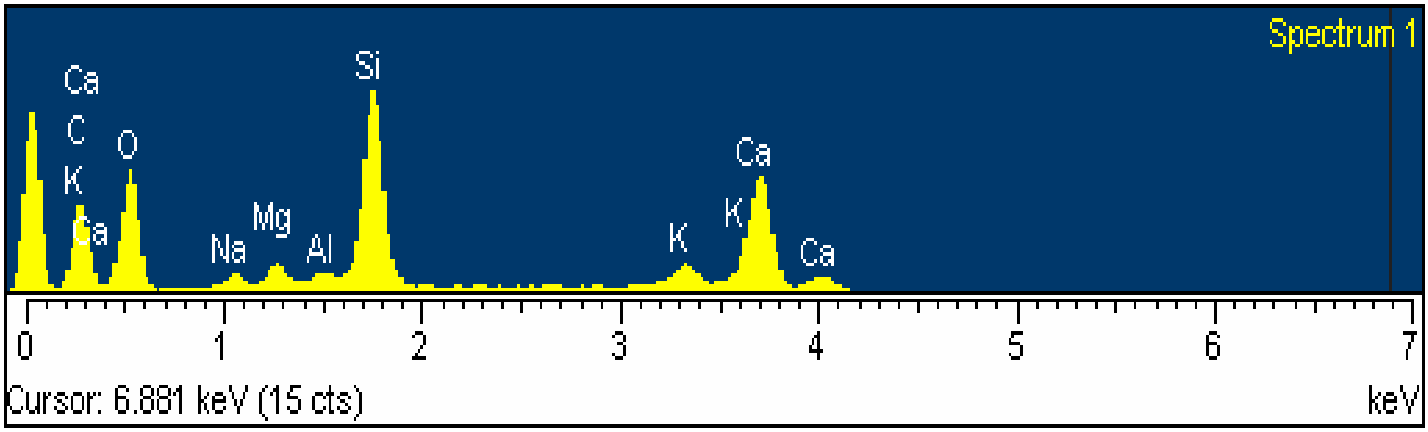

Element	Weight %	Compound	Compound %
Ca	29.56	CaO	41.37
Si	21.22	SiO_2	45.40
K	4.26	K_2O	5.13
Mg	2.49	MgO	4.13
Na	2.09	Na_2O	2.82
Al	0.61	AL_2O_3	1.15
O	39.76		

Figure C-6: EDX results for alkali-silica gel present as a secondary deposit on a air void surface in Prism 40d prepared with Sudbury gravel aggregate concrete (1.2 % Na_2Oe and no lithium admixture).

Appendix D

Appendix D
Compressive strength measurements

Mix	Specimen	Strength [MPa]	
		28 days	365 days
00-F1/F1/0.5/0	a	53.78	53.78
	b	53.50	54.81
	c	48.26	55.64
01-F1/NG/0.5/0	a	37.30	41.16
	b	35.09	39.51
	c	37.30	37.85
02-HA/NG/1.0/0	a	34.13	45.51
	b	38.13	43.85
	c	36.75	45.78
03-HA/F1/1.0/0	a	47.99	56.47
	b	50.75	56.47
	c	51.71	57.57
04-HA/GG/1.0/0	a	36.75	47.71
	b	37.30	46.06
	c	37.16	47.16
05-F1/GG/0.5/0	a	43.30	51.57
	b	45.64	51.02
	c	46.33	53.23
06-F1/F2/0.5/0	a	47.85	50.47
	b	46.61	52.12
	c	45.23	52.40
07-HA/F2/1.0/0	a	43.85	51.02
	b	43.85	50.75
	c	43.30	52.12
08-F1/F1/1.0/0	a	45.51	50.19
	b	43.44	52.40
	c	43.57	48.68
09-F1/F1/1.2/0	a	43.71	50.06
	b	42.75	51.02
	c	43.44	51.43
10-F1/F1/1.0/1	a	46.33	50.75
	b	45.64	51.85
	c	44.40	51.57
11-F1/F1/1.2/1	a	47.71	53.23
	b	47.16	53.50
	c	47.44	51.57
12-F1/F1/1.0/2	a	46.19	52.12
	b	47.16	53.78
	c	46.33	53.50
13-F1/F1/1.2/2	a	43.85	53.23
	b	46.19	53.37
	c	44.95	53.09

14-F1/GG/1.0/0	a	34.27	42.82
	b	35.09	44.95
	c	35.09	43.09
15-F1/GG/1.2/0	a	38.13	50.75
	b	38.96	48.81
	c	37.71	51.02
16-F1/GG/1.0/1	a	34.27	49.09
	b	34.82	47.99
	c	35.92	46.61
17-F1/GG/1.0/2	a	43.85	51.85
	b	43.30	51.85
	c	42.26	51.85
18-F1/GG/1.2/1	a	41.16	49.37
	b	39.78	49.64
	c	40.89	48.81
19-F1/GG/1.2/2	a	40.06	49.92
	b	40.61	50.19
	c	41.44	53.78
20-F1/NG/1.0/0	a	36.75	43.57
	b	35.65	43.44
	c	35.09	43.30
21-F1/NG/1.2/0	a	36.75	45.37
	b	36.47	45.51
	c	37.02	45.51
22-F1/NG/1.0/1	a	37.30	46.06
	b	38.40	44.40
	c	37.71	47.30
23-F1/NG/1.0/2	a	36.75	43.30
	b	37.30	45.37
	c	37.85	42.47
24-F1/NG/1.2/1	a	33.99	39.23
	b	34.27	42.82
	c	35.09	41.71
25-F1/NG/1.2/2	a	37.85	46.61
	b	39.23	458.09
	c	39.51	45.37
26-F1/F2/1.0/0	a	43.30	44.95
	b	43.02	46.47
	c	42.82	46.61
27-F1/F2/1.2/0	a	38.40	42.95
	b	38.96	45.78
	c	39.23	44.68
28-F1/F2/1.0/1	a	41.16	47.16
	b	41.44	45.78
	c	41.71	47.44
29-F1/F2/1.2/1	a	38.40	43.16
	b	38.68	44.13
	c	38.54	43.30

30-F1/H1/0.5/0	a	43.85	51.16
	b	45.51	52.12
	c	44.68	51.02
31-F1/H1/1.0/0	a	38.40	44.95
	b	38.54	45.64
	c	37.58	43.44
32-F1/H1/1.2/0	a	39.51	45.78
	b	38.96	46.06
	c	40.33	47.16
33-F1/H1/1.0/1	a	38.96	48.13
	b	39.09	46.06
	c	39.51	48.54
34-F1/H1/1.0/2	a	40.61	49.92
	b	41.16	51.30
	c	42.26	49.92
35-F1/H1/1.2/1	a	40.33	47.85
	b	40.06	47.71
	c	40.20	48.26
36-F1/H1/1.2/2	a	39.51	48.26
	b	40.06	47.85
	c	39.23	48.54
37-HA/H1/1.0/0	a	40.06	50.88
	b	39.51	49.92
	c	40.61	49.09
38-F1/H2/0.5/0	a	45.51	46.88
	b	45.78	47.99
	c	44.95	49.37
39-F1/H2/1.0/0	a	37.30	43.30
	b	36.75	43.85
	c	37.02	43.30
40-F1/H2/1.2/0	a	36.75	40.82
	b	35.65	41.71
	c	36.20	40.47
41-F1/H2/1.0/1	a	35.65	41.30
	b	36.20	40.47
	c	36.75	40.61
42-F1/H2/1.2/1	a	38.40	43.30
	b	37.30	44.54
	c	37.85	43.85
43-HA/H2/1.0/0	a	38.68	44.40
	b	37.02	43.30
	c	37.30	43.85
44-F1/F3/0.5/0	a	30.20	33.16
	b	29.10	31.65
	c	29.65	31.51
45-F1/F3/1.0/0	a	30.75	32.75
	b	31.23	33.44
	c	30.20	31.65

46-F1/F3/1.2/0	a	30.75	25.79
	b	29.65	30.06
	c	30.20	30.75
47-F1/F3/1.0/1	a	27.99	30.82
	b	26.89	30.06
	c	27.44	29.23
48-F1/F3/1.2/1	a	27.44	29.10
	b	25.79	27.17
	c	26.34	27.99
49-HA/F3/1.0/0	a	27.99	31.78
	b	26.89	33.30
	c	27.44	32.89
53-F1/F1/1.0/0/NFA	a	37.02	44.95
	b	38.40	42.82
	c	37.85	43.99
54-F1/H1/1.0/0/NFA	a	38.96	27.58
	b	37.30	23.03
	c	36.75	23.58
55-F1/H2/1.0/0/NFA	a	32.89	37.44
	b	31.78	33.44
	c	31.78	36.89

X. REFERENCES

[1] Powers, R.G. and Kessler, R., "Corrosion Evaluation of Substructure, Long Key Bridge," Corrosion Report No. 87-9A, Florida Department of Transportation, Gainesville, FL, 1987.

[2] Powers, R.G., "Corrosion of Epoxy-Coated Rebar, Keys Segmental Bridges Monroe County, Report No. 88-8A, Florida Department of Transportation, Gainesville, FL, August, 1988.

[3] Zayed, A.M. and Sagues, A.A., "Corrosion of Epoxy-Coated Reinforcing Steel in Concrete," Paper No. 386 presented at CORROSION/89, New Orleans, LA, April 21, 1989.

[4] Glass, G.K. and Buenfeld, N.R., "Chloride Threshold Levels for Corrosion Induced Deterioration of Steel in Concrete," paper no. 3 presented at RILEM International Workshop on Chloride Penetration into Concrete, Oct. 15-18, 1995, Saint Rémy-les-Chevreuse.

[5] Hartt, W.H., Nam, J., Kim, K., and Li, L., "Effect of Cement Alkalinity upon Time-to-Corrosion of Reinforcing Steel in Concrete undergoing Chloride Exposure," paper no. 03290 presented at CORROSION/03, San Diego, March 17-21, 2003, San Diego.

[6] Hartt, W.H., Nam, J., and Li, L., "Critical Issues Related to Corrosion Induced Deterioration Projection for Concrete Marine Bridge Substructures," Final Report submitted to FDOT by Florida Atlantic University for Project BD166, December 30, 2002.

[7] Nam, J., Hartt, W.H., and Kim, K., "Time-to-Corrosion of Reinforcing Steel in Concrete Specimens as Affected by Cement Alkalinity and Rebar Surface Condition," paper no. 05256 presented at CORROSION/05, April 3-7, 2005, Houston.

[8] Hartt, W.H. and Nam, J., "Critical Parameters for Corrosion Induced Deterioration of Marine Bridge Substructures in Florida," Final Report submitted to FDOT by Florida Atlantic University for Project BD166, April 9, 2004.

[9] Hausmann, D.A., Materials Protection, Vol. 6(10), 1967, p. 23.

[10] Gouda, V.K., British Corrosion Journal, Vol. 5, 1970, p. 198.

[11] Hausmann, D.A., Materials Performance, Vol. 37(10), 1998, p. 64.

[12] Breit, W., Mater. Corrosion, Vol. 49, 1998, p. 539.

[13] Charvin, S., Hartt, W.H., and Lee, S. K., "Influence of Permeability Reducing and Corrosion Inhibiting Admixtures in Concrete upon Initiation of Salt Induced Embedded Steel Corrosion," paper no. 00802 presented at CORROSION/00, March 26-31, 2000, Orlando.

[14] Li, L. and Sagüés, A.A., Corrosion, Vol. 57, 2001, p. 19.

[15] Hausmann, D.A., Materials Protection, Vol. 6(11), 1967, p. 19.

[16] Richardson, M., *Fundamentals of Durable Reinforced Concrete*, Spon Press, NY, 2002.

[17] Folliard, K., Thomas, M., and Kurtis, K., "Guidelines for the Use of Lithium to Mitigate or Prevent ASR", Federal Highway Administration, Washington, DC, Report No. FHWA-RD-03-047, 2003.

[18] ASTM C150, "Standard Specification for Portland Cement," Vol. 04.01, Annual Book of ASTM Standards, American Society for Testing and Materials, Philadelphia.

[19] Neville, A., "Neville on Concrete", American Concrete Institute, Farmington Hills, MI, 2003.

[20] Papadakis, V.G., "Effect of Fly Ash on Portland Cement Systems. Part I. Low-Calcium Fly Ash", Cement and Concrete Research, Vol. 29, 1999, p. 1727.

[21] Ampadu, K., Torii, K., and Kawamura, M., "Beneficial Effect of Fly Ash on Chloride Diffusivity of Hardened Cement Paste", Cement and Concrete Research, Vol. 29, 1999, p. 585.

[22] ASTM C295 "Standard Guide for Petrographic Examination of Aggregates for Concrete," Vol. 04.02, Annual Book of ASTM Standards, American Society for Testing and Materials, Philadelphia.

[23] "Manual of Concrete Practice - Guide to Durable Concrete," Publication 01.2R-01, American Concrete Institute, Farmington Hills, MI, 2000.

[24] Steffens, A., Li, K., and Coussy, O., "Aging Approach to Water Effect on Alkali-Silica Reaction Degradation of Structures", Journal of Engineering Mechanics, Vol. 129, 2003, p. 50.

[25] Fournier, B. and Malhotra, M., "Evaluation of Laboratory Test Methods for Alkali-Silica Reactivity", Cement, Concrete and Aggregates, CCAGDP. Vol. 21, 1999, p.173.

[26] Ollivier, J.P., Maso, J.C., and Bourdette, B., "Interfacial Transition Zone in Concrete," Advanced Cement Based Materials, Vol. 2, 1995, p. 30.

[27] Stark, D., Morgan, B., Okamoto, P., and Diamond, S., "Eliminating or Minimizing Alkali-Silica Reactivity," Strategic Highway Research Program (SHRP) Document SHRP-C-343, 1993.

[28] Gudmundsson, G. and Olafsson, O., "Alkali-Silica Reactions and Silica Fume: 20 Years of Experience in Iceland," Cement and Concrete Research, Vol. 29, 1999, p. 1289.

[29] Duchesne, J., and Berube, M.A., "Long-Term Effectiveness of Supplementary Cementing Materials Against Alkali-Silica Reaction," Cement and Concrete Research, Vol. 31, 2001, p. 1057.

[30] Duchesne, J., and Berube, M.A., "The Effectiveness of Supplementary Cementing Materials in Suppressing Expansion Due to ASR: Another Look at the Reactions Mechanisms. Part 1: Concrete Expansion and Portlandite Depletion," Cement and Concrete Research, Vol. 24, 1993, p. 73.

[31] Duchesne, J., and Berube, M.A., "The Effectiveness of Supplementary Cementing Materials in Suppressing Expansion Due to ASR: Another Look at the Reactions Mechanisms. Part 2: Pore Solution Chemistry," Cement and Concrete Research, Vol. 24, 1994, p. 221.

[32] Lane, S.D. and Ozyildirum, H.C. "Evaluation of the Effect of Portland Cement Alkali Content, Fly Ash, Ground Slag, and Silica Fume on Alkali-Silica Reactivity," Cement, Concrete, and Aggregates, CCAGDP, Vol.21, No.2, December, 1999, P. 126.

[33] Duchesne, J., and Berube, M.A., "Effect of Supplementary Cementing Materials on the Composition of Cement Hydration Products," Advanced Cement-Based Materials, Vol. 2, 1995, p. 43.

[34] Kawamura, M. et. al., "Effectiveness of Various Silica Fumes in Preventing Alkali-Silica Expansion," Katherine and Bryant Mather International Conference on Concrete Durability, American Concrete Institute Publication SP-100, Vol. 2, 1988, P. 1809.

[35] Boddy, A.M. et. al., "The Effect of Silica Content of Silica Fume on Its Ability to Control Alkali-Silica Reaction," Cement and Concrete Research, Vol. 33, 2003, p. 1263.

[36] Hasparyk, N.P. et. al., "Effect of Silica Fume and Rice Husk Ash on Alkali-Silica Reaction," American Concrete Materials Journal, July-August, 2000, p. 486.

[37] Malvar, L.J. et. al., "Alkali-Silica Reaction Mitigation: State of the Art and Recommendations," American Concrete Institute Materials Journal, Sept.-Oct., 2002, p. 480.

[38] Shehata, M.H. et. al., "The Effect of Fly Ash Composition on the Expansion of Concrete Due to Alkali-Silica Reaction," Cement and Concrete Research, Vol. 30, 2000, p. 1063.

[39] Bhatty, M.S.Y., "Mechanism of Pozzolanic Reactions and Control of Alkali-Aggregate Expansion," Cement, Concrete, and Aggregates, CCAGDP, Vol. 7, No. 2, 1985, p. 69.

[40] Monteiro, P.J.M. et. al., "Influence of Mineral Admixtures on the Alkali-Aggregate Reaction," Cement and Concrete Research, Vol. 27, 1997, p. 1899.

[41] Collins, C., Ideker, J., Willis, G., and Kurtis, K., "Examination of the Effects of LiOH, LiCl, and $LiNO_3$ on Alkali-Silica Reaction", Cement and Concrete Research, Vol. 34, 2004, p.1403.

[42] Berube, M., Tremblay, C., Fournie,r B., Thomas, M., and Stokes, D., "Influence of Lithium-Based Products Proposed for Counteracting ASR on the Chemistry of Pore Solution and Cement Hydrates" Cement and Concrete Research, Vol. 34, 2004, p. 1645.

[43] Feng, X., Thomas, M., Bremmer, T. Balcom B., and Folliard K., "Studies on Lithium Salts to Mitigate ASR-Induced Expansion in New Concrete: A Critical Review", Cement and Concrete Research, DTD 5, 2004, p. 1.

[44] Glass, B. and Buenfeld, N., "The Influence of Chloride Binding on the Chloride Induced Risk in Reinforced Concrete", Corrosion Science, Vol. 42, 2000, p. 329.

[45] Glass, B., Reddy, B., and Buenfeld, N., "The Participation of Bound Chloride in Passive Film Breakdown on Steel in Concrete", Corrosion Science, Vol. 42, 2000, p. 2013.

[46] Bryant, J., "Non-Invasive Permeability Assessment of High-Performance Concrete Bridge Mixtures", Virginia Polytechnic Institute and State University, Department of Civil Engineering, Doctoral Dissertation, 2001.

[47] Polder, R. and Peelen, W., "Characterization of Chloride Transport and Reinforcement Corrosion in Concrete under Cyclic Wetting and Drying by Electrical Resistivity", Cement and Concrete Research, Vol. 24, 2002, p. 427.

[48] Whiting, D. and Nagi, M., "Electrical Resistivity of Concrete- A Literature Review", PCA R&D Serial No.2457, Portland Cement Association, IL, 2003.

[49] ASTM 1202, "Standard Test Method for Electrical Indication of Concrete's Ability to Resist Chloride Ion Penetration," Vol. 04.02, Annual Book of ASTM Standards, American Society for Testing and Materials, Philadelphia.

[50] Wee, T., Suryavanshi A., and Tin, S., "Evaluation of Rapid Chloride Permeability Test Results for Concrete Containing Mineral Admixtures", ACI Materials Journal, Vol. 97, 2000, p. 221.

[51] Morris, W. and Vazquez, V., "Chloride Induced Corrosion of Reinforcing Steel Evaluated by Concrete Resistivity Measurements", Electrochimica Acta, Vol. 49, 2004, p. 4447.

[52] "Florida Method of Test for Concrete Resistivity as an Electrical Indicator of Its Permeability," Florida Department of Transportation, Test Method FM5-578, FL, 2004.

[53] Garci, M. and Jennings, H., "Effects of High Alkalinity on Cement Pastes", ACI Materials Journal, Vol. 98, 2001, p. 251.

[54] Tritthart, J., "Chloride binding in cement II. The Influence of the Hydroxide Concentration in the Pore Solution of Hardened Cement Paste on Chloride Binding", Cement and Concrete Research, Vol. 19, 1989, p. 683.

[55] Smaoui, N., Berube, M., Fournier, B., Bissonnette, B., and Durand, B., "Effects of Alkali Addition on the Mechanical Properties and Durability of Concrete", Cement and Concrete Research, Vol. 35, 2005, p. 203.

[56] Shayan, A., "Effect of NaOH and NaCl Solutions and Temperature on the Behavior of Specimens Subjected to Accelerated AAR Tests", Cement and Concrete Research, Vol. 28, 1998, p. 25.

[57] Diamond, S. and Ong, S., "Effects of Added Alkali Hydroxides in Mix Water on Long-Term SO_4^{2+} Concentrations in Pore Solution", Cement and Concrete Composites, Vol. 16, 1994, p. 219.

[58] Jawed, I. and Skalny, J., "Aalkali in Cement - A Review: II. Effects of Alkalies on Hydration and Performance of Portland Cement", Cement and Concrete Research, Vol. 8, 1978, p. 37.

[59] ASTM C231 "Standard Test Method for Density (Unit Weight), Yield, and Air Content (Gravimetric) of Concrete," Vol. 04.02, Annual Book of ASTM Standards, American Society for Testing and Materials, Philadelphia.

[60] ASTM C 192 "Standard Practice for Making and Curing Concrete Test Specimens in the Laboratory," Vol. 04.02, Annual Book of ASTM Standards, American Society for Testing and Materials, Philadelphia.

[61] ASTM C1293, "Standard Test Method for Determination of Length Change of Concrete Due to Alkali-Silica Reaction," Vol. 04.02, Annual Book of ASTM Standards, American Society for Testing and Materials, Philadelphia.

[62] ASTM C856, "Standard Practice for Petrographic Examination of Hardened Concrete," Vol. 04.02, Annual Book of ASTM Standards, American Society for Testing and Materials, Philadelphia.

[63] ASTM C295, "Standard Practice for Petrographic Examination of Aggregates for Concrete," Vol. 04.02, Annual Book of ASTM Standards, American Society for Testing and Materials, Philadelphia.

[64] ASTM C294, "Standard Descriptive Nomenclature for Constituents of Concrete Aggregates," Vol. 04.02, Annual Book of ASTM Standards, American Society for Testing and Materials, Philadelphia.

[65] Barneyback, R. and Diamond, S., "Expression and Analysis of Pore Fluids from Hardened Cement Pastes and Mortars", Cement and Concrete Research, Vol. 11, 1981, p. 279.

[66] Sagües, A., Moreno, E., and Andrade, C., "Evolution of pH During In-Situ Leaching in Small Concrete Cavities", Cement and Concrete Research, Vol. 27, 1997, p. 1747.

[67] L. Li, J. Nam, and W.H. Hartt, "Ex-Situ Leaching Measurement of Concrete Alkalinity," Cement and Concrete Research, Vol. 35, 2005, p. 277.

[68] ASTM C39, "Standard Test Method for Compressive Strength of Cylindrical Concrete Specimens," Vol. 04.02, Annual Book of ASTM Standards, American Society for Testing and Materials, Philadelphia.

[69] ASTM C78, "Standard Test Method for Flexural Strength of Concrete," Vol. 04.02, Annual Book of ASTM Standards, American Society for Testing and Materials, Philadelphia.

[70] Mindess, S. and Young, J., *Concrete*, Civil Engineering and Engineering Mechanics Series, Prentice Hall, Englewood Cliffs, NJ, 1981.

[71] Taylor, H.F.W., *Cement Chemistry*. 2nd Edition", Thomas Telford Publishing, London, UK, 1997.

[72] Duchesne, J. and Berube, M-A., "Available Alkalies from Supplementary Cementing Materials" ACI Materials Journal, Vol. 91, 1994, p. 289.

[73] Diamond, S. "Effects of Two Danish Flyashes on Alkali Contents of Pore Solutions of Cement-Flyash Pastes", Cement and Concrete Research, Vol. 11, 1981, p. 383.

[74] Duchesne, J. and Berube, M.A., "The Effectiveness of Supplementary Cementing Materials in Suppressing Expansion Due to ASR: Another Look at the Reaction Mechanisms. Part 2: Pore Solution Chemistry", Cement and Concrete Research, Vol. 24, 1994, p. 221.

[75] Al-Amoudi, O.S.B., Maslehuddin, M., and Asi, I., "Performance and Correlation of the Properties of Fly Ash Cement Concrete", Cement, Concrete, and Aggregates, Vol. 18, 1996, p. 71.

[76] ASTM C33 "Standard Specification for Concrete Aggregates" Vol. 04.02, Annual Book of ASTM Standards, American Society for Testing and Materials, Philadelphia.

[77] Rogers, C., "Multi-laboratory study of the accelerated mortar bar test (ASTM C 1260) for alkali-silica reaction", Cement, Concrete, and Aggregates, Vol.21, No.2, December, 1999, p. 185-194).

[78] Ranc, R., Isabelle, H, Clement, J., and Sorrentino, D., "Limits of Application of the ASTM C227 Mortar Bar Test. Comparison with Two Others Standards on Alkali Aggregate Reactivity", Cement, Concrete, and Aggregates, Vol. 16, June 1994, p. 63.

[79] Alasali, M., Malhotra, V., and Soles, J., "Performance of Various Test Methods for Assessing the Potential Alkali Reactivity of Some Canadian Aggregates", American Concrete Institute Materials Journal, November-December 1991, p. 613.

[80] Thomas, M. and Innis, F., "Use of the Accelerated Mortar Bar Test for Evaluating the Efficacy of Mineral Admixtures for Controlling Expansion due to Alkali-Silica Reaction", Cement, Concrete, and Aggregates, Vol. 21, No. 2, December 1999, p. 157.

[81] ASTM C78, "Flexural Strength of Concrete (Using Simple Beam with Third Point Loading)," Vol. 04.02, Annual Book of ASTM Standards, American Society for Testing and Materials, Philadelphia.

[82] Chatterji, S. and Kawamura M., "Electrical double Layer, Ion Transport and Reactions in Hardened Cement Paste", Cement and Concrete Research, Vol. 22, 1992, p. 774.

[83] Chatterji S., "Aspects of Ionic Diffusion Through Thick Matrices of Charged Particles", Journal of Colloid and Interface Science, Vol. 30, 2006, p.820.

[84] Glass, G.K., Buenfeld, N.R., "Chloride-Induced Corrosion of Steel in Concrete", Progress in Structural Engineering and Materials, Vol. 2, 2000, p. 448.

[85] Kruyt, H.R., *Colloid Science*, 4th Edition, Vol. 1, Chapter IV, Elsevier Publishing Company, Netherlands, 1965.

[86] Chatterji, S., "Colloid Electrochemistry of Saturated Cement Paste and Some Properties of Cement Based Materials", Advanced Cement Based Materials, Vol. 7, 1998, p. 102.